

THEORETICAL AND EXPERIMENTAL ANALYSIS OF
ANNULAR, ANNULAR SECTOR AND CIRCULAR SECTOR
PRINTED CIRCUIT ANTENNAS

A Thesis

Presented to
the Faculty of the Department of Electrical Engineering
University of Houston

In Partial Fulfillment
of the Requirements for the Degree
Master of Science in Electrical Engineering

by
Jia-Dong Ou
July 1981

ACKNOWLEDGEMENT

I am greatly indebted to my advisor, Dr. W. F. Richards, for his invaluable help and encouragement throughout the development of this material. In particular, I am grateful to Dr. Richards and the personnel at Harry Diamond Laboratory for supplying the experimental antennas and measurements reported in this thesis. My appreciation is also extended to Dr. L. C. Shen, Dr. S. A. Long and Dr. G. W. Batten for their service on my thesis committee. My special thanks are also due to my parents, Mr. and Mrs. P. G. Ou, and my wife, L. G. Shen. Without their patronage and encouragement, this thesis could not be completed.

THEORETICAL AND EXPERIMENTAL ANALYSIS OF
ANNULAR, ANNULAR SECTOR AND CIRCULAR SECTOR
PRINTED CIRCUIT ANTENNAS

An Abstract of a Thesis
Presented to the
the Faculty of the Department of Electrical Engineering
University of Houston

In Partial Fulfillment
of the Requirements for the Degree
Master of Science in Electrical Engineering

by
Jia-Dong Ou
July 1981

ABSTRACT

An analysis of three different shaped microstrip antennas is performed. The three shapes were an annular patch, a sector of an annular patch, and a sector of a circular disk patch. The method used to analyze these antennas was based on the "cavity model." Briefly, the analysis method consists of first computing the fields between the patch and ground plane based on the assumption that the edge of the patch represents an ideal open. From these "internal fields," a "magnetic current" at the patch edge can be defined. Using some simple approximations, a radiated field produced by the magnetic current can be found. From this, the power radiated by the antenna can be approximated. Also, from the internal fields, the power lost to heating the dielectric and metal parts of the antenna can be approximated, as well as the time average stored energy under the patch. From these quantities, the quality factor of the antenna can be accurately calculated. Finally, from the quality factor, a correction to the imaginary part of the resonant frequencies of the antenna can be constructed. Once the complex resonant frequencies of the antenna have been found, the input impedance can be easily calculated. Experiments were performed for each of the structures analyzed. Very good agreement between measured and calculated impedances were found.

TABLE OF CONTENTS

Chapter		Page
1	INTRODUCTION	1
2	ANALYSIS OF THE PRINTED-CIRCUIT MICROSTRIP ANTENNAS ..	5
2-1	The Cavity Model	5
2-2	The Internal Field Structure	10
2-2-1	The Internal Fields of the Annular Antenna Element	12
2-2-2	The Internal Field of Annular Sector Antenna	19
2-2-3	The Internal Fields of Circular Sector ...	23
2-3	The Electric and Magnetic Stored Energy	29
2-3-1	Annulus Microstrip Antenna	29
2-3-2	Annular Sector Microstrip Antenna	31
2-3-3	Circular Sector Microstrip Antenna	32
2-4	Dielectric Loss	33
2-5	Copper Loss	33
2-6	Radiated Power	34
2-6-1	The Annular Microstrip Antenna	39
2-6-2	The Annular Sector Antenna	44
2-6-3	The Circular Sector Antennas	47
2-7	The Input Impedance	49
2-7-1	Annular Microstrip Antenna	52
2-7-2	Annular Sector Microstrip Antenna	52
2-7-3	Annular Sector	52

Chapter		Page
	2-8 Acceleration of Series	53
	2-8-1 Annular Microstrip Antenna	54
	2-8-2 Annular Sector Microstrip Antenna	55
	2-8-3 Circular Sector Microstrip Antenna	55
	2-8-4 The Efficient Summation of Series of Asymptotic Forms	56
3	ANALYTIC AND EXPERIMENTAL RESULTS	58
	3-1 The Loss Tangent and the Conductivity	58
	3-2 The Quality Factor	58
	3-3 The Resonant Frequency	62
	3-4 The Input Impedance	62
4	APPLICATIONS AND CONCLUSIONS	99
	REFERENCES	101

CHAPTER 1

INTRODUCTION

This thesis provides a simple yet accurate analysis of a variety of microstrip antennas. A microstrip antenna is generally constructed from double clad, printed circuit board. It is a member of a general class of antennas constructed from printed circuit boards called "printed circuit antennas." In the case of a microstrip antenna, the "ground plane" (i.e., one side of the printed circuit board) is left intact. Most of the cladding on the other side of the board is etched away leaving a region of metal usually with at least one linear dimension on the order of a half dielectric wavelength. An example of such an antenna is the circular microstrip antenna illustrated in figure 1-1. An equivalent parallel plate antenna is shown in figure 1-2 if the ground plane is sufficiently large so that image theory can be applied.

Microstrip antennas have recently been applied to a variety of systems, especially where light weight and simple fabrication are required. These antennas are low-profile, conformable, rugged, and inexpensive to fabricate by common printed-circuit techniques such as photoetching. They are well suited for high velocity vehicles where aerodynamic drag is an important design consideration. The main advantage is their narrow band characteristics. For many applications, however, the bandwidth limitations are acceptable. There is active interest in finding simple analytic models to describe and predict their behavior.

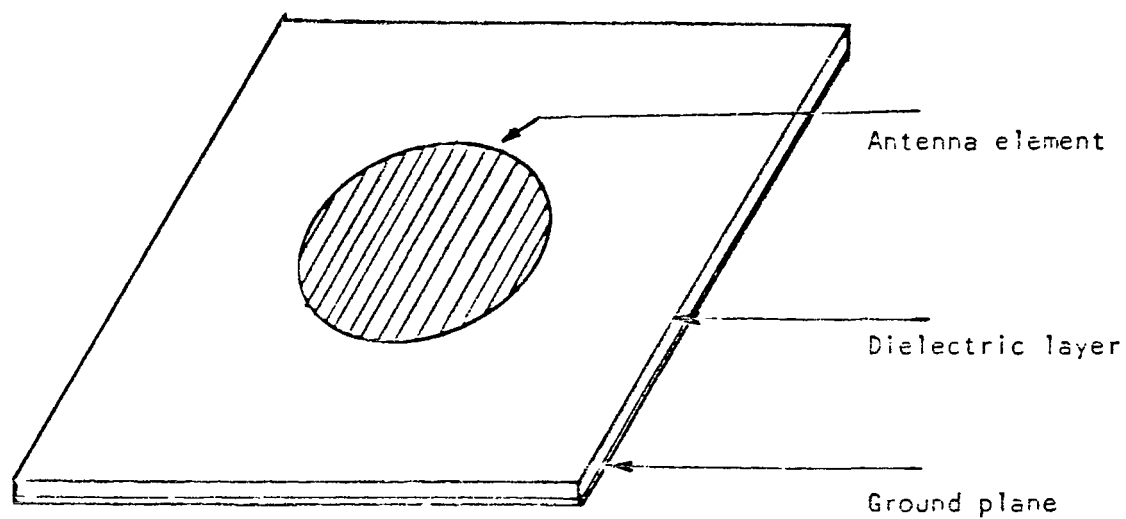


Figure 1-1: A general circular disk microstrip antenna element

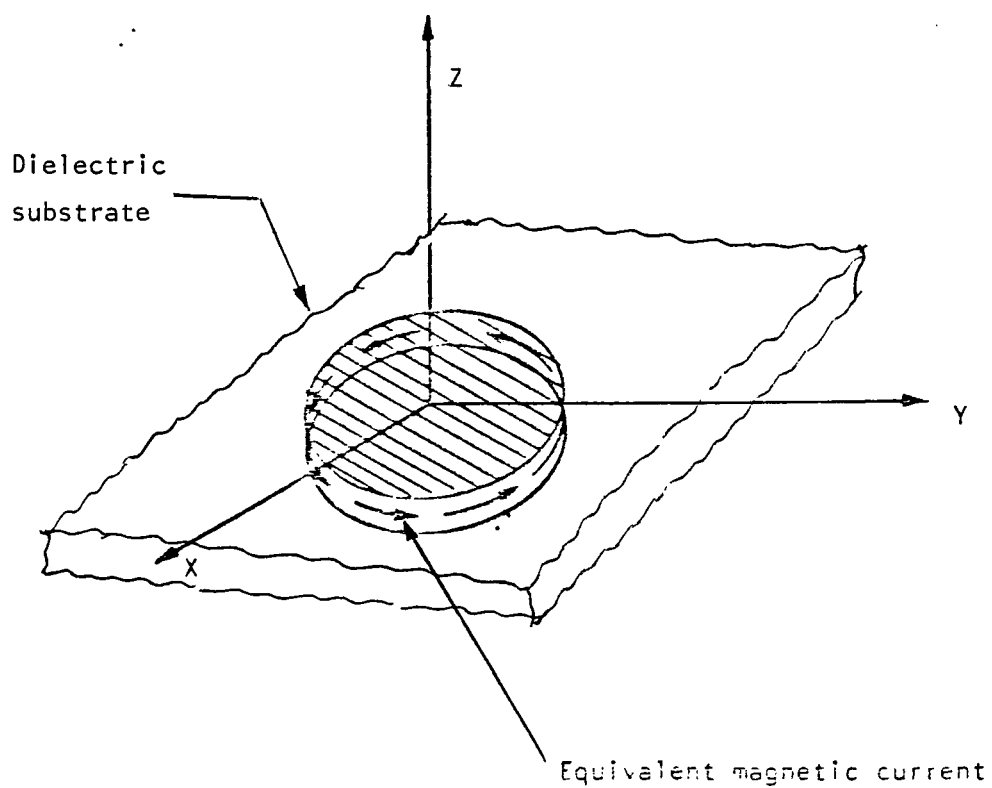


Figure 1-2: The simple cavity model and the equivalent magnetic current

Extensive analysis has been done for microstrip antennas of several different shapes, including the circular disk, rectangle, square and triangle [1,2,3,4,5]. In this thesis, the microstrip antennas with the shapes of an annulus, an annular sector and a circular sector are studied analytically by the simple "resonant cavity model." This resonant cavity is formed by connecting the antenna patch to the ground plane by a perfect magnetic wall around the side. The antenna can be replaced by this cavity to compute the approximate fields under the patch. This can be done because the magnetic field tangent to the patch edge is small. Thinking of this antenna as a parallel plate waveguide, we see that this model, as it is, would predict complete reflection of the fields incident upon the truncation (i.e., patch edge) of the waveguide. In the actual antenna, of course, some energy is radiated at the patch edge although most is reflected. Indeed this is consistent with the experimental result that the quality factor of these antennas is typically high. That is, for a given amount of radiated power (and other types of power loss), the stored energy in the antenna is large.

For each case, the fields are studied by two methods: the cavity mode expansion and mode matching. For the resonant mode expansion method, the field is expressed by a double, infinite series of resonant cavity modes. On the other hand, for the mode matching method, the field is expressed by a single infinite series. After the internal fields are determined, an equivalent magnetic current around the aperture can be computed. From this equivalent magnetic current,

the radiation pattern and the radiated power can be found.

In searching for the solution, the free-space Green's function is used. This, of course, is an approximation. The accuracy of the prediction will degrade if the thickness or the dielectric constant of the substrate is large. However, for the most practical applications, the prediction by this model is very good. In fact, it was found [4] that the dielectric effect on the radiation field intensity can be neglected when the thickness of the substrate is very small with respect to the dielectric wavelength or when ϵ_r goes to 1. The bandwidth increases when the ratio of the thickness of the dielectric substrate to the free space wavelength increases. For the case of thicker substrates, we must use the Green's function for a two-layer medium to account for the dielectric effect. Here, we just study the electrically thin microstrip antenna for simplicity.

CHAPTER 2

ANALYSIS OF THE PRINTED-CIRCUIT MICROSTRIP ANTENNAS

In this chapter, three different microstrip antennas (as shown in figures 2-1, 2-2, 2-3) are analyzed in detail. The internal fields of these antennas are found by using a "modal expansion" or by "mode matching." From these fields, we easily find the stored energy, radiated power, power lost to heating of the cladding (here called "copper loss") and heating of the dielectric (called "dielectric loss"). Using these parameters, the driving point impedance and radiation pattern of the antenna are computed.

2-1 The Cavity Model

If we view the region between the patch and the ground plane as a parallel plate wave guide, then the edge of the patch represents an "open circuit." This, of course, is not an ideal open circuit. Indeed if it were, the antenna would not radiate at all. However, if the antenna is very thin, then as far as the shape of the internal field distribution is concerned, it makes little difference whether or not this "open" radiates. It is important to make a distinction here. The shape of the field distribution is relatively insensitive to the details of the open. However, the amplitude of the distribution is intimately dependent on how much power is radiated from the open circuit.

In this analysis, we first predict the shape of the distribution. This is done by idealizing the open circuit in such a way that the problem of finding the internal fields becomes separable. (The geometry of the antenna elements dictates the use of cylindrical coordinates.)

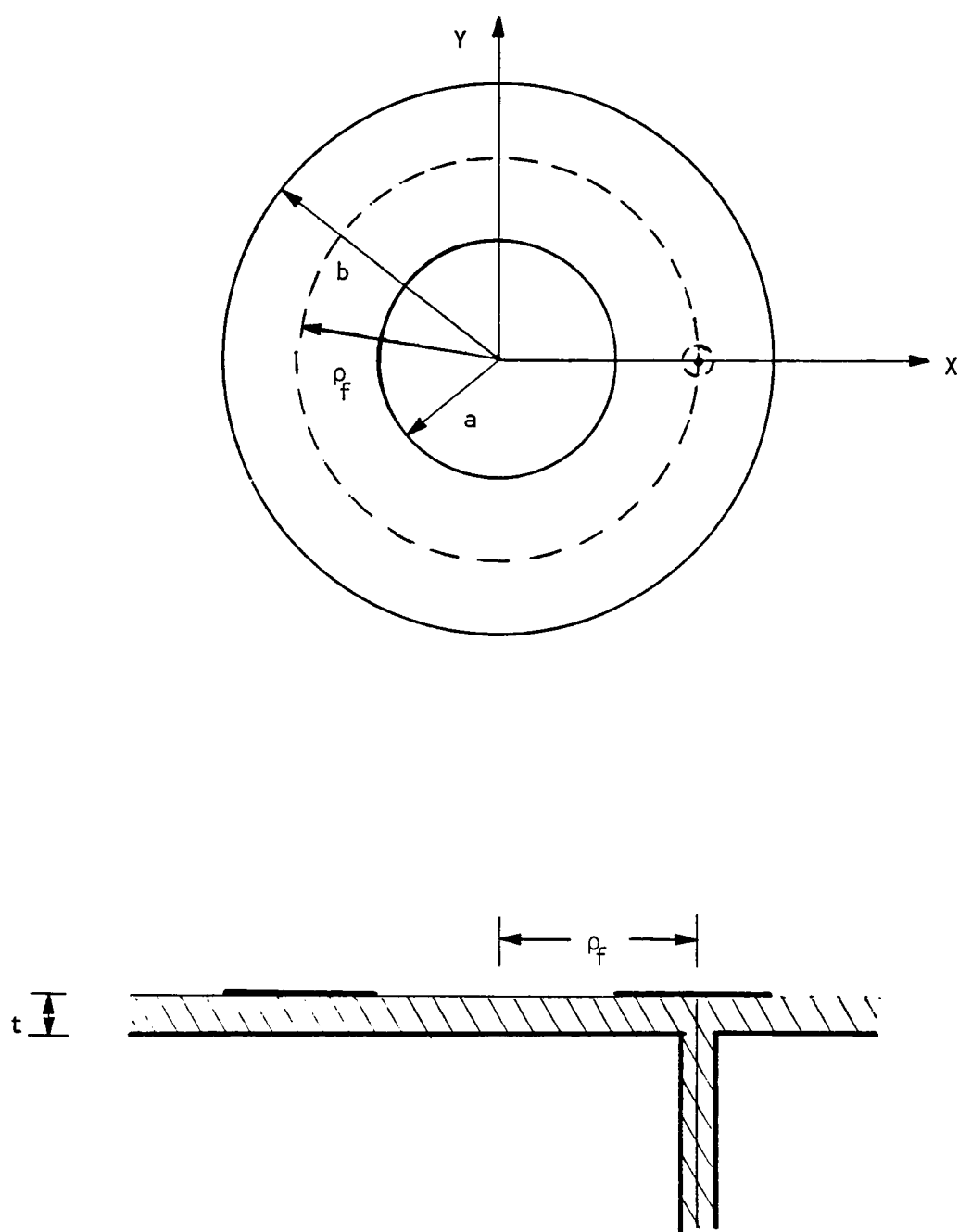


Figure 2-1: An annulus microstrip antenna, showing coaxial feed method

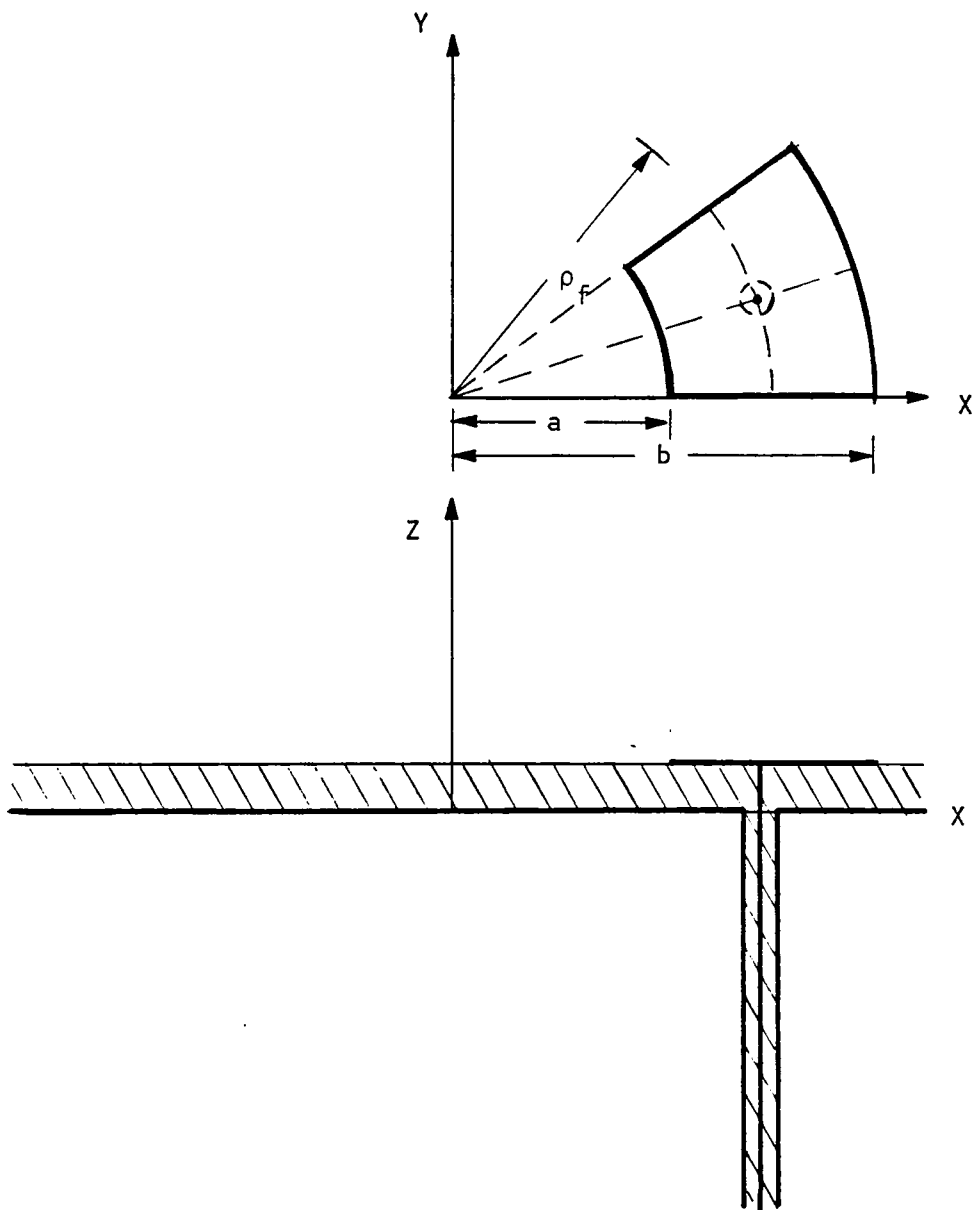


Figure 2-2: An annular sector microstrip antenna, showing coaxial feed method

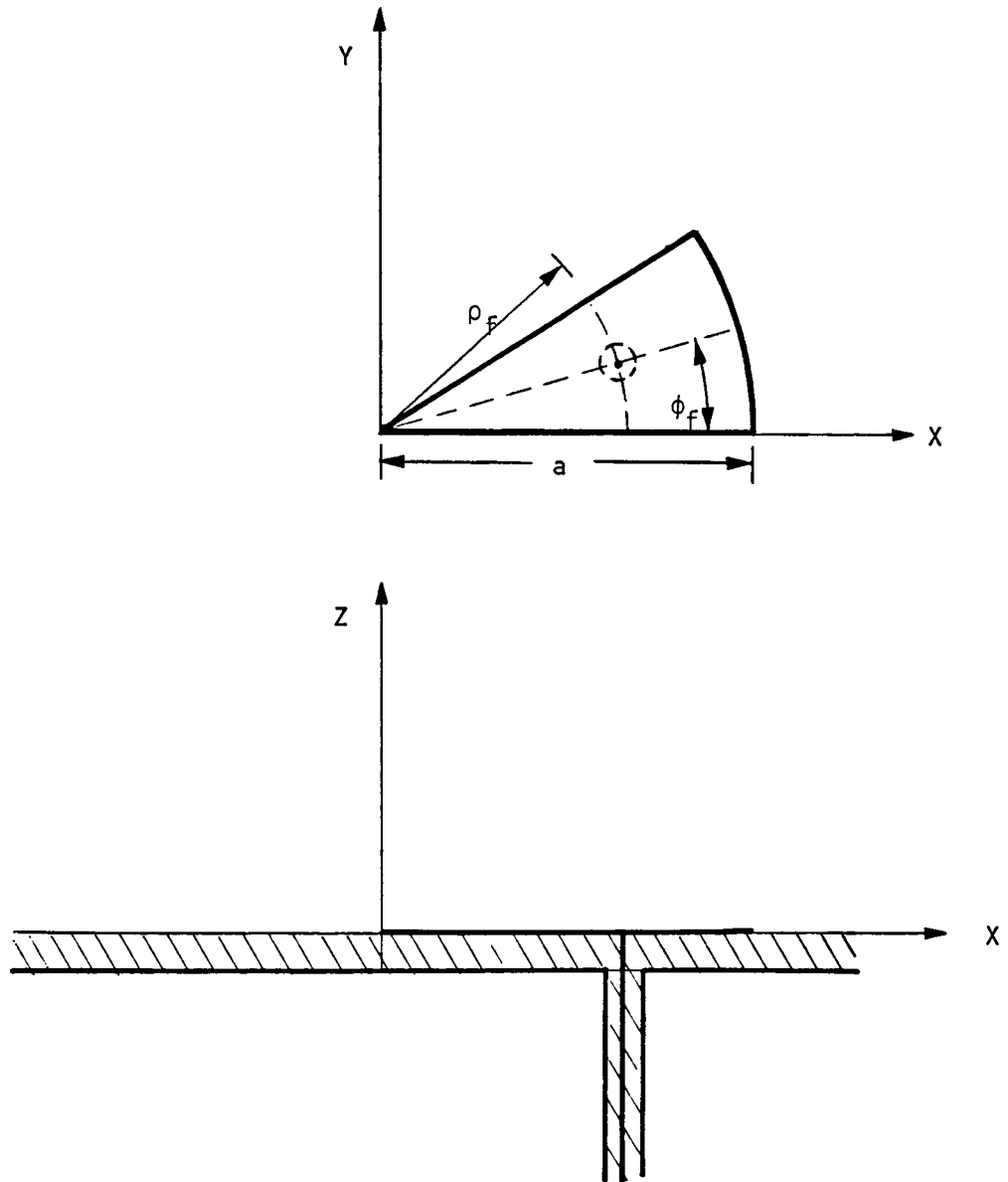


Figure 2-3: A circular sector microstrip antenna, showing coaxial feed method

Next from these internal fields, we compute the stored energy and the total power absorbed and radiated by the antenna. Since the amplitude of the field distribution is not correctly predicted, but is off by some constant factor, say A , the stored energy and total power loss will be off by a factor of A^2 . However, if we compute the quality factor, Q , of the antenna, these factors of A^2 will cancel out since Q is proportional to the ratio of stored energy to power loss. Thus, in order to correctly predict the quality factor of the antenna, we need only be able to correctly predict the shape of the internal field distribution.

Finally it will become clear from the equations which follow that the amplitude of the field distribution can be accurately estimated if the antenna Q is known. With the field distribution determined, the impedance and pattern can be computed.

The first problem becomes how to idealize the open circuit. This is done by replacing the aperture between the edge of the patch and the ground plane by a perfect magnetic conductor (PMC). This model for the open circuit is chosen since it is expected that the component of the electric current under the patch normal to the patch edge is very small. Therefore, the component of magnetic field tangential to the aperture plane is also expected to be small. Hence, the introduction of a magnetic conductor should not appreciably disturb the fields. We further idealize this "cavity" by initially assuming that all the metal cladding is a perfect electric conductor (PEC). A detailed analysis of these internal fields is given below.

2-2 The Internal Field Structure

In order to excite the antenna element, power has to be fed to the antenna by some method. This can be done by either a coaxial cable with the connection of the outer conductor to the ground plane and the inner conductor (piercing the substrate) to the antenna element, or by a microstrip transmission line at the edge of the antenna patch.

For electrically thin microstrip antennas, the internal fields are approximately independent of z . Actually, for the frequencies of interest, all z dependent parallel plate waveguide modes are well below their cutoff frequencies and are negligible everywhere except very near the feed and patch edge. Also, the electric field must be z directed within the ideal cavity.

There are many representations for the field in the cavity [10]. In this thesis, two convenient ones are chosen in which the electric field is expanded in terms of single or double infinite series of "modes."

(1) Representation by Expansion in Resonant Modes:

This expansion converges slowly but gives more physical insight for the antenna excited near a resonant frequency.

(2) Representation by Modal Matching:

This expansion converges faster than the former. It will be used for actual computation to save computer time.

Within the cavity, the fields have to satisfy the boundary conditions and the vector Helmholtz equation. For the resonant mode

expansion, it is required that each mode term satisfies the boundary conditions, and the total field (i.e., a double infinite series of modes) satisfies the inhomogeneous Helmholtz equation. On the other hand, using mode matching, each term of the series satisfies the source free Helmholtz equation and the boundary conditions in their respective source-free regions. The sum of these modes is then used to match to the source.

To find the electric field, \vec{E} , and the magnetic field, \vec{H} , we must find the Green's function of cavity. We have:

$$\nabla \times \vec{E} = -j\omega\mu\vec{H} \quad (2.2.1)$$

$$\nabla \times \vec{H} = j\omega\epsilon\vec{E} + \hat{z}\delta(\phi - \phi_f)/\delta(\rho - \rho_f)/\rho_f \quad (2.2.2)$$

$$\hat{n} \times \vec{H} = 0 \quad \text{on the magnetic wall} \quad (2.2.3)$$

$$\hat{n} \times \vec{E} = 0 \quad \text{on the electric wall} \quad (2.2.4)$$

The last term of 2.2.2 represents a z directed, uniform, filamentary unit current flowing from the ground plane to the patch. A z independent field solution is sought.

Let $\vec{E} = \hat{z} E(\rho, \phi)$. Thus,

$$\nabla \times \vec{E} = \nabla \vec{E} \times \hat{z} \quad (2.2.5)$$

and

$$\nabla \times \nabla \times \vec{E} = k^2 E \hat{z} - j\omega\mu \hat{z} \delta(\rho - \rho_f) \delta(\phi - \phi_f)/\rho_f = -\hat{z} \nabla^2 E$$

$$\nabla^2 E + k^2 E = j\omega\mu \delta(\rho - \rho_f) \delta(\phi - \phi_f)/\rho_f \quad (2.2.6)$$

where $k = \omega\sqrt{\mu\epsilon}$ is the wavenumber of the dielectric.

This differential equation can now be solved for a variety of cavity shapes.

2-2-1 The Internal Fields of the Annular Antenna Element

For the annular antenna, the boundary conditions are

$$H_\phi(a, \phi) = H_\phi(b, \phi) = 0 \quad ,$$

where a and b are the inner and the outer radius, respectively.

(A) Resonant mode expansion method

For this method, we first solve the homogeneous equation

$$\nabla^2 \psi_{mn} + k_{mn}^2 \psi_{mn} = 0 \quad , \quad (2.2.7)$$

where ψ_{mn} is a function of ρ, ϕ . A solution to this equation, subject to the continuity condition that

$$\psi_{mn}(\rho, 0) = \psi_{mn}(\rho, 2\pi) \quad ,$$

is

$$\psi_{mn} = g_2 [J_n(k_{mn}\rho) + g_1 N_n(k_{mn}\rho)] \cos(n\phi) \quad , \quad (2.2.8)$$

where $J_n(x)$ is the Bessel function of the first kind and $N_n(x)$ is the Neumann function (or Bessel function of the second kind). Here g_1 is a constant to be determined by one of the boundary conditions and g_2 is an arbitrary constant. Let $E_{zmn} = A_{mn} \psi_{mn}$. Then the corresponding magnetic field, \vec{H}_{mn} , is

$$\vec{H}_{mn} = A_{mn} \frac{1}{\omega\mu} \left(\hat{\rho} \frac{1}{\rho} \frac{\partial \psi_{mn}}{\partial \phi} - \hat{\phi} \frac{\partial \psi_{mn}}{\partial \rho} \right) \quad (2.2.9)$$

If we require H_{mn} to satisfy the PMC boundary conditions, then,

$$\frac{\partial \psi_{mn}(a, \phi)}{\partial \rho} = \frac{\partial \psi_{mn}(b, \phi)}{\partial \rho} = 0 \quad (2.2.10)$$

This implies that

$$-k_{mn} (J'_n(k_{mn} a) + g_1 N'_n(k_{mn} a)) = 0 \quad (2.2.11)$$

or

$$g_1 = -\frac{J'_n(k_{mn} a)}{N'_n(k_{mn} a)} \quad \text{or} \quad k_{mn} = 0 \quad .$$

Applying the condition at $\rho = b$,

$$J'_n(k_{mn} b) - N'_n(k_{mn} b) \frac{J'_n(k_{mn} a)}{N'_n(k_{mn} a)} = 0 \quad (2.2.13)$$

$$N'_n(k_{mn} a) J'_n(k_{mn} b) - N'_n(k_{mn} b) J'_n(k_{mn} a) = 0 \quad . \quad (2.2.14)$$

Thus, either k_{mn} is zero, or k_{mn} is a root of equation 2.2.14. A computer program has been developed to find the roots of this equation. Some of the roots are listed in table 2-1. For convenience, let $g_2 = N'_n(k_{mn} a)$. Thus, electric field is

$$E = \sum_{m,n=0}^{\infty} A_{mn} \psi_{mn} \quad ;$$

$$\psi_{mn} = N'_n(k_{mn} a) J_n(k_{mn} \rho) - J'_n(k_{mn} a) N_n(k_{mn} \rho) \quad .$$

Requiring the total field to satisfy the inhomogeneous wave equation yields

$$j\omega\mu\delta(\rho - \rho_f) \delta(\phi)/\rho_f = (\nabla^2 + k^2) \sum_{m,n=0}^{\infty} A_{mn} \psi_{mn} = \sum_{m,n=0}^{\infty} A_{mn} (k^2 - k_{mn}^2) \quad (2.2.15)$$

TABLE 2-1: The roots of $J'_\nu(\lambda x)N'_\nu(x) - J'_\nu(x)N'_\nu(\lambda x) = 0$
 where $\nu=n$ for annulus and $\nu=p\pi/\phi$ for annular sector

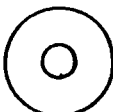
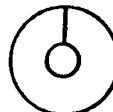
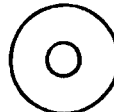


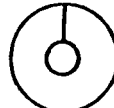


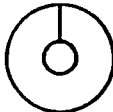
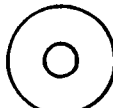
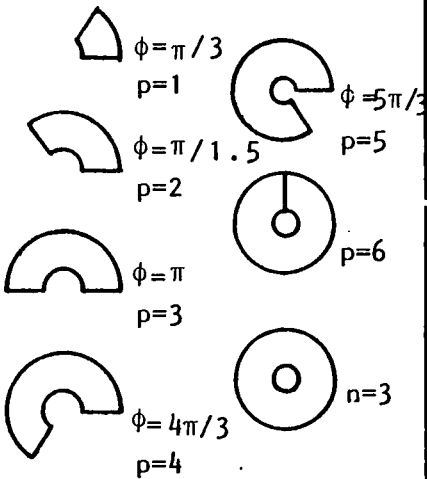
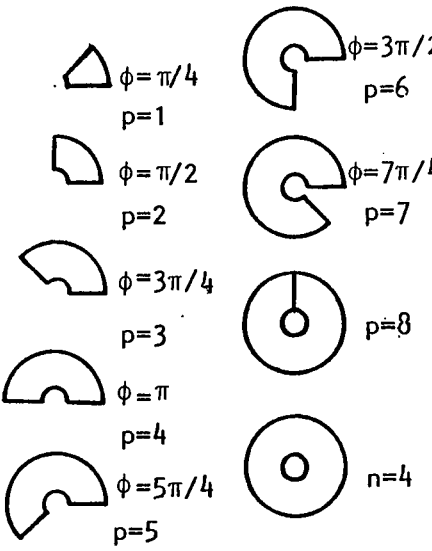
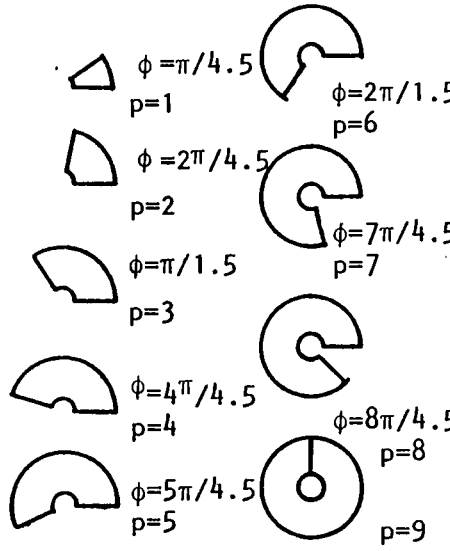
	$m \backslash \nu$	 n=0	 p=1	 n=1	 $\phi = 2\pi/3$ p=1	 $\phi = \pi/2$ p=1
		 p=2	 $\phi = \pi/3$ p=2	 $\phi = 3\pi/2$ p=3	 p=4	 n=2
		0	0.5	1	1.5	2
$\lambda = 2$	1	0	0.33958	0.67733	1.01150	1.34060
	2	3.19657	3.21820	3.28247	3.38796	3.53129
	3	6.31231	6.32257	6.35321	6.40403	6.47471
	4	9.44442	9.45119	9.47133	9.50433	9.55158
$\lambda = 2.5$	1	0	0.29463	0.58471	0.86636	1.13695
	2	2.15645	2.18356	2.26364	2.39312	2.56640
	3	4.22309	4.23567	4.27330	4.33569	4.42238
	4	6.30657	6.31474	6.33923	6.37992	6.43665
$\lambda = 3$	1	0	0.26067	0.51362	0.75321	0.97743
	2	1.63561	1.66669	1.75776	1.90238	2.09009
	3	3.17884	3.19318	3.23611	3.30738	3.40667
	4	4.73809	4.74730	4.77493	4.82089	4.88506

TABLE 2-1 : Continued

	$m \setminus \nu$			
		3	4	4.5
$\lambda = 2$	1	1.97888	2.58761	2.88152
	2	3.92005	4.41822	4.69302
	3	6.67380	6.94614	7.10825
	4	9.68421	9.86768	9.97786
$\lambda = 2.5$	1	1.64327	2.11284	2.33839
	2	3.01411	3.54103	3.81551
	3	4.66643	5.00039	5.19909
	4	6.59744	6.81965	6.95321
$\lambda = 3$	1	1.38803	1.76922	1.95449
	2	2.54219	3.01972	3.25069
	3	3.68720	4.06812	4.28321
	4	5.06762	5.32232	5.47692

(Since the annulus has rotational symmetry, the source is taken to be at $(\rho_f, \phi_f = 0)$.)

To determine the A_{mn} , the orthogonality of ψ_{mn} is used. We write

$$\begin{aligned} j\omega\mu \int_{\phi} \int_{\rho} \frac{\delta(\rho - \rho_f) \delta(\phi)}{\rho} \psi_{pq} \rho d\rho d\phi \\ = \sum_{m,n=0}^{\infty} A_{mn} (k^2 - k_{mn}^2) \int_{\rho} \int_{\phi} \psi_{mn} \psi_{pq} \rho d\rho d\phi \end{aligned} \quad (2.2.16)$$

Using the orthogonality of $\cos(n\phi)$, and the identity [8],

$$\begin{aligned} \int_a^b U_n(k_{mn}\rho) U_n(k_{pn}\rho) \rho d\rho \\ = \begin{cases} 0 & k_{mn} \neq k_{pn} \\ \frac{\rho}{2} \left\{ [U_n(k_{mn}\rho)]^2 + \left(1 - \frac{n^2}{(k_{mn}\rho)^2}\right) [U'_n(k_{mn}\rho)]^2 \right\} & k_{mn} = k_{pn} \end{cases} \end{aligned} \quad (2.2.17)$$

(where U_n is any linear combination of J_n and N_n), we have

$$\begin{aligned} \int_{\rho} \int_{\phi} \psi_{mn} \psi_{pn} \rho d\rho d\phi \\ = \begin{cases} 0 & m \neq p \\ \pi(1 + \delta_{on}) D & m = p \end{cases} \end{aligned} \quad (2.2.18)$$

$$\text{where } D = \frac{2}{\pi^2 k_{nm}^2} \left\{ \left(1 - \frac{n^2}{k_{mn}^2 b^2}\right) \left(\frac{J'_n(k_{mn}a)}{J'_n(k_{mn}b)}\right)^2 - 1 + \frac{n^2}{k_{mn}^2 a^2} \right\} ; \quad (2.2.19)$$

δ_{mn} is the Kronecker delta. Therefore, we find that

$$A_{mn} = \frac{j\omega\mu [N'_n(k_{mn}a) J_n(k_{mn}\rho_f) - J'_n(k_{mn}a) N_n(k_{mn}\rho_f)]}{(k^2 - k_{mn}^2) \pi(1 + \delta_{on}) D}, \quad (2.2.20)$$

and

$$E_z = \sum_{m,n=0}^{\infty} A_{mn} [N'_n(k_{mn}a) J_n(k_{mn}\rho) - J'_n(k_{mn}a) N_n(k_{mn}\rho)] \quad . \quad (2.2.21)$$

(B) Mode matching method

In this approach, the antenna structure is divided into two parts, $a < \rho < \rho_f$ for region II and $\rho_f < \rho < b$ for region I. We need to solve the homogeneous equation in each source-free region. That is, we must solve

$$\nabla^2 \psi_m + k^2 \psi_m = 0 \quad . \quad (2.2.22)$$

In region I, assume

$$E_{z1} = \sum_{m=0}^{\infty} \{A_m J_m(k\rho) + B_m N_m(k\rho)\} \cos(m\phi) \quad . \quad (2.2.23)$$

From equation 2.2.9, we have

$$H_{\phi 1} = -j/\omega\mu \partial E_{z1} / \partial \rho \quad . \quad (2.2.24)$$

From the orthogonality of $\cos(m\phi)$ and the boundary condition $H_{\phi}(b, \phi) = 0$, we have

$$\{A_m J'_m(kb) + B_m N'_m(kb)\} = 0 \quad . \quad (2.2.25)$$

In region II, assume

$$E_{z2} = \sum_{m=0}^{\infty} \{C_m J_m(k\rho) + D_m N_m(k\rho)\} \cos(m\phi) \quad . \quad (2.2.26)$$

Similarly, $H_{\phi}(a, \phi) = 0$ implies

$$\{C_m J'_m(ka) + D_m N'_m(ka)\} = 0 \quad . \quad (2.2.27)$$

The source can be expressed as

$$\vec{J} = \hat{z} \delta(\phi) \delta(\rho - \rho_f) / \rho_f \quad (2.2.28)$$

Since E_z has to be continuous at $\rho = \rho_f$, we have

$$A_m J_m(k\rho_f) + B_m N_m(k\rho_f) = C_m J_m(k\rho_f) + D_m N_m(k\rho_f) \quad (2.2.29)$$

Around the source, $H_{\phi 1} - H_{\phi 2} = \frac{\delta(\phi)}{\rho_f}$. This implies that

$$\begin{aligned} \sum_{m=0}^{\infty} [-jk/\omega\mu (A_m J'_m(k\rho_f) + B_m N'_m(k\rho_f)) \\ + jk/\omega\mu (C_m J'_m(k\rho_f) + D_m N'_m(k\rho_f))] \cos(m\phi) = \frac{\delta(\phi)}{\rho_f} \end{aligned} \quad (2.2.30)$$

Using the identity

$$\delta(\phi) = \frac{1}{\pi} \sum_{m=0}^{\infty} \frac{\cos(m\phi)}{1 + \delta_{m0}} \quad (2.2.31)$$

We have

$$\begin{aligned} \frac{jk}{\omega\mu} [(C_m - A_m) J'_m(k\rho_f) + (D_m - B_m) N'_m(k\rho_f)] \\ = \frac{1}{\pi\rho_f(1 + \delta_{m0})} \end{aligned} \quad (2.2.32)$$

We have four equations (2.2.25, 2.2.27, 2.2.29, and 2.2.32) in four unknowns (A_m, B_m, C_m, D_m). Solving these equations, we find that

$$A_m = \frac{-j\omega\mu}{2(1 + \delta_{om})\Delta_m} N'_m(kb) [J_m(k\rho_f) N'_m(ka) - J'_m(ka) N_m(k\rho_f)] \quad (2.2.33)$$

$$B_m = \frac{j\omega\mu}{2(1 + \delta_{om})\Delta_m} J'_m(kb) [J_m(k\rho_f) N'_m(ka) - J'_m(ka) N_m(k\rho_f)] \quad (2.2.34)$$

$$C_m = \frac{j\omega\mu J'_m(ka)}{2(1 + \delta_{om})\Delta_m} [J_m(k\rho_f) N'_m(kb) - J'_m(kb) N_m(k\rho_f)] \quad (2.2.35)$$

$$\Delta_m = \frac{j\omega\mu J'_m(ka)}{2(1 + \delta_{om})\Delta_m} [J_m(k\rho_f) N'_m(kb) - J'_m(kb) N_m(k\rho_f)] \quad (2.2.36)$$

Here

$$\Delta_m = J'_m(kb) N'_m(ka) - N'_m(kb) J'_m(ka) \quad (2.2.37)$$

Compare this to the characteristic equation for the resonant mode expansion method (2.2.14). If k approaches a zero of Δ , then the demoninators of A_m , B_m , C_m , and D_m approach zero, and the internal fields go to infinity. Under this condition, the cavity is at resonance. This result is, of course, consistent with the results of the equivalent cavity mode expansion method.

These four sets of coefficient equations, 2.2.23, and 2.2.26, can be used to find the electric field everywhere in the cavity, due to a point source.

The resonant mode expansion, equation (2.2.21), is a double summation while the mode matching expressions (2.2.23), (2.2.26), yield single summations. The latter technique is computationally faster than the former.

2-2-2 The Internal Field of Annular Sector Antenna

This kind of antenna is like the case in section 2-2-1 except that we must use fractional order Bessel functions. The boundary conditions which must be satisfied are

$$\begin{cases} H_\rho = 0 & \text{at } \phi = 0, \phi_0 \\ H_\phi = 0 & \text{at } \rho = a, b \end{cases}$$

(A) Resonant mode expansion

Similar to what was done in section 2-2-1, we can write

$$\psi_{mp} = [N'_{\nu_p}(k_{mv}a) J_{\nu_p}(k_{mv}\rho) - J'_{\nu_p}(k_{mv}a) N_{\nu_p}(k_{mv}\rho)] \cos(\nu_p\phi) \quad (2.2.38)$$

$$\cos(\nu_p\phi)$$

where $p = 0, 1, 2, \dots$ and ν_p are determined from the boundary conditions.

The boundary conditions at $\phi = 0$ and $\phi = \phi_0$ requires that $\nu_p = \frac{p\pi}{\phi_0}$.

Write

$$E_z = \sum_{m,p=0}^{\infty} A_{mp} \psi_{mp} \quad (2.2.39)$$

Requiring the total field to satisfy the inhomogeneous wave equation gives

$$j\omega\mu\delta(\rho - \rho_f) \delta(\phi - \phi_f)/\rho_f = \sum_{m,p=0}^{\infty} (k^2 - k_{mv}^2) A_{mp} \psi_{mp} \quad (2.2.40)$$

By the same procedure as in section 2-2-1, we have

$$\begin{aligned} & j\omega\mu [N'_{\nu}(k_{mv}a) J_{\nu}(k_{mv}\rho_f) - J'_{\nu}(k_{mv}a) N_{\nu}(k_{mv}\rho_f)] \cos(\nu\phi_f) \\ & - (k^2 - k_{mv}^2) A_{mp} \frac{(1 + \delta_{op})}{2} \phi_0 \cdot D \end{aligned} \quad (2.2.41)$$

where

$$D = \frac{2}{\pi^2 k_{mv}^2} \left\{ \left(1 - \frac{\nu^2}{k_{mv}^2 b^2} \right) \left(\frac{J'_1(k_{mv}a)}{J'_1(k_{mv}b)} \right)^2 - 1 + \frac{\nu^2}{k_{mv}^2 a^2} \right\},$$

$$A_{mn} = \frac{2j\omega\mu [N'_v(k_{mv}a)J_v(k_{mv}\rho_f) - J'_v(k_{mv}a)N_v(k_{mv}\rho_f)]}{(k^2 - k_{mv}^2)(1 + \delta_{op})\phi_0^D} \cos(v\phi_f) , \quad (2.2.42)$$

and the subscript, p , of v_p has been omitted for convenience.

(B) Mode matching method

The antenna structure is divided into two parts as in figure 2-2.

Let

$$E_{z1} = \sum_{p=0}^{\infty} \{A_p J_v(k\rho) + B_p N_v(k\rho)\} \cos(v\phi) , \quad (2.2.43)$$

$$E_{z2} = \sum_{p=0}^{\infty} \{C_p J_v(k\rho) + D_p N_v(k\rho)\} \cos(v\phi) . \quad (2.2.44)$$

The source current is

$$\vec{J} = \hat{z} \delta(\rho - \rho_f) \delta(\phi - \phi_f) / \rho_f . \quad (2.2.45)$$

It follows that

$$H_{\rho 1} = \frac{-j}{\omega\mu\rho} \sum_{p=0}^{\infty} v [A_p J_v(k\rho) + B_p N_v(k\rho)] \sin(v\phi) , \quad (2.2.46)$$

$$H_{\phi 1} = \frac{-jk}{\omega\mu} \sum_{p=0}^{\infty} [A_p J'_v(k\rho) + B_p N'_v(k\rho)] \cos(v\phi) , \quad (2.2.47)$$

$$H_{\rho 2} = \frac{-j}{\omega\mu\rho} \sum_{p=0}^{\infty} v [C_p J_v(k\rho) + D_p N_v(k\rho)] \sin(v\phi) , \quad (2.2.48)$$

$$H_{\phi 2} = \frac{-jk}{\omega\mu} \sum_{p=0}^{\infty} [C_p J'_v(k\rho) + D_p N'_v(k\rho)] \cos(v\phi) . \quad (2.2.49)$$

Applying the boundary condition,

$$H_{\rho 1} = H_{\rho 2} = 0 \quad \text{at } \phi = 0, \phi_0 ,$$

we find that

$$v_p = p\pi/\phi_0 \quad .$$

We have four other conditions that must be satisfied:

$$\begin{aligned} H_{\phi 1} &= 0 & \text{at } \rho &= b \quad , \\ H_{\phi 2} &= 0 & \text{at } \rho &= a \quad , \\ E_{z1} &= E_{z2} & \text{at } \rho &= \rho_f \quad , \\ H_{\phi 1} - H_{\phi 2} &= \delta(\phi - \phi_f)/\rho_f & \text{at } \rho &= \rho_f \quad . \end{aligned} \tag{2.2.50}$$

Using the identity

$$\delta(\phi - \phi_f) = \frac{2}{(1 + \delta_{op})\phi_0} \sum_{p=0}^{\infty} \cos(v\phi) \cos(v\phi_f) \quad , \tag{2.2.51}$$

we have the equations

$$A_p J'_v(k\rho) + B_p N'_v(k\rho) = 0 \quad , \tag{2.2.52}$$

$$C_p J'_v(k\rho) + D_p N'_v(k\rho) = 0 \quad , \tag{2.2.53}$$

$$A_p J_v(k\rho_f) + B_p N_v(k\rho_f) - C_p J_v(k\rho_f) - D_p N_v(k\rho_f) = 0 \quad , \tag{2.2.54}$$

$$\begin{aligned} &A_p J'_v(k\rho_f) + B_p N'_v(k\rho_f) - C_p J'_v(k\rho_f) - D_p N'_v(k\rho_f) \quad , \\ &= \frac{j\omega\mu}{k} \frac{2\cos(v\phi_f)}{(1 + \delta_{op})\phi_0\rho_f} \quad . \end{aligned}$$

Solving, we find these four sets of coefficients:

$$A_p = \frac{-j\omega\mu\pi\cos(v\phi_f)}{(1 + \delta_{op})\phi_0\Delta_p} N'_v(kb) [J_v(k\rho_f)N'_v(ka) - J'_v(ka) N_v(k\rho_f)] , \quad (2.2.56)$$

$$B_p = \frac{j\omega\mu\pi\cos(v\phi_f)}{(1 + \delta_{op})\phi_0\Delta_p} J'_v(kb) [J_v(k\rho_f) N'_v(ka) - J'_v(ka) N_v(k\rho_f)] , \quad (2.2.57)$$

$$C_p = \frac{-j\omega\mu\pi\cos(v\phi_f)}{(1 + \delta_{op})\phi_0\Delta_p} N'_v(ka) [N'_v(kb) J_v(k\rho_f) - J'_v(kb) N_v(k\rho_f)] , \quad (2.2.58)$$

$$D_p = \frac{j\omega\mu\pi\cos(v\phi_f)}{(1 + \delta_{op})\phi_0\Delta_p} J'_v(ka) [N'_v(kb) J_v(k\rho_f) - J'_v(kb) N_v(k\rho_f)] , \quad (2.2.60)$$

where

$$\Delta_p = J'_v(kb) N'_v(ka) - N'_v(kb) J'_v(ka) .$$

Using these four parameters, the internal fields can be found easily everywhere in the cavity by equations 2.2.43 and 2.2.44.

2-2-3 The Internal Fields of Circular Sector

The structure is pictured in figure 2-3. The boundary condition is

$$\begin{cases} H_\rho = 0 & \text{at } \phi = 0, \phi_0 \\ H_\phi = 0 & \text{at } \rho = a \end{cases} .$$

(A) Resonant mode expansion

We can still assume that the E_z is a function of ρ and ϕ only. Again, the differential equation is

$$\nabla^2 \psi_{mp} + k_{mv}^2 \psi_{mp} = 0 \quad , \quad (2.2.61)$$

$$\psi_{mp} = J_v(k_{mv}\rho) \cos(v\phi) \quad .$$

Here we do not have the term of $N_n(k_{mv}\rho)$ because the fields must be finite at $\rho = 0$.

Let

$$E_z = \sum_{m,p=0}^{\infty} A_{mp} \psi_{mp} \quad . \quad (2.2.62)$$

Since

$$H_{\rho mp} = 0 \quad \text{at } \phi = 0, \phi_0 \quad ,$$

and

$$H_{\rho mp} = -1/\rho J'_v(k_{mv}\rho) \cos(v\phi) = 0 \quad \text{for } \phi = \phi_0 \quad , \quad (2.2.63)$$

then

$$v_p = p\pi/\phi_0 \quad p = 1, 2, 3, \dots \quad . \quad (2.2.64)$$

The condition $H_\phi = 0$ at $\rho = a$ implies

$$k_{mv}(J'_v(k_{mv}a)) = 0 \quad ,$$

whence

$$k_{mv} = 0 \quad \text{or} \quad k_{mv} = \chi'_{mv}/a \quad , \quad (2.2.65)$$

where χ'_{mv} are the roots of $J'_v(x) = 0$.

A computer program has been written and some numerical values of χ_{mv} are listed in table 2-2.

Requiring the total field to satisfy the inhomogeneous wave equation, and assuming the source is

$$j\omega\mu\delta(\rho - \rho_f) \delta(\phi - \phi_f)/\rho \quad , \quad (2.2.66)$$

TABLE 2-2 : The roots of $J'_\nu(x) = 0$, where $\nu=n$ for circular disk and $\nu=p\pi/\phi$ for circular sector

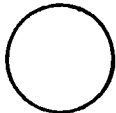
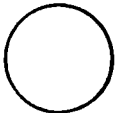
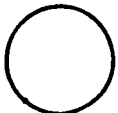
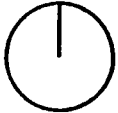



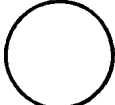
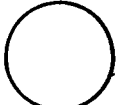














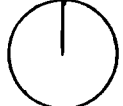
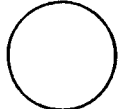






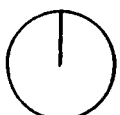







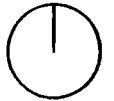
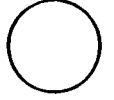









	 n=0	 p=1	 n=1  p=2  p=1	 $\phi=2\pi/3$ p=1  $\phi=4\pi/3$ p=2  p=3	 n=2  $\phi=\pi/2$ p=1  p=2  $\phi=3\pi/2$ p=3  p=4	 $\phi=\pi/2.5$ p=1  $\phi=2\pi/2.5$ p=2  $\phi=3\pi/2.5$ p=3  $\phi=4\pi/2.5$ p=4  p=5
m \ ν	0	0.5	1	1.5	2	2.5
1	0	1.16556	1.84113	2.46053	3.05424	3.63280
2	3.83170	4.60422	5.33143	6.02929	6.70612	7.36701
3	7.01559	7.78989	8.53631	9.26139	9.96946	10.66356
4	10.17347	10.94994	11.70601	12.44526	13.17037	13.88336

TABLE 2-2: Continued

	 $\phi=\pi/3$ $p=1$  $\phi=2\pi/3$ $p=2$  $p=3$  $\phi=4\pi/3$ $p=4$  $\phi=5\pi/3$ $p=5$  $p=6$  $n=3$	 $\phi=\pi/3.5$ $p=1$  $\phi=2\pi/3.5$ $p=2$  $\phi=3\pi/3.5$ $p=3$  $\phi=4\pi/3.5$ $p=4$  $\phi=5\pi/3.5$ $p=5$  $\phi=6\pi/3.5$ $p=6$  $p=7$	 $\phi=\pi/4$ $p=1$  $\phi=\pi/2$ $p=2$  $\phi=3\pi/4$ $p=3$  $p=4$  $\phi=5\pi/4$ $p=5$  $\phi=3\pi/2$ $p=6$  $\phi=7\pi/4$ $p=7$  $p=8$  $n=4$	 $\phi=\pi/4.5$ $p=1$  $\phi=2\pi/4.5$ $p=2$  $\phi=3\pi/4.5$ $p=3$  $\phi=4\pi/4.5$ $p=4$  $\phi=5\pi/4.5$ $p=5$  $\phi=6\pi/4.5$ $p=6$  $\phi=7\pi/4.5$ $p=7$  $\phi=8\pi/4.5$ $p=8$  $p=9$
$m \backslash v$	3	3.5	4	4.5
1	4.20119	4.76219	5.31754	5.86841
2	8.01523	8.65312	9.28239	9.90430
3	11.34529	12.01825	12.68191	13.33792
4	14.58585	15.27907	15.96410	16.64179

(a unit current feeding the antenna at (ρ_f, ϕ_f)), we have

$$j\omega\mu\delta(\rho - \rho_f) \delta(\phi - \phi_f)/\rho_f = \sum_{m,p=0}^{\infty} (k^2 - k_{mv}^2) A_{mp} \psi_{mp} \quad (2.2.67)$$

By the same procedure as in section 2-2-1, we get

$$A_{mp} = \frac{4j\omega\mu J_v(k_{mv}\rho_f) \cos(v\phi_f)}{(k^2 - k_{mv}^2)(1 + \delta_{op})\phi_0 J_v^2(k_{mv}a)(a^2 - \frac{v^2}{k_{mv}^2 a^2})} \quad (2.2.68)$$

(B) Mode matching method

We divide the antenna into two parts, $\rho_f < \rho < a$ for region I and $0 < \rho < \rho_f$ for region II.

The electric field in region I can be written as

$$E_{z1} = \sum_{p=0}^{\infty} [A_v J_v(k\rho) + B_v N_v(k\rho)] \cos(v\phi) \quad (2.2.69)$$

Also,

$$H_{\rho 1} = \frac{-j}{\omega\mu\rho} \sum_{p=0}^{\infty} [A_v J_v(k\rho) + B_v N_v(k\rho)] \sin(v\phi) \quad (2.2.70)$$

and

$$H_{\phi 1} = \frac{-jk}{\omega\mu} \sum_{p=0}^{\infty} [A_v J'_v(k\rho) + B_v N'_v(k\rho)] \cos(v\phi) \quad (2.2.71)$$

Similarly, we can write E and H in region II as

$$E_{z2} = \sum_{p=0}^{\infty} C_p J_v(k\rho) \cos(v\phi) \quad ; \quad (2.2.72)$$

$$H_{\rho 2} = \frac{-j}{\omega\mu\rho} \sum_{p=0}^{\infty} v C_p J_v(k\rho) \sin(v\phi) \quad ; \quad (2.2.73)$$

$$H_{\phi 2} = \frac{-jk}{\omega\mu} \sum_{p=0}^{\infty} C_p J'_v(k\rho) \cos(v\phi) \quad . \quad (2.2.74)$$

From the boundary and continuity conditions

$$\begin{cases} H_\phi = 0 & \text{at } \rho = a \\ E_{z1} = E_{z2} & \text{at } \rho = \rho_f \\ H_{\phi1} - H_{\phi2} = \hat{z} \delta(\phi - \phi_f) / \rho_f \end{cases} \quad (2.2.75)$$

and the identity 2.2.51, we have three equations:

$$A_p J'_\nu(ka) + B_p N'_\nu(ka) = 0 \quad ; \quad (2.2.76)$$

$$A_p J_\nu(k\rho_f) + B_p N_\nu(k\rho_f) - C_p J_\nu(k\rho_f) = 0 \quad ; \quad (2.2.77)$$

$$A_p J'_\nu(k\rho_f) + B_p N'_\nu(k\rho_f) - C_p J'_\nu(k\rho_f) = \frac{2\cos(\nu\phi_f) j\omega\mu}{\rho_f k \phi_0 (1 + \delta_{op})} \quad (2.2.78)$$

Solving, we get

$$A_p = \frac{-j\omega\mu\pi}{(1 + \delta_{op})\phi_0} \cos(\nu\phi_f) \frac{N'_\nu(ka)}{J'_\nu(ka)} J_\nu(k\rho_f) \quad ; \quad (2.2.79)$$

$$B_p = \frac{j\omega\mu\rho}{(1 + \delta_{op})\phi_0} \cos(\nu\phi_f) J_\nu(k\rho_f) \quad ; \quad (2.2.80)$$

$$C_p = \frac{j\omega\mu\pi}{(1 + \delta_{op})\phi_0} \cos(\nu\phi_f) \left[N_\nu(k\rho_f) - \frac{J_\nu(k\rho_f)}{J'_\nu(ka)} N'_\nu(ka) \right] . \quad (2.2.81)$$

By equations 2.2.69, 72, 79, 80, 82, the internal fields can be determined everywhere. Again, if k is the zero of $J'_\nu(ka)$, the internal fields will go to infinity.

2-3 The Electric and Magnetic Stored Energy

To find the quality factor needed to accurately analyze the antenna, we must estimate the energy stored in the fields generated by the antenna. The time average electric stored energy, W_e , is

$$W_e = \frac{\epsilon}{2} \int_v |E|^2 dv \quad (2.3.1)$$

and the time average magnetic stored energy, W_m , is given by

$$W_m = \frac{\mu}{2} \int_v |H|^2 dv \quad (2.3.2)$$

where v is the volume between the patch and the ground plane. But

$$\vec{H} = \frac{1}{j\omega\mu_0} \nabla E \times \hat{z} \quad ,$$

so that $\vec{H} \cdot \vec{H}^*$ is

$$\vec{H} \cdot \vec{H}^* = \frac{1}{(k_0\eta_0)^2} |\nabla E \times \hat{z}|^2 = \frac{1}{(k_0\eta_0)^2} |\nabla E|^2$$

Therefore,

$$W_m = \frac{\mu}{2(k_0\eta_0)^2} \int_v |\nabla E|^2 dv \quad (2.3.3)$$

2-3-1 Annulus Microstrip Antenna

From equations 2.2.23 and 2.2.26,

$$E_{z1} = \sum_{m=0}^{\infty} \{A_m J_m(k\rho) + B_m N_m(k\rho)\} \cos(m\phi) \quad , \quad (2.3.4)$$

$$E_{z2} = \sum_{m=0}^{\infty} \{ C_m J_m(k\rho) + D_m N_m(k\rho) \} \cos(m\phi) \quad . \quad (2.3.5)$$

Let

$$A_m J_m(k\rho) + B_m N_m(k\rho) = P_m(k\rho) \quad ,$$

$$C_m J_m(k\rho) + D_m N_m(k\rho) = O_m(k\rho) \quad . \quad (2.3.6)$$

Then,

$$W_e = \frac{\varepsilon t}{2} \sum_{m=0}^{\infty} \sum_{n=0}^{\infty} \left\{ \int_a^{\rho_f} O_m(k\rho) O_n^*(k\rho) \rho d\rho \right. \\ \left. + \int_{\rho_f}^b P_m P_n^* \rho d\rho \right\} \int_0^{2\pi} \cos(m\phi) \cos(n\phi) d\phi \quad .$$

From the orthogonality of $\cos(m\phi)$, we have

$$W_e = \frac{\varepsilon t \pi}{2} \sum_{m=0}^{\infty} (1 + \delta_{om}) \left[\int_a^{\rho_f} |O_m|^2 \rho d\rho + \int_{\rho_f}^b |P_m|^2 \rho d\rho \right] \quad (2.3.7)$$

This equation can be integrated in closed form by using equation 2.2.17.

Performing the integration, we have

$$W_e = \frac{\omega^2 \varepsilon t \pi \mu^2}{8} \sum_{m=0}^{\infty} \frac{1}{(1 + \delta_{om}) \Delta_m^2} \left\{ \frac{2}{\pi^2 k^2} \left[1 - \frac{m^2}{(kb)^2} \right] \cdot [J_m(k\rho_f) N_m'(ka) \right. \\ - J_m'(ka) N_m(k\rho_f)]^2 - \frac{2}{\pi^2 k^2} \left[1 - \frac{m^2}{(ka)^2} \right] \cdot [J_m(k\rho_f) N_m'(kb) \\ - J_m'(kb) N_m(k\rho_f)]^2 + \frac{\rho_f^2}{2} \left[[N_m'(kb) J_m(k\rho_f) - J_m'(kb) N_m(k\rho_f)]^2 \right. \\ \cdot [N_m'(ka) J_m(k\rho_f) - J_m'(ka) N_m(k\rho_f)]^2 - [J_m(k\rho_f) N_m'(ka) \\ - J_m'(ka) N_m(k\rho_f)]^2 [J_m(k\rho_f) N_m'(kb) - J_m'(kb) N_m(k\rho_f)]^2 \Big\} \quad (2.3.8)$$

where Δ_m is defined in equation (2.2.37).

2-3-2 Annular Sector Microstrip Antenna

Similar to section 2-3-1, by using the equations 2.2.43 and 2.2.44, we get

$$\begin{aligned}
 W_e = \frac{\epsilon t}{4} \sum_{p=0}^{\infty} \frac{\omega^2 \mu^2 \pi^2 \cos^2(v\phi_f)}{(1 + \delta_{op}) \phi_0 \Delta_p^2} & \left\{ \frac{2(1 - v^2/(kb)^2)}{\pi^2 k^2} [J_v(k\rho_f) N'_v(ka) \right. \\
 & - J'_v(ka) N_v(k\rho_f)]^2 - \frac{2}{\pi^2 k^2} \left[1 - \frac{v^2}{(ka)^2} \right] \\
 & \cdot [J_v(k\rho_f) N'_v(kb) - J'_v(kb) N_v(k\rho_f)]^2 + \frac{\rho_f^2}{2} ([N'_v(kb) J_v(k\rho_f) \\
 & - J'_v(kb) N_v(k\rho_f)]^2 [N'_v(ka) J'_v(k\rho_f) - J'_v(ka) N'_v(k\rho_f)]^2 \\
 & - [J_v(k\rho_f) N'_v(ka) - J'_v(ka) N_v(k\rho_f)]^2 \cdot [J'_v(k\rho_f) N'_v(kb) \\
 & \left. - J'_v(kb) N'_v(k\rho_f)]^2 \right\} \quad (2.3.9)
 \end{aligned}$$

where Δ_p is given by equation (2.2.60).

2-3-3 Circular Sector Microstrip Antenna

From equations 2.2.69 and 2.2.72,

$$E_{z1} = \sum_{p=0}^{\infty} [A_p J_v(k\rho) + B_p N_v(k\rho)] \cos(v\phi) \quad ,$$

$$E_{z2} = \sum_{p=0}^{\infty} C_p J_v(k\rho) \quad .$$

Let

$$P_p(k\rho) = A_p J_v(k\rho) + B_p N_v(k\rho) \quad , \quad (2.3.10)$$

$$O_p(k\rho) = C_p J_v(k\rho) \quad . \quad (2.3.11)$$

From equation 2.3.6, we have

$$W_e = \frac{\epsilon t}{2} \frac{\phi_0}{2} \sum_{p=0}^{\infty} (1 + \delta_{op}) \left(\int_0^{\rho_f} |O_p|^2 \rho d\rho + \int_{\rho_f}^a |P_p|^2 \rho d\rho \right) \quad . \quad (2.3.12)$$

Performing the integration by using the identity 2.2.17

$$W_e = \frac{\epsilon t \omega^2 \mu^2 \pi^2 \rho_f^2 a^2}{8\phi_0} \sum_{p=0}^{\infty} \frac{1}{(1 + \delta_{op})} \left(1 - \frac{v^2}{(ka)^2} \right) \cdot \left(J_v(k\rho_f) N'_v(ka) - \frac{N'_v(ka)}{N'_v(ka)} J_v(k\rho_f) J_v(ka) \right)^2 \quad . \quad (2.3.13)$$

We now turn our attention to the computation of the power lost to heating of the dielectric and the metal cladding.

2-4 Dielectric Loss

The power absorbed by the dielectric is

$$\begin{aligned} P_d &= \sigma \int_V |E|^2 dv \\ &= 2 \omega \tan \delta W_e \end{aligned} \quad (2.4.1)$$

where $\tan \delta$ is the dielectric loss tangent, defined by $\tan \delta = \sigma/\omega\epsilon$, and W_e is the stored electric energy determined in section 2-3.

2-5 Copper Loss

The copper loss is approximated by first solving the problem (as has been done) using the ideal boundary condition, $\hat{n} \times \vec{E} = 0$, to find the surface current, \vec{J}_s . In general, the copper loss is related to the H field tangent to, and the E field normal to the copper plates. It can be shown that the loss associated with the normal E field is negligible. Therefore we will concentrate on the loss associated with the tangential H field on the wall.

For a good conductor, the skin depth is

$$\Delta = \sqrt{\frac{2}{\omega\mu\sigma}} \quad . \quad (2.5.1)$$

Furthermore, within the finitely conductive copper, if it is many skin depths thick as it is in the practical cases, then J , the current density, can be approximated by

$$J = \gamma J_s e^{-\gamma z} \quad , \quad (2.5.2)$$

where γ is the complex attenuation factor

$$\gamma = \sqrt{j\omega\sigma\mu_0} = 1/\Delta + j1/\Delta \quad (2.5.3)$$

Then the copper loss is

$$P_{cu} = 2/\sigma \int_V |J|^2 dv \quad (2.5.4)$$

where here, V is the volume of the metal. Since

$$|J|^2 = 2/\Delta^2 e^{-2z/\Delta} |J_s|^2, \quad (2.5.5)$$

then

$$P_{cu} = \frac{4W_m}{\sigma\Delta\mu t} = \frac{2\Delta\omega}{t} W_m. \quad (2.5.6)$$

In order to obtain this equation, use was made of the fact that

$|\vec{J}_s| = |\vec{H}|$ and \vec{H} is independent of z so that

$$\int_a^b \int_0^{\phi_0} |J_s|^2 \rho d\rho d\phi = \frac{2}{\mu t} \frac{1}{2} \mu \int_V |\vec{H}|^2 dv. \quad (2.5.7)$$

The factor of "2" introduced into 2.2.5 accounts for the loss on both top and bottom plates of the cavity.

Next, we turn to the remaining most important loss mechanism, the radiated field.

2-6 The Radiated Power

Determining the radiated power is the most important and difficult part of the analysis of the microstrip antenna. An equivalence principle, illustrated in figure 2-4, is used to calculate the radiation fields. A circular disk microstrip antenna is employed to illustrate

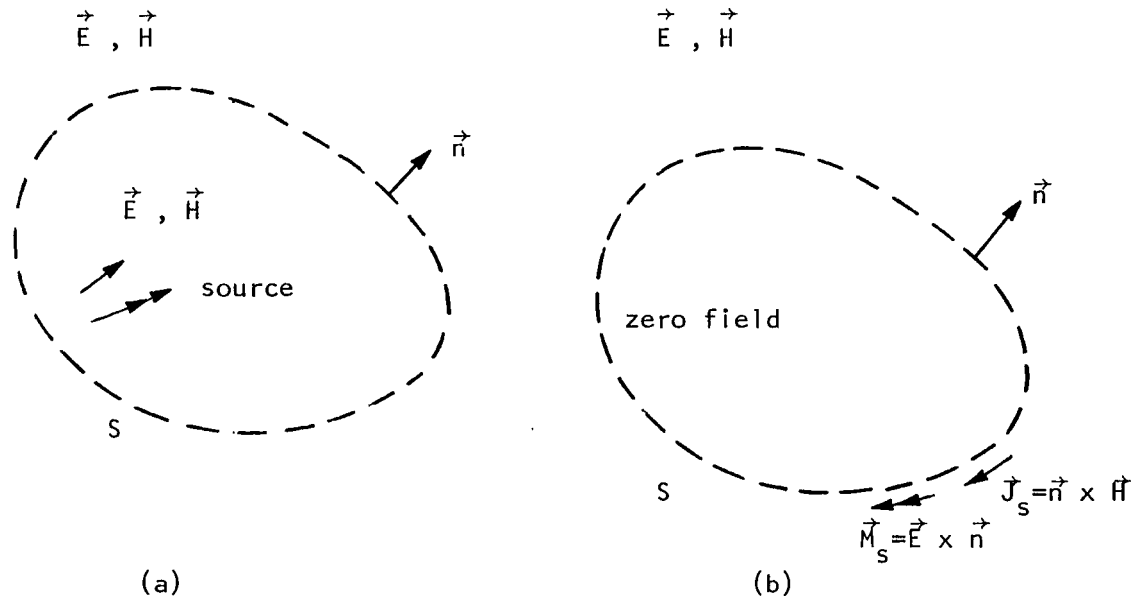


Figure 2-4: The equivalent (b) produces the same field external to S as do the original sources (a).

the use of this equivalence principle.

As shown in figure 2-5-a, the circular disk microstrip antenna is composed of a conducting patch (radius a) over a ground plane. To find the radiated fields, we can extend the patch to infinity by introducing an equivalent magnetic current ($M(x)$) on the top surface of the infinite conductor over the dielectric substrate as shown in figure 2-5-b). (Since an electric current just above the metal will not radiate in the presence of the conductor, it is ignored.) From the equivalence principle, we know that by appropriately choosing this equivalent magnetic current, the fields above the dielectric substrate will be the same as in the original antenna.

The next step, then, is to find the distribution of this equivalent magnetic current. First of all, it is plausible to assume this equivalent magnetic current is concentrated on the edge. Indeed, the edge condition requires that the equivalent magnetic current goes to infinity at the edge and drops to a relatively small value away from the edge quickly. In this case, we can assume that the most significant contribution of the magnetic current to the radiated field comes from a small region of the distribution, say $a < x < x_0$, around the edge of the patch. We neglect the contribution from the remaining part of the equivalent magnetic current. Furthermore, because the range of the magnetic current distribution is so small compared to a wavelength, we can shrink this distribution into a line current, \vec{M}_s , at the edge without changing the fields significantly. Then,

$$M_s = \int_a^{x_0} M(x) dx \quad . \quad (2.6.1)$$

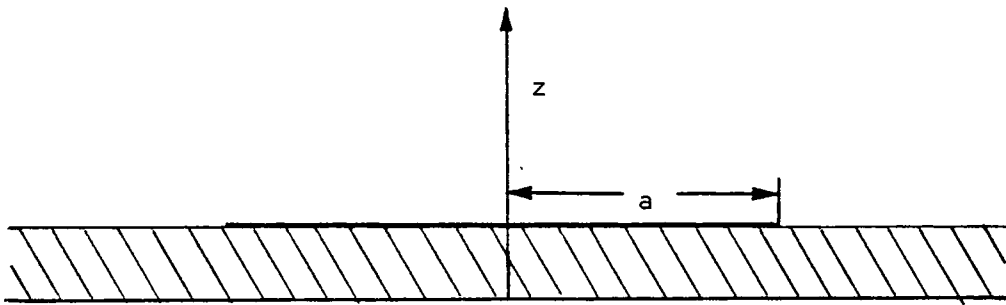


Figure 2-5-a

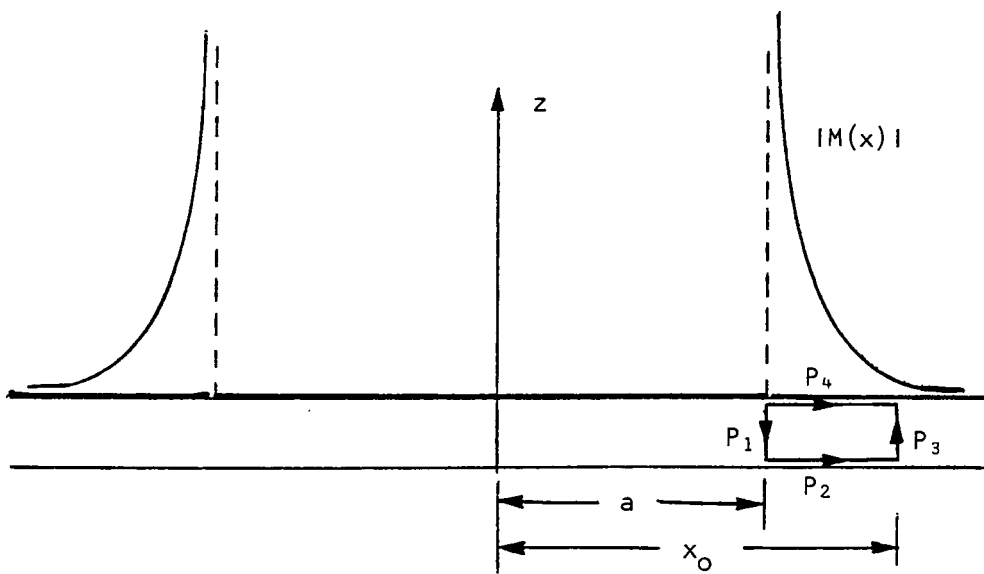


Figure 2-5-b

From the loop shown in figure 2-5-b, we have

$$\begin{aligned}
 & \left| \int_{p1} \vec{E} \cdot d\vec{r} + \int_{p2} \vec{E} \cdot d\vec{r} + \int_{p3} \vec{E} \cdot d\vec{r} + j\omega\mu \iint_s \vec{H} \cdot \hat{n} \, dS \right| \\
 & \qquad \qquad \qquad (2.6.2) \\
 & = \left| \int_{p4} \vec{E} \cdot d\vec{r} \right| = \left| M_s \right|
 \end{aligned}$$

We know that the first term of the left side is just the voltage at the edge of "cavity." The second term is zero because of the presence of the ground plane. Furthermore, the third and the fourth terms are very small compared to the first term since the field drops dramatically away from the edge and because of the boundary condition that the ϕ component of the magnetic field is very small near the edge. Finally, we can conclude that the equivalent magnetic current (which is the only source of the radiated fields now) is equal to the voltage at the edge of "cavity." This approximation will introduce some error, of course, because we neglect the contribution from part of the equivalent magnetic current distribution. However, the part we neglected is essentially associated with the surface wave and space wave in a direction parallel to the ground plane and has a small effect on the radiated fields. Actually, it can be shown the the power loss associated with this surface wave is insignificant compared to the radiated power in most practical applications.

When this equivalent magnetic current is found, we can determine the corresponding far-field electric vector potential defined by

$$\vec{F} = \frac{e^{-jkr}}{4\pi r} \iiint \vec{M}(\vec{r}') e^{jkr' \cos \xi} \, dV' \quad . \quad (2.6.3)$$

From the equation,

$$\vec{E} = -\vec{\nabla} \times \vec{F} \quad , \quad (2.6.4)$$

we have the far-field electric field equal to

$$\vec{E} = -jk_0 F_\phi \hat{\theta} + jk_0 F_\theta \hat{\phi} \quad . \quad (2.6.5)$$

Thus,

$$E_\theta = -jk_0 F_\theta \quad \text{and} \quad E_\phi = jk_0 F_\theta \quad . \quad (2.6.6)$$

Once the far field is known, the radiation power pattern can be calculated by the Poynting vector defined by

$$\vec{S} = \vec{E}^* \times \vec{H} \quad . \quad (2.6.7)$$

From this, the radiated power is found by the equation

$$P_r = 1/\eta_0 \int_{\theta=0}^{\pi/2} \int_{\phi=0}^{2\pi} |E|^2 r^2 \sin\theta d\theta d\phi \quad (2.6.8)$$

where $|E|^2 = |E_\phi|^2 + |E_\theta|^2$ and η_0 is the intrinsic impedance of free space.

2-6-1 The Annular Microstrip Antenna

From equations 2.2.3, 2.2.33, and 2.2.34, the electric field at $z = b$ can be simplified to

$$E_{z1} \Big|_{\rho=b} = \sum_{m=0}^{\infty} \frac{j\eta_0}{(1 + \delta_{om}) \sqrt{\epsilon_r}} \frac{1}{\pi b} \left\{ \frac{[J'_m(ka) N_m(k\rho') - J_m(k\rho') N'_m(ka)]}{[J'_m(kb) N'_m(ka) - N'_m(kb) J'_m(ka)]} \right\} \cos(m\phi) \quad , \quad (2.6.9)$$

where ϕ is the azimuth angle with respect to the source. Let \vec{M}_{s1} be the magnetic current ribbon around the aperture at $\rho = b$ as shown in figure 2-6,

$$\vec{M}_{s1} = \vec{E}_{z1} \Big|_{\rho'=b} \hat{\chi} \hat{n} = \hat{\phi}_1 E_{z1} \Big|_{\rho'=b} \quad . \quad (2.6.10)$$

From equation 2.6.3 the electric vector potential due to \vec{M}_{s1} is

$$\vec{F}_1(r) = \frac{e^{-jk_0 r}}{4\pi r} \text{tb} \int_0^{2\pi} \vec{M}_{s1} e^{jkr' \cos(\xi)} d\phi' \quad (2.6.11)$$

where ξ is polar angle. Thus

$$\vec{F}_1 = \frac{e^{-jk_0 r}}{2\pi r} \text{tb} \int_0^{2\pi} \vec{M}_{s1} e^{jk_0 b \sin \theta \cos(\phi - \phi')} d\phi' \quad (2.6.12)$$

where the primed variables are source coordinates as shown in figure 2-6 and the factor of 2 is introduced into the integral to account for the contribution from the image. Using

$$\hat{\phi}' = \sin \theta \sin(\phi - \phi') \hat{r} + \cos \theta \sin(\phi - \phi') \hat{\theta} \quad (2.6.13)$$

$$+ \cos(\phi - \phi') \hat{\phi} \quad ,$$

and letting $k_0 b \sin \theta = \alpha_1$, we have

$$\begin{aligned} F_{1\phi} = \frac{e^{-jk_0 r}}{2\pi r} \text{tb} \sum_{m=0}^{\infty} \left\{ \frac{j\eta_0}{(1 - \delta_{om}) \sqrt{\epsilon_r}} \frac{1}{\pi} \frac{[J'_m(ka) N_m(k\rho_f) - J_m(k\rho_f) N'_m(ka)]}{[J'_m(kb) N'_m(ka) - N'_m(kb) J'_m(ka)]} \right. \\ \left. \cdot \int_0^{2\pi} \cos m\phi' \cos(\phi - \phi') e^{j\alpha_1 \cos(\phi - \phi')} d\phi' \quad , \quad (2.6.14) \right. \end{aligned}$$

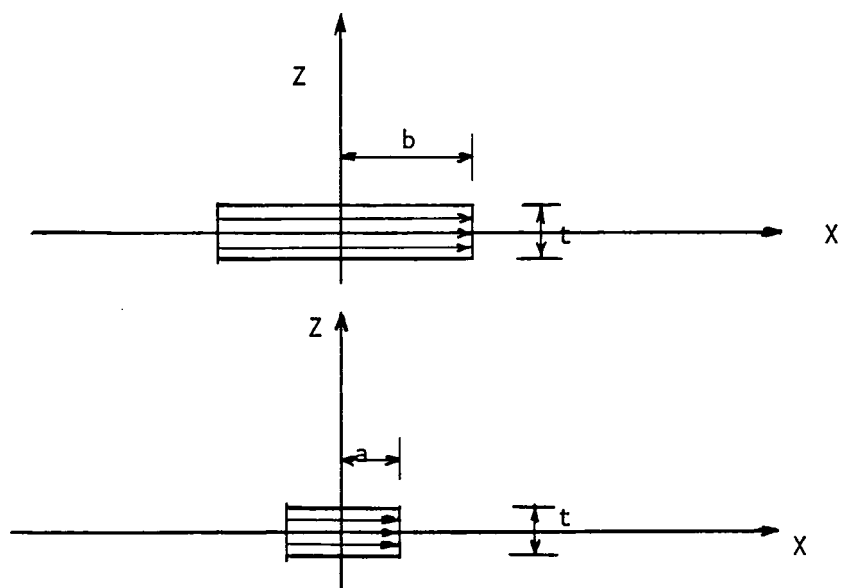
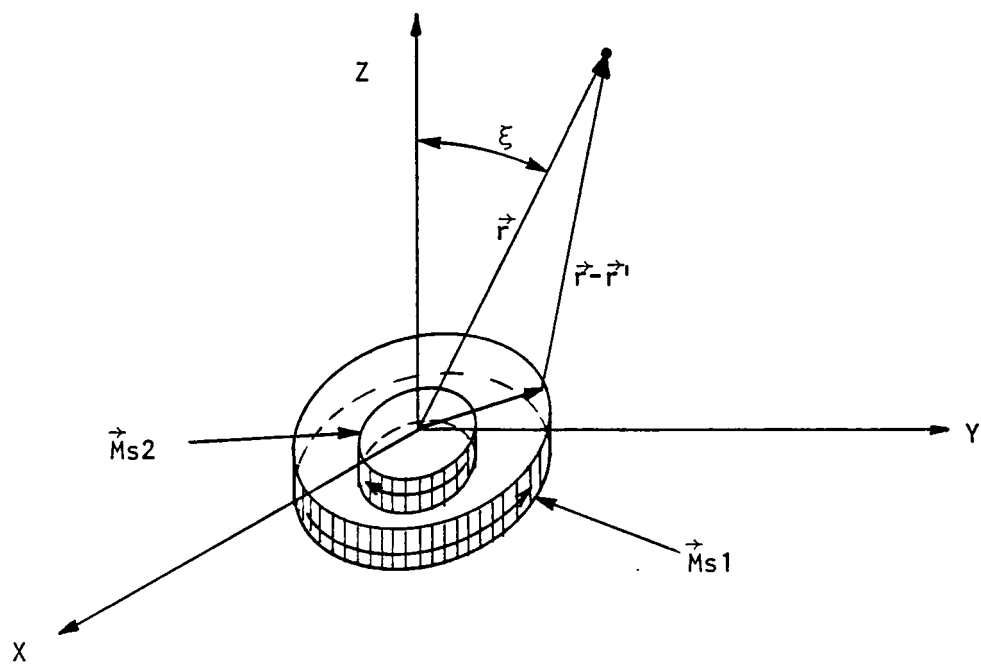


Figure 2- 6

$$F_{1\theta} = \frac{e^{-jk_0 r}}{2\pi r} \cdot \sum_{m=0}^{\infty} \frac{j\eta_0}{(1 + \delta_{om})\sqrt{\epsilon_r}} \cdot \frac{1}{\pi} \frac{[J'_m(ka)N_m(k\rho_f) - J_m(k\rho_f)N'_m(ka)]}{[J'_m(kb)N'_m(ka) - N'_m(kb)J'_m(ka)]} \cdot \cos\theta \int_0^{2\pi} \sin(\phi - \phi') \cos m\phi' e^{-j\alpha_1 \cos(\phi - \phi')} d\phi' \quad (2.6.15)$$

Using the identity

$$e^{j\alpha_1 \cos u} = 2 \sum_{n=0}^{\infty} \frac{j^n J_n(\alpha_1)}{1 + \delta_{on}} \cos nu \quad , \quad (2.6.16)$$

the equations 2.6.14 and 15 can be written as

$$F_{1\phi} = G(r) \cdot \left\{ jJ_1(\alpha_1) \frac{[J'_0(ka)N_0(k\rho_f) - J_0(k\rho_f)N'_0(ka)]}{[J'_0(kb)N'_0(ka) - N'_0(kb)J'_0(ka)]} + \sum_{m=1}^{\infty} (\cos(m\phi)) \cdot j^{m+1} \left(J_{m+1}(\alpha_1) - \frac{J_{m-1}(\alpha_1)}{1 + \delta_{m,1}} \right) \cdot \frac{[J'_m(ka)N_m(k\rho_f) - J_m(k\rho_f)N'_m(ka)]}{[J'_m(kb)N'_m(ka) - N'_m(kb)J'_m(ka)]} \right\} \quad (2.6.17)$$

$$F_{1\theta} = -G(r) \sum_{m=1}^{\infty} \frac{[J'_m(ka)N_m(k\rho_f) - J_m(k\rho_f)N'_m(ka)]}{[J'_m(kb)N'_m(ka) - N'_m(kb)J'_m(ka)]} \cdot \cos\theta \cdot j^{m+1} \sin(m\phi) \left(J_{m+1}(\alpha_1) + \frac{J_{m-1}(\alpha_1)}{m,1 + 1} \right) \quad (2.6.18)$$

where

$$G(r) = \frac{e^{-jk_0 r}}{2\pi r} \cdot \frac{j\eta_0}{\sqrt{\epsilon_r}}$$

and

$$k_0 b \sin \theta = \alpha_1 \quad .$$

The magnetic current at the aperture at $\rho = a$ is

$$\vec{M}_{s2} = \vec{E}_{z2} \Big|_{\rho'=a} \times \hat{n} = \vec{E}_{z2} \Big|_{\rho'=a} \times (-\hat{\rho}') = -\hat{\phi}' \vec{E}_{z2} \Big|_{\rho=a} \quad (2.6.19)$$

From equation 2.2.26, we similarly find $F_{2\phi}$ and $F_{2\theta}$. Replacing a by b in the numerators of equations 2.6.17 and 2.6.18, and replacing α_1 by α_2 , we find that

$$F_{2\phi} = -G(\gamma) \left\{ jJ_1(\alpha_2) \frac{[J'_0(kb)N_0(k\rho_f) - N'_0(kb)J_0(k\rho_f)]}{[J'_0(kb)N'_0(ka) - N'_0(kb)J'_0(ka)]} + \sum_{m=1}^{\infty} (\cos(m\phi)) \right. \\ \left. \cdot j^{m+1} \left[J_{m+1}(\alpha_2) - \frac{J_{m-1}(\alpha_2)}{1 + \delta_{m,1}} \right] \cdot \frac{[J'_m(kb)N_m(k\rho_f) - J_m(k\rho_f)N'_m(kb)]}{[J'_m(kb)N'_m(ka) - N'_m(kb)J'_m(ka)]} \right\}, \quad (2.6.20)$$

$$F_{2\theta} = G(r) \sum_{m=1}^{\infty} \frac{J'_m(kb)N_m(k\rho_f) - J_m(k\rho_f)N'_m(kb)}{J'_m(kb)N'_m(ka) - N'_m(kb)J'_m(ka)} \cdot \cos\theta \\ \cdot j^{m+1} \sin(m\phi) \left[J_{m+1}(\alpha_2) + \frac{J_{m-1}(\alpha_2)}{1 + \delta_{m,1}} \right], \quad (2.6.21)$$

where $\alpha_2 = k_0 a \sin\theta$. Then the electric far fields in any direction can be determined by

$$E_{\theta} = -jk_0 F_{\phi} = -jk_0 (F_{1\phi} + F_{2\phi}) \quad (2.6.22)$$

and

$$E_{\phi} = jk_0 F_{\theta} = jk_0 (F_{1\theta} + F_{2\theta}) \quad (2.6.23)$$

From this, the radiated power can be found by integrating the Poynting vector over the whole upper hemisphere as in equation 2.6.8. The orthogonality of $\cos(m\phi)$ and $\sin(m\phi)$ can be used to simplify the

integration. The integration over ϕ can be integrated in closed form and the integration over θ will be done by using Gaussian quadrature.

2-6-2 The Annular Sector Antenna

As illustrated in figure 2-7, we can divide the magnetic current into four parts, \vec{M}_{s1} , \vec{M}_{s2} , \vec{M}_{s3} , \vec{M}_{s4} . For \vec{M}_{s1} , we have

$$\vec{F}_1 = \frac{e^{-jk_0 r}}{2\pi r} \text{tb} \int_0^{\phi_0} \hat{\phi}' M_{s1} e^{-jk_0 b \sin \theta \cos(\phi - \phi')} d\phi' , \quad (2.6.24)$$

where

$$M_{s1} = \sum_{p=0}^{\infty} (A_p J_p(k\rho) + B_p N_p(k\rho)) \cos v\phi .$$

Then

$$\begin{aligned} F_{1\phi} &= \frac{e^{-jk_0 r}}{2\pi r} \text{tb} \sum_{p=0}^{\infty} (A_p J_p(k\rho) + B_p N_p(k\rho)) \\ &\cdot \int_0^{\phi} \cos(v\phi') \cos(\phi - \phi') e^{jk_0 b \sin \theta \cos(\phi - \phi')} d\phi' ; \end{aligned} \quad (2.6.25)$$

$$\begin{aligned} F_{1\theta} &= \frac{e^{-jk_0 r}}{2\pi r} \text{tb} \sum_{p=0}^{\infty} (A_p J_p(kb) + B_p N_p(kb)) \cos \theta \\ &\cdot \int_0^{\phi_0} \cos(v\phi') \sin(\phi - \phi') e^{jk_0 b \sin \theta \cos(\phi - \phi')} d\phi' . \end{aligned} \quad (2.6.26)$$

By using the identity in 2.6.16, equations 2.6.24 and 2.6.25 can be integrated in closed form. Similarly, we find, due to the magnetic current sheet \vec{M}_{s2} , that

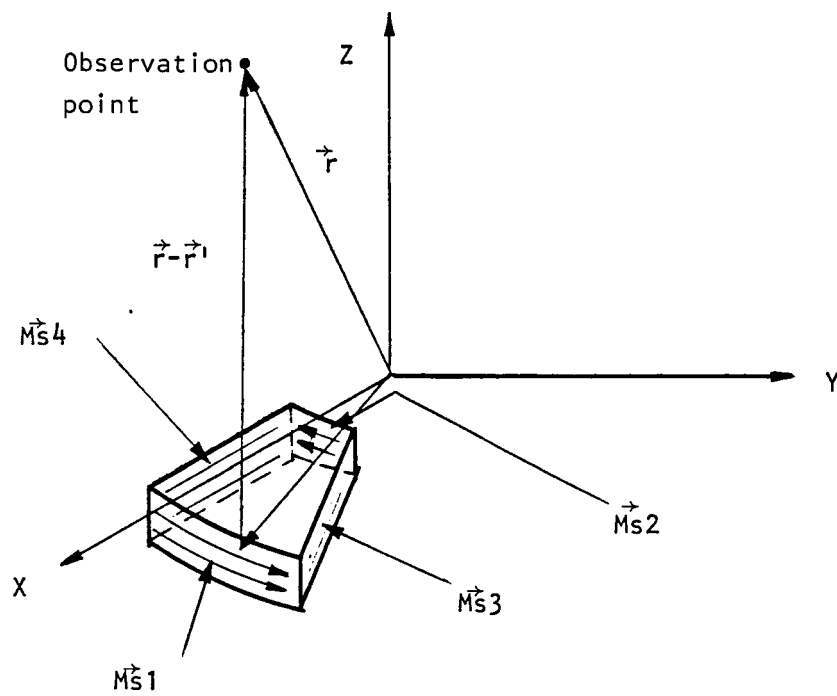


Figure 2-7

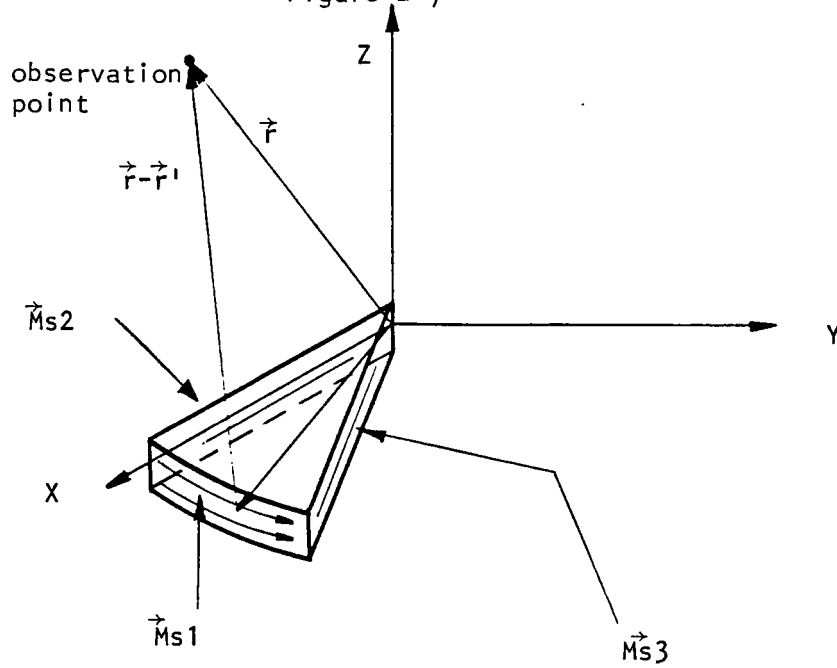


Figure 2-8

$$F_{2\phi} = \frac{e^{-jk_0 r}}{2\pi r} \tan \sum_{p=0}^{\infty} (C_p J_\nu(ka) + D_p N_\nu(ka)) \cdot \int_0^{\phi_0} \cos(\nu\phi') \cos(\phi - \phi') e^{jk a \sin\theta \cos(\phi - \phi')} d\phi' ; \quad (2.6.27)$$

$$F_{2\theta} = -\frac{e^{-jk_0 r}}{2\pi r} \tan \sum_{p=0}^{\infty} (C_p J_\nu(ka) + D_p N_\nu(ka)) \cos\theta \cdot \int_0^{\phi_0} \cos(\nu\phi') \sin(\phi - \phi') e^{jk a \sin\theta \cos(\phi - \phi')} d\phi' . \quad (2.6.28)$$

The electric vector potential $F_{4\phi}, F_{4\theta}$, due to magnetic current sheet \vec{M}_{s4} is found by

$$F_{4\phi} = \frac{e^{-jk_0 r}}{2\pi r} \tan \sin(-\phi) \sum_{p=0}^{\infty} \text{INTE}_p(\theta, \phi) \quad (2.6.29)$$

$$F_{4\theta} = \frac{e^{-jk_0 r}}{2\pi r} \tan \cos\theta \cos\phi \sum_{p=0}^{\infty} \text{INTE}_p(\theta, \phi) \quad (2.6.30)$$

where

$$\begin{aligned} \text{INTE}_p(\theta, \phi) = & \int_a^{\rho_f} (C_p J_\nu(k\rho) + D_p N_\nu(k\rho)) \cdot e^{jk_0 \rho \sin\theta \cos\phi} d\rho \\ & + \int_{\rho_f}^b (A_p J_\nu(k\rho) + B_p N_\nu(k\rho)) e^{jk_0 \rho \sin\theta \cos\phi} d\rho \end{aligned}$$

which can be evaluated by Gaussian quadrature. Here the identity

$$\hat{\rho}' = \hat{r} \sin\theta \cos(\phi - \phi') + \hat{\theta} \cos\theta \cos(\phi - \phi') + \hat{\phi} \sin(\phi - \phi') \quad (2.6.31)$$

was used to derive $F_{4\phi}$ and $F_{4\theta}$ from \vec{F}_4 .

Similarly,

$$F_{3\phi} = \frac{e^{-jk_0 r}}{2\pi r} t \sin(\phi_0 - \phi) \sum_{p=0}^{\infty} \text{INTE2}_p(\theta, \phi) , \quad (2.6.32)$$

$$F_{3\theta} = \frac{e^{-jk_0 r}}{2\pi r} t \cos\theta \cos(\phi - \phi_0) \sum_{p=0}^{\infty} \text{INTE2}_p(\theta, \phi) , \quad (2.6.33)$$

where

$$\text{INTE2}_p(\theta, \phi) = \int_a^{\rho_f} (C_p J_\nu(k\rho) + D_p N_\nu(k\rho)) e^{jk_0 \rho \sin\theta \cos(\phi - \phi_0)} d\rho .$$

Then, in the far field,

$$E_\theta = -jk_0 (F_{1\phi} + F_{2\phi} + F_{3\phi} + F_{4\phi}) , \quad (2.6.34)$$

$$E_\phi = jk_0 (F_{1\theta} + F_{2\theta} + F_{3\theta} + F_{4\theta}) , \quad (2.6.35)$$

and the radiated power can be determined by integrating the Poynting vector over the upper hemisphere by Gaussian quadrature.

2-6-3 The Circular Sector Antennas

As shown in figure 2-8, we divide the magnetic current into three parts \vec{M}_{s1} , \vec{M}_{s2} and \vec{M}_{s3} . From equations 2.2.62 and 2.2.68, we have

$$\vec{M}_{s1} = \vec{E} \Big|_{\rho=a} \times \hat{n} = \sum_{m,p=0}^{\infty} A_{mp} J_\nu(k_{mv} a) \cos(\nu\phi)$$

and

$$\begin{aligned}
\vec{F}_1 &= \frac{e^{-jk_0 r}}{2\pi r} \tan \int_0^{\phi_0} \hat{\phi}' M_{s1} e^{jk_0 a \sin \theta \cos(\phi - \phi')} \\
&= \frac{e^{-jk_0 r}}{2\pi r} \tan \sum_{m,p=0}^{\infty} A_{mp} J_{\nu}(k_{mv} a) \int_0^{\phi_0} \hat{\phi}' \cos(\nu \phi') e^{jk_0 a \sin \theta \cos(\phi - \phi')} d\phi'.
\end{aligned}
\tag{2.6.36}$$

By identity 2.6.13, we have

$$\begin{aligned}
F_{1\phi} &= \frac{e^{-jk_0 r}}{2\pi r} \tan \sum_{m,p=0}^{\infty} A_{mp} J_{\nu}(k_{mv} a) \int_0^{\phi_0} \cos(\nu \phi') \cos(\phi - \phi') \\
&\quad \cdot e^{jk_0 a \sin \theta \cos(\phi - \phi')} d\phi' ;
\end{aligned}
\tag{2.6.37}$$

$$\begin{aligned}
F_{1\theta} &= \frac{e^{-jk_0 r}}{2\pi r} \tan \sum_{m,p=0}^{\infty} A_{mp} J_{\nu}(k_{mv} a) \int_0^{\phi_0} \cos \theta \\
&\quad \cdot \sin(\phi - \phi') \cos(\nu \phi') e^{jk_0 a \sin \theta \cos(\phi - \phi')} d\phi'.
\end{aligned}
\tag{2.6.38}$$

Equations 2.6.37 and 2.6.38 can be integrated in closed form.

To find the electric vector potential due to \vec{M}_{s2} and \vec{M}_{s3} , we have

$$\vec{M}_{s2} = \vec{M}_{s3} = \sum_{m,p=0}^{\infty} A_{mp} J_{\nu}(k_{mv} \rho) \hat{\rho}' ;
\tag{2.6.39}$$

$$\vec{F}_2 = \frac{e^{-jk_0 r}}{2\pi r} \tan \sum_{m,p=0}^{\infty} A_{mp} \int \hat{\rho}' J_{\nu}(k_{mv} \rho') e^{jk_0 \rho' \sin \theta \cos \phi} d\rho' ;
\tag{2.6.40}$$

$$\vec{F}_3 = \frac{e^{-jk_0 r}}{2\pi r} \tan \sum_{m,p=0}^{\infty} A_{mp} \int \hat{\rho}' J_{\nu}(k_{mv} \rho') e^{jk_0 \rho' \sin \theta \cos(\phi - \phi')} d\rho' .
\tag{2.6.41}$$

By using series expansions of $J_{\nu}(k_{mv} \rho')$ and $e^{jk_0 \rho' \sin \theta \cos(\phi - \phi')}$, we can integrate 2.6.40 and 2.6.51 in closed form. The far electric

field is

$$E_{\theta} = -jk_0(F_{1\phi} + F_{2\phi} + F_{3\phi}) \quad , \quad (2.6.46)$$

$$E_{\phi} = jk_0(F_{1\theta} + F_{2\theta} + F_{3\theta}) \quad . \quad (2.6.47)$$

Of course, the radiated power is found from this as in the case of section 2-6-2.

2-7 The Input Impedance

In general, the driving point admittance is

$$Y(\omega) = \{[P_r + P_{sw} + P_c + P_d] + j2\omega[W_e - W_m]\}/|V|^2, \quad (2.7.1)$$

where

P_r = radiated power ,

P_{sw} = surface wave loss ,

P_c = copper loss ,

P_d = dielectric loss ,

W_e = time averaged electric stored energy ,

W_m = time averaged magnetic stored energy.

We can show that P_{sw} is negligible [7] compared to P_c , P_d , and P_r for thin dielectrics and will be omitted here for simplicity.

Let $P = P_r + P_c + P_d$, then we can write

$$Z_{in}(\omega) = \frac{P + j2\omega(W_e - W_m)}{I^2} = V/I \quad (2.7.2)$$

If we choose $I = 1$ amp., and t = thickness of the dielectric substrate,

$Z_{in}(\omega)$ can be reduced to

$$Z_{in} = t E_z \quad (2.7.3)$$

since that E_z is independent of z . As mentioned above, the copper loss and radiated power are calculated using perturbation of an ideal resonant cavity. Therefore, it can not be expected that equation 2.7.3 will agree with the experiments since the expression for the internal electric field, E_z , takes no account of these losses. Obviously (if we neglect the dielectric loss) equation 2.7.3 predicts the implausible result that the driving point impedance is infinite at the resonant frequency. This inconsistency can be avoided in two ways. One was proposed in [3]. There the antenna was modelled as a cavity with a finite admittance wall instead of a magnetic wall. Another one was proposed in [1], where the power losses were redistributed throughout the dielectric within the cavity. The system will then consist of a perfect cavity with a modified lossy dielectric. This approximation is accurate only if the microstrip antenna has a high Q . Here the Q is the quality factor defined by

$$Q = \frac{\omega \cdot \text{stored energy}}{\text{total power loss}} \quad (2.7.4)$$

The reason for this is that if the power losses are very small compared to the stored energy, then this redistribution will not change the internal field structure significantly. Now by modifying the dielectric loss tangent to account for the power loss, we have a new effective loss tangent defined by

$$\delta_{\text{eff}} = \frac{P}{2\omega W_e} \quad . \quad (2.7.5)$$

It is very interesting to note from this definition of the effective loss tangent that it just equal to the reciprocal of the quality factor of the microstrip antenna. Actually

$$Q = \frac{\omega(W_e + W_m)}{P} \quad , \quad (2.7.6)$$

but $W_e = W_m$ at resonance.

The complex wave number for the modified system is then

$$K_{\text{eff}} = \sqrt{\omega(1 - j\delta_{\text{eff}})\mu\epsilon} \quad (2.7.8)$$

Using this complex wave number, we can re-express the internal fields and find the input impedance by using equation 2.7.3.

However, there is a problem. Because we made the assumption that the feed line is vanishingly thin we will have an infinite inductive impedance. This can be corrected by modeling the feed line as a finite width, thin strip of uniform current. This idea was first proposed in the literature [7] and worked very well. Then by superposing the expressions of internal fields for this current distribution, we will have another factor $(\sin(v\phi_W)/(v\phi_W))$ in the series expressions for internal field. Since the field between the ground plane and the patch varies over this feed strip, the field is averaged over the strip. This introduces an additional factor of $(\sin(v\phi_W)/(v\phi_W))$. The expressions for the fields computed in this way can be obtained from their corresponding Green's functions by

setting $\rho = \rho_f$, $\phi = \phi_f$, and by multiplying the summand by $\sin^2(v\phi_W)/(\nu\phi_W)$.

2-7-1 Annular Microstrip Antenna

From equations 2.2.23, 2.2.33, and 2.2.34, we have

$$Z_{in} = t \sum_{m=0}^{\infty} \left\{ \frac{-j\omega\mu}{2(1 + \delta_{om})\Delta_m} [J_m(k\rho_f)N'_m(ka) - J'_m(ka)N_m(k\rho_f)] \right. \\ \left. \cdot [N'_m(kb)J_m(k\rho_f) - J'_m(kb)N_m(k\rho_f)] \right\} \frac{\sin^2(m\phi_W)}{(m\phi_W)^2} . \quad (2.7.9)$$

2-7-2 Annular Sector Microstrip Antenna

From equations 2.2.43, 2.2.56, and 2.2.57 ,

$$Z_{in} = t \sum_{p=0}^{\infty} \left\{ \frac{-j\omega\mu\cos^2(v\phi_f)}{(1 + \delta_{op})\phi_0} \frac{[J_v(k\rho_f)N'_v(ka) - J'_v(ka)N_v(k\rho_f)]}{[J'_v(kb)N'_v(ka) - N'_v(kb)J'_v(ka)]} \right. \\ \left. \cdot [N'_v(kb)J_v(k\rho_f) - J'_v(kb)N_v(k\rho_f)] \right\} \frac{\sin^2(v\phi_W)}{(\nu\phi_W)^2} , \quad (2.7.10)$$

where

$$\nu = p\pi/\phi_W .$$

2-7-3 Annular Sector

From equations 2.2.72 and 2.2.81,

$$Z_{in} = t \sum_{p=0}^{\infty} \left\{ \frac{j\omega\mu}{(1 + \delta_{0m})\phi_0} \cos^2(v\phi_f) \left[N_v(k\rho_f) - \frac{J_v(k\rho_f)}{J'_v(ka)} N'_v(ka) \right] \right\} \\ \cdot J_v(k\rho_f) (\sin v\phi_W / v\phi_W)^2, \quad (2.7.11)$$

where again, $v = p\pi/\phi_0$.

2-8 Acceleration of Series

As found in the previous sections, the fields are represented by infinite series. Let

$$S_1 = \sum_{m=1}^{\infty} A_m, \quad (2.8.1)$$

$$S_2 = \sum_{m=1}^{\infty} [A_m - \lambda_m] + \sum_{m=1}^{\infty} \lambda_m, \quad (2.8.2)$$

where the summand of S_1 , A_m , is asymptotic to λ_m as m goes to infinity. Then $S_1 = S_2$ and the first series of S_2 converges faster than the series for S_1 . This acceleration technique is useful if the second series of S_2 can be summed easily. In fact, for the series to be evaluated in this study, the asymptotic forms of the summands can be summed very efficiently.

In our investigation, we must sum series involving Bessel and Neumann functions. For large order, the Bessel functions have asymptotic forms of [11]

$$J_m(z) \sim \frac{1}{\sqrt{2\pi m}} (ez/2m)^m; \quad (2.8.3)$$

$$N_m(z) \sim \frac{-\sqrt{2}}{\sqrt{m\pi}} (ez/2m)^{-m}; \quad (2.8.4)$$

$$J'_m(z) \underset{m \rightarrow \infty}{\sim} \frac{e}{2\sqrt{2m\pi}} (ez/2m)^{m-1} ; \quad (2.8.5)$$

$$N'_m(z) \underset{m \rightarrow \infty}{\sim} \frac{e}{\sqrt{2m\pi}} (ez/2m)^{-m-1} . \quad (2.8.6)$$

2-8-1 Annular Microstrip Antenna

Substituting the asymptotic forms of the Bessel functions into equations 2.2.23 and 2.2.26 gives

$$E_{z1m} \underset{m \rightarrow \infty}{\sim} - \frac{j\omega\mu}{2m\pi} \frac{[(\rho_f/a)^m + (a/\rho_f)^m]2[(\rho/b)^m + (b/\rho)^m]}{[(b/a)^m - (a/b)^m]} \cdot \left(\frac{\sin(m\phi_W)}{m\phi_W} \right)^2 , \quad (2.8.7)$$

$$E_{z2m} \underset{m \rightarrow \infty}{\sim} - \frac{j\omega\mu}{2m\pi} \frac{[(\rho_f/b)^m + (b/\rho_f)^m][(\rho/a)^m + (b/\rho)^m]}{[(b/a)^m + (a/b)^m]} \cdot \left(\frac{\sin(m\phi_W)}{m\phi_W} \right)^2 . \quad (2.8.8)$$

At the feed point, $\rho = \rho_f$, and

$$E_{z1m} = E_{z2m} \underset{m \rightarrow \infty}{\sim} - \frac{j\omega\mu}{2\pi m} \frac{[(\rho_f/b)^m + (b/\rho_f)^m][(\rho_f/a)^m + (a/\rho_f)^m]}{(b/a)^m + (a/b)^m} \cdot \left(\frac{\sin(m\phi_W)}{m\phi_W} \right)^2 . \quad (2.8.9)$$

This can be simplified further using the fact that $(\rho_f/b)^m$ and $(a/b)^m$ approach 0, as $m \rightarrow \infty$. Then

$$E_{z1m} = E_{z2m} \underset{m \rightarrow \infty}{\sim} - \frac{j\omega\mu}{2m\pi} \left(\frac{\sin(m\phi_W)}{m\phi_W} \right) . \quad (2.8.10)$$

2-8-2 Annular Sector Microstrip Antenna

From equations 2.2.43 and 2.2.44, we have

$$E_{z1_p} \underset{p \rightarrow \infty}{\sim} - \frac{j\omega\mu\cos^2(v\phi_f)}{v\phi_0} \frac{[(\rho_f/a)^v + (a/\rho_f)^v][(\rho/b)^v + (b/\rho)^v]}{[(a/b)^v + (b/a)^v]} \cdot \left(\frac{\sin(v\phi_W)}{v\phi_W} \right)^2, \quad (2.8.11)$$

$$E_{z2_p} \underset{p \rightarrow \infty}{\sim} - \frac{j\omega\mu\cos^2(v\phi_f)}{\phi_0 v} \frac{[(\rho_f/b)^v + (b/\rho_f)^v][(\rho/a)^v + (a/\rho)^v]}{[(b/a)^v - (a/b)^v]} \cdot \left(\frac{\sin(v\phi_W)}{v\phi_W} \right)^2. \quad (2.8.12)$$

At the feed point, $\rho = \rho_f$, and

$$E_{z1_p} = E_{z2_p} \underset{p \rightarrow \infty}{\sim} - \frac{j\omega\mu\cos^2(v\phi)}{v\phi_0} \frac{[(\rho_f/b)^v + (b/\rho_f)^v][(\rho_f/a)^v + (a/\rho_f)^v]}{[(a/b)^v + (b/a)^v]} \cdot \left(\frac{\sin(v\phi_W)}{v\phi_W} \right)^2 - \frac{j\omega v \cos^2(v\phi)}{\phi_0 v} \cdot \left(\frac{\sin(v\phi_W)}{v\phi_W} \right)^2. \quad (2.8.14)$$

2-8-3 Circular Sector Microstrip Antenna

From equations 2.2.69 and 2.2.72, we have

$$E_{z1_p} \underset{p \rightarrow \infty}{\sim} \frac{-j\omega v \pi}{\phi_0} \cos^2(v\phi_f) \frac{1}{v\pi} (\rho_f/a)^v \cdot [(\rho/a)^v + (a/\rho)^v] \cdot \left(\frac{\sin(v\phi_W)}{v\phi_W} \right)^2, \quad (2.8.15)$$

$$E_{z2} \underset{p \rightarrow \infty}{\sim} \frac{-j\omega\mu\pi}{\phi_0} \cos^2(v\phi_f) \frac{1}{v\pi} (\rho/a)^v \cdot [(a/\rho_f)^v + (\rho_f/a)^v] \cdot \left(\frac{\sin(v\phi_W)}{v\phi_W} \right)^2, \quad (2.8.16)$$

which at feed point, $\rho = \rho_f$, becomes

$$E_{z1p} = E_{z2p} \underset{p \rightarrow \infty}{\sim} \frac{-j\omega\mu\pi}{\phi_0} \cos^2(v\phi_f) \cdot \frac{1}{v\pi} (\rho_f/a)^v \cdot [(a/\rho_f)^v + (\rho_f/a)^v] \cdot \left(\frac{\sin(v\phi_W)}{v\phi_W} \right)^2 \quad (2.8.17)$$

$$\sim - \frac{j\omega\mu\pi}{\phi_0} \cos^2(v\phi_f) \frac{\sin(v\phi_W)^2}{v\phi_W} \quad (2.8.18)$$

2-8-4 The Efficient Summation of Series of Asymptotic Forms

It was seen in sections 2-8-1, 2, 3 that we must find the value of infinite series

$$\sum_{m=1}^{\infty} (\sin(m\phi_W))^2 / m^3, \quad (2.8.19)$$

or

$$\sum_{m=1}^{\infty} \cos^2(m\phi_f) \sin^2(m\phi_W) / m^3 \quad (2.8.20)$$

First,

$$\begin{aligned} \sum_{m=1}^{\infty} \sin^2(m\phi_W) / m^3 &= \sum_{m=1}^{\infty} \frac{1}{2} \left(\frac{1}{m^3} - \frac{\cos(m(2\phi_W))}{m^3} \right) \\ &= \frac{1}{2} \left(1.202057 - \sum_{m=1}^{\infty} \frac{\cos(m(2\phi_W))}{m^3} \right) \quad (2.8.21) \end{aligned}$$

The Taylor series expansion of this function of ϕ can be found through [7]

$$\sum_{m=1}^{\infty} \frac{\cos(m\theta)}{m^3} = 1.202057 - \theta^2 \left(\frac{3}{4} - \frac{1}{2} \ln \theta \right) + \sum_{k=1}^{\infty} \frac{\zeta(2k)}{k(2k+1)(2k+2)} \cdot (\theta/2\pi)^{2k} \quad , \quad (2.8.22)$$

where ζ is the Rieman-Zeta function. It can be seen that equation 2.8.22 converges quickly so that equation 2.8.19 can be found very efficiently.

Similarly, equations 2.8.20 can be expressed as

$$\sum_{m=1}^{\infty} \cos^2(m\phi_f) \sin^2(m\phi_W) / m^3 = \frac{1}{4} \sum_{m=1}^{\infty} \left\{ \frac{1}{m^3} - \frac{\cos(2m\phi_W)}{m^3} + \frac{\cos(2m\phi_f)}{m^3} - \frac{\cos(2m(\phi_W + \phi_f))}{2m^3} - \frac{\cos(2m(\phi_f - \phi_W))}{2m^3} \right\} . \quad (2.8.23)$$

This is also efficiently evaluated using 2.8.22.

CHAPTER 3

ANALYTIC AND EXPERIMENTAL RESULTS

3-1 The Loss Tangent and the Conductivity

In analyzing the microstrip antenna, it is important to specify the dielectric loss tangent and the conductivity of copper in order to determine the quality factor. It is found that the values supplied by the manufacturers often differ from the measured values of these parameters [14]. In the present case, the measured conductivity and dielectric loss tangent are 222×10^5 ohms/m and 0.0012 respectively. These values were used in all the computations.

3-2 The Quality Factor

Probably the single most important parameter used to characterize (and by this method, to analyze) the microstrip antenna is the quality factor. From the quality factor, we can determine the effective wave number and then the input impedance. The quality factor of some lower modes for five differently shaped antennas are listed in table 3-1.

The shape of the measured and calculated input impedances is usually circular in the Smith Chart. Points on the plot corresponding to different frequencies (of a fixed frequency increment) will be close together for a low Q antenna and further apart for a higher Q antenna. Therefore, by comparing the spread of points in the Smith Chart of an equal frequency increment, we can compare Q's directly on the Smith Chart. It can be seen from the figures of impedance locus below that this method predicts the Q very well.

TABLE 3-1: Some calculated value of Quality Factor
for microstrip antenna

Antenna Element	Mode (n,m) (v,p,m)	Quality Factor	Efficiency %
Figure 3-1-a	(1,1)	191.3	57.6
Figure 3-2-a	(2,3,1)	165.4	34.7
Figure 3-3-a	(4.5,1,1)	88.33	72.5
Figure 3-4-a	(1,1,1)	161.4	26.6
Figure 3-5-a	(4.5,1,1)	65.24	79.9

TABLE 3-2-a: The calculated and the measured resonant frequency for the microstrip antenna element of figure 3-1-a (annulus).

n	m	Calculated Resonant Freq.	Measured Resonant Freq.	Deviation %
1	1	375.5	382	1.74
2	1	714.5	720	0.77
3	1	1014.6	1016	0.13
0	2	1195.6	1158	3.15
1	2	1284.9	1260	1.93
4	1	1293.3	1298	0.36

TABLE 3-2-b: The calculated and the measured resonant frequencies for the microstrip antenna of figure 3-2-a. (270° annular sector)
(Mhz)

(ν , p, m)	Calculated Resonant Freq.	Measured Resonant freq.	Deviation %
(2, 3, 1)	714.5	714	0.07
($2^2/3$, 4, 1)	917.9	914	0.43
($3^1/3$, 5, 1)	1109.1	1102	0.64
(0, 0, 2)	1195.0	1152	3.61
($2/3$, 1, 2)	1235.6	1206	2.35
(4, 6, 1)	1293.3	1288	3.80
($4/3$, 2, 2)	1351.5	1330	1.59

TABLE 3-2-c: The calculated and the measured resonant frequencies for the microstrip antenna of figure 3-3-a. (40° annular sector)
(Mhz)

(ν , p, m)	Calculated Resonant Freq.	Measured Resonant Freq.	Deviation %
(0, 0, 2)	1195.6	1172	1.93
(4.5, 1, 1)	1428.7	1390	2.71
(0, 0, 3)	2323.7	2280	1.88
(4.5, 1, 2)	2376.2	2305	3.0

TABLE 3-2-d: The calculated and the measured resonant frequencies for the microstrip antenna of figure 3-4-a. (half disk)
(Mhz)

(ν , p, m)	Calculated Resonant Freq.	Measured Resonant Freq.	Deviation %
(1, 1, 1)	470.5	470	0.10
(2, 2, 1)	780.5	774	0.83
(0, 0, 2)	979.1	966	1.34
(3, 3, 1)	1073.6	1068	0.52
(4, 4, 1)	1358.8	1358	0.06

TABLE 3-2-e: The calculated and the measured resonant frequencies for the microstrip antenna of figure 3-5-a. (40° circular sector)
(Mhz)

(ν , p, m)	Calculated Resonant Freq.	Measured Resonant Freq.	Deviation %
(4.5, 1, 1)	1499.6	1460	2.64
(0, 0, 3)	1792.7	1770	1.27

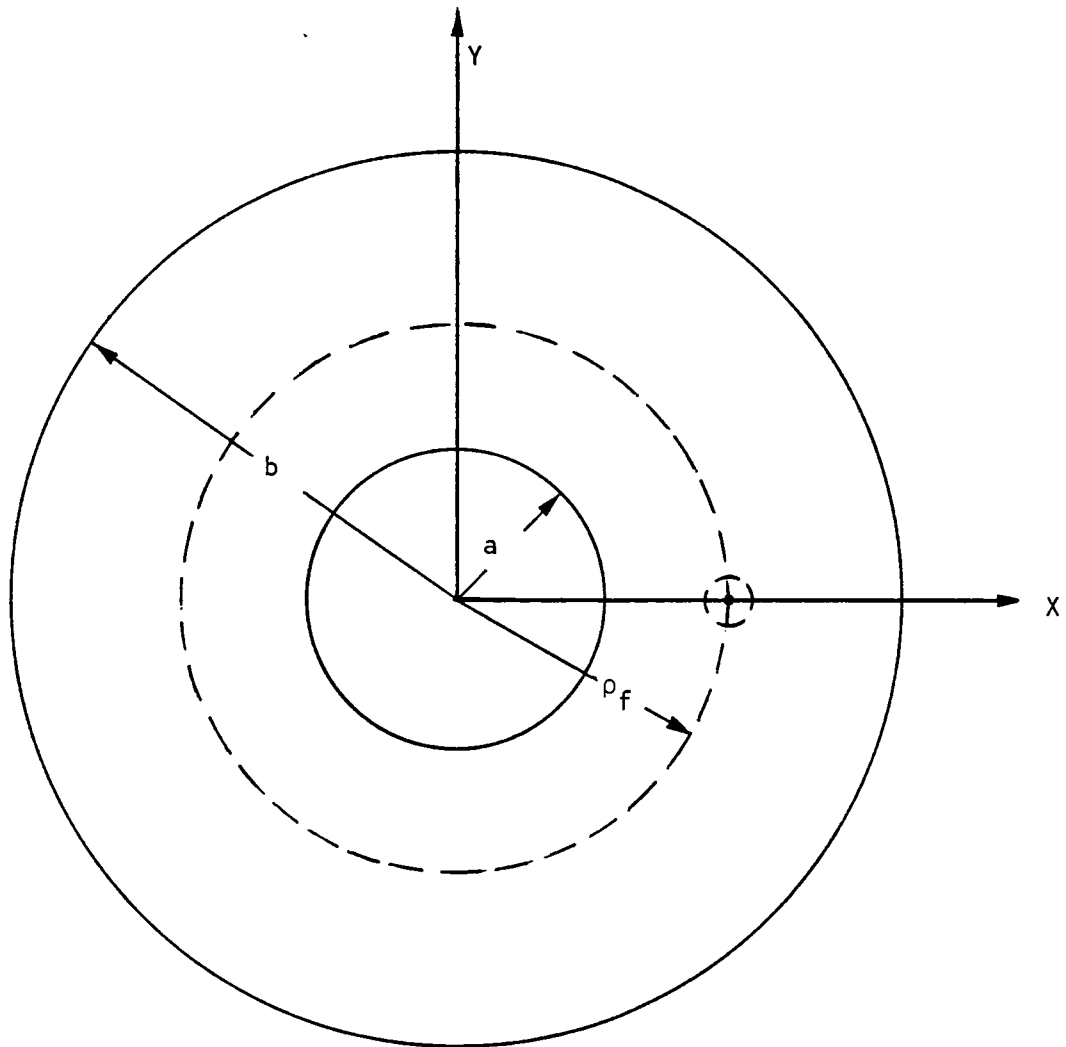
3-3 The Resonant Frequency

It was found that the resonant frequencies obtained by the characteristic equations in Chapter 2 agree with the measured resonant frequencies very well. (Here, the resonant frequencies were determined by identifying the frequency of minimum reflection coefficient). The tables 3-2-a,b,c,d,e compare these values for some of the lower modes.

3-4 The Input Impedance

As mentioned in Chapter 2, the input impedance can be computed by using the effective wave number very efficiently with the use of an acceleration method.

Figures 3-1 to 3-5 represent plots of the driving point impedance of five different microstrip antennas. Impedance was plotted both on Smith Charts and *versus* frequency. Measured results are plotted on the same of the same figures for comparison. It is clear from these results that the theory agrees well with the experimental measurements.



$a = 4.09 \text{ cm}$

$b = 12.26 \text{ cm}$

$\rho_f = 7.4 \text{ cm}$

Thickness = 0.146 cm

Dielectric const. = 2.55

Conductivity $\sigma = 222 \times 10^5 \text{ mho/m}$

Loss tangent $\delta = 0.0012$

Figure 3-1-a

18 MAR 81

ANNULUS

4.09CM IR, 12.26CM O

1.00

.30

3.00

X=0

MEAS 1

 R/Z_0
 $=$
 2.055

 $IMAG$
 $=$
 -2.321

 $FREQ$
 $=$
 382.000

REF PLANE EXT= 1.15CM

 $\Gamma_{max}=1.0000$

NEXT

Figure 3-1-b: The experimental loci of the input impedance
for the antenna element of figure 3-1-a

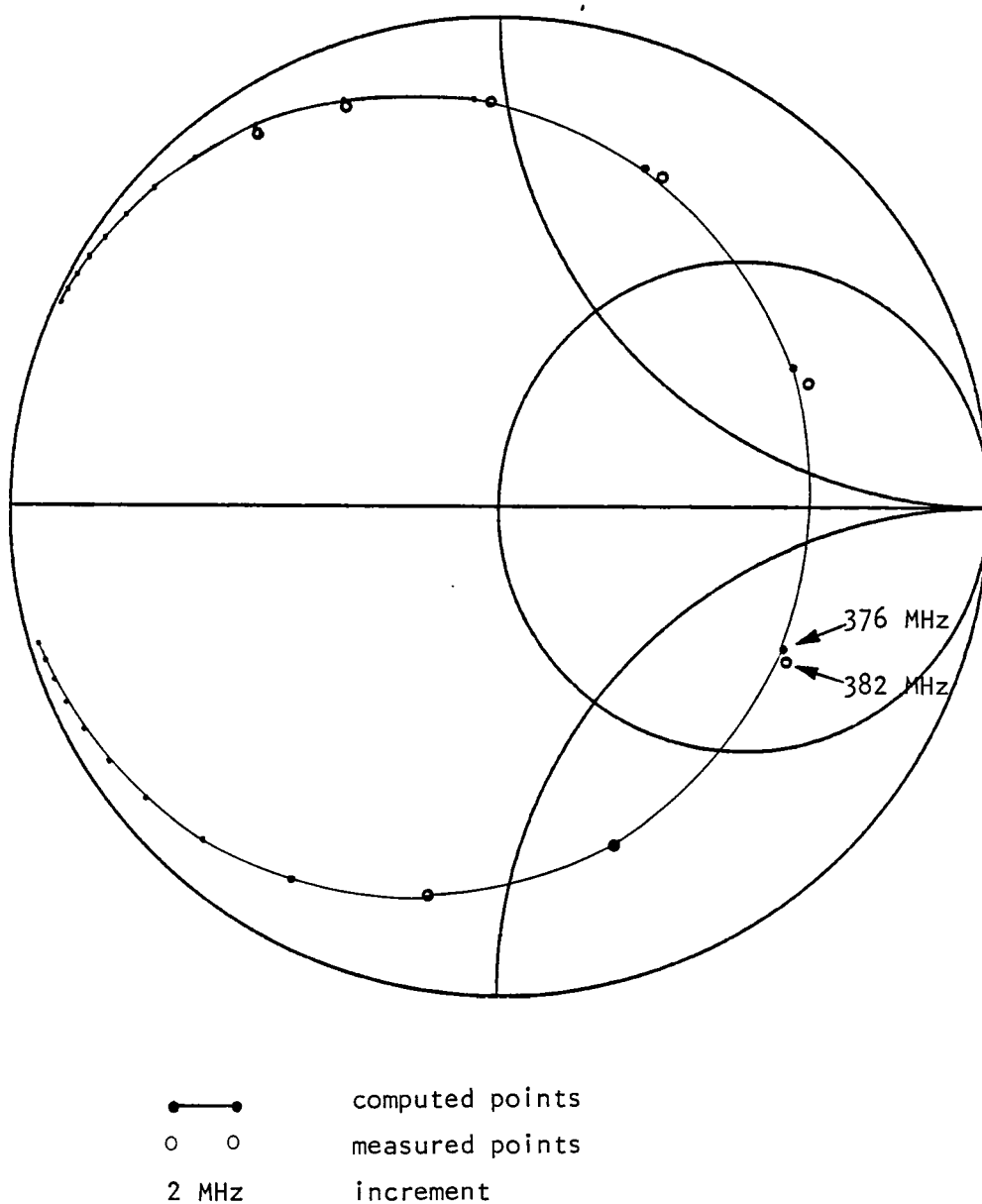


Figure 3-1-c: Calculated and measured input impedance loci for the antenna element of figure 3-1-a

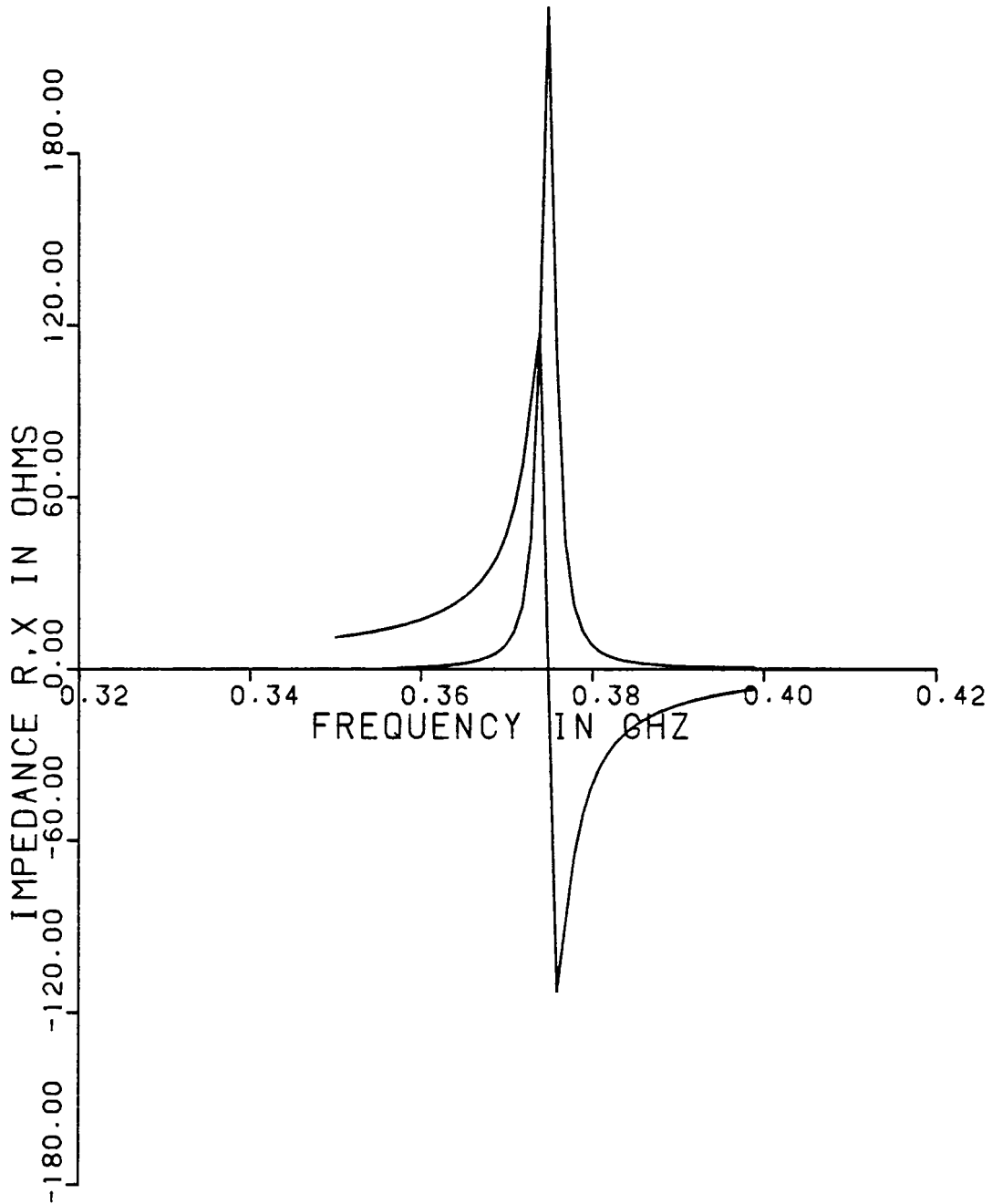
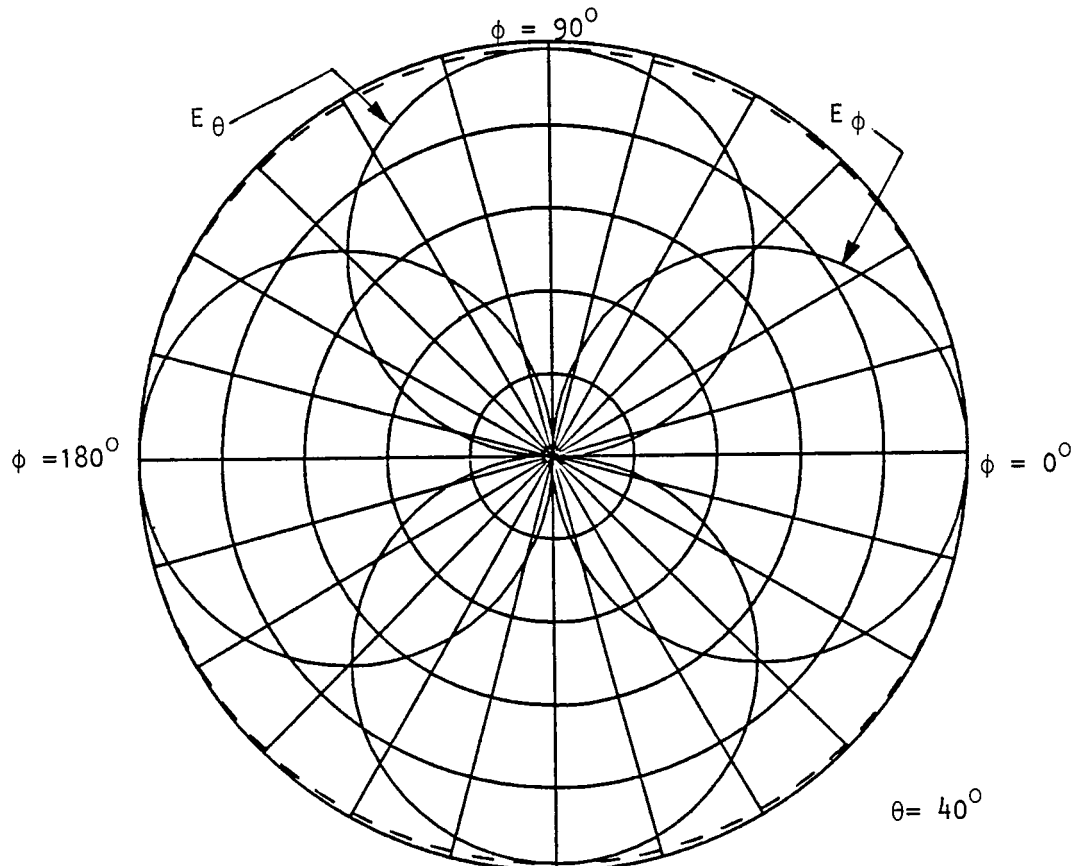


Figure 3-1-d: Calculated input impedance vs. freq. for the antenna element of figure 3-1-a



Mode $(n,m) = (1,1)$

$\phi = 270^\circ$ ---- Poynting vector

Frequency = 375.5 MHz

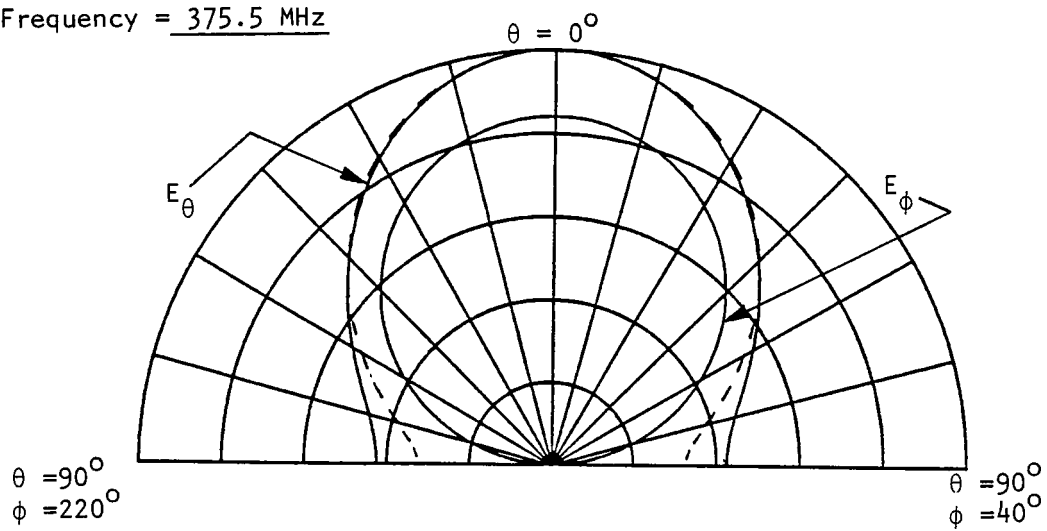


Figure 3-1-e: Calculated radiation pattern for the antenna element of figure 3-1-a

18 MAR 81

ANNULUS

4.09CM IR, 12.26CM O

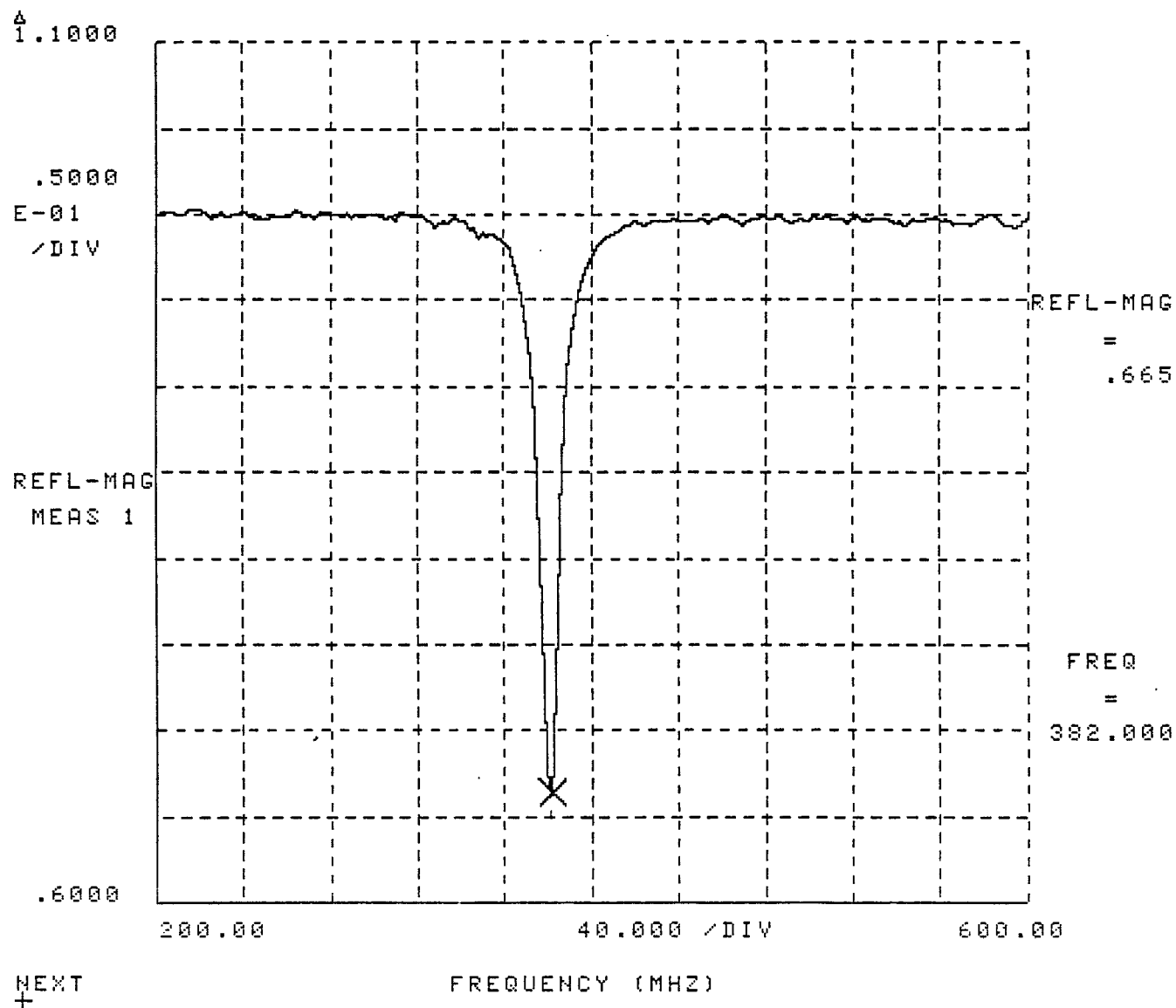


Figure 3-1-f: Experimental reflection coefficient for the microstrip element of figure 3-1-a

18 MAR 81

ANNULUS
4.09CM IR 12.26CM OR

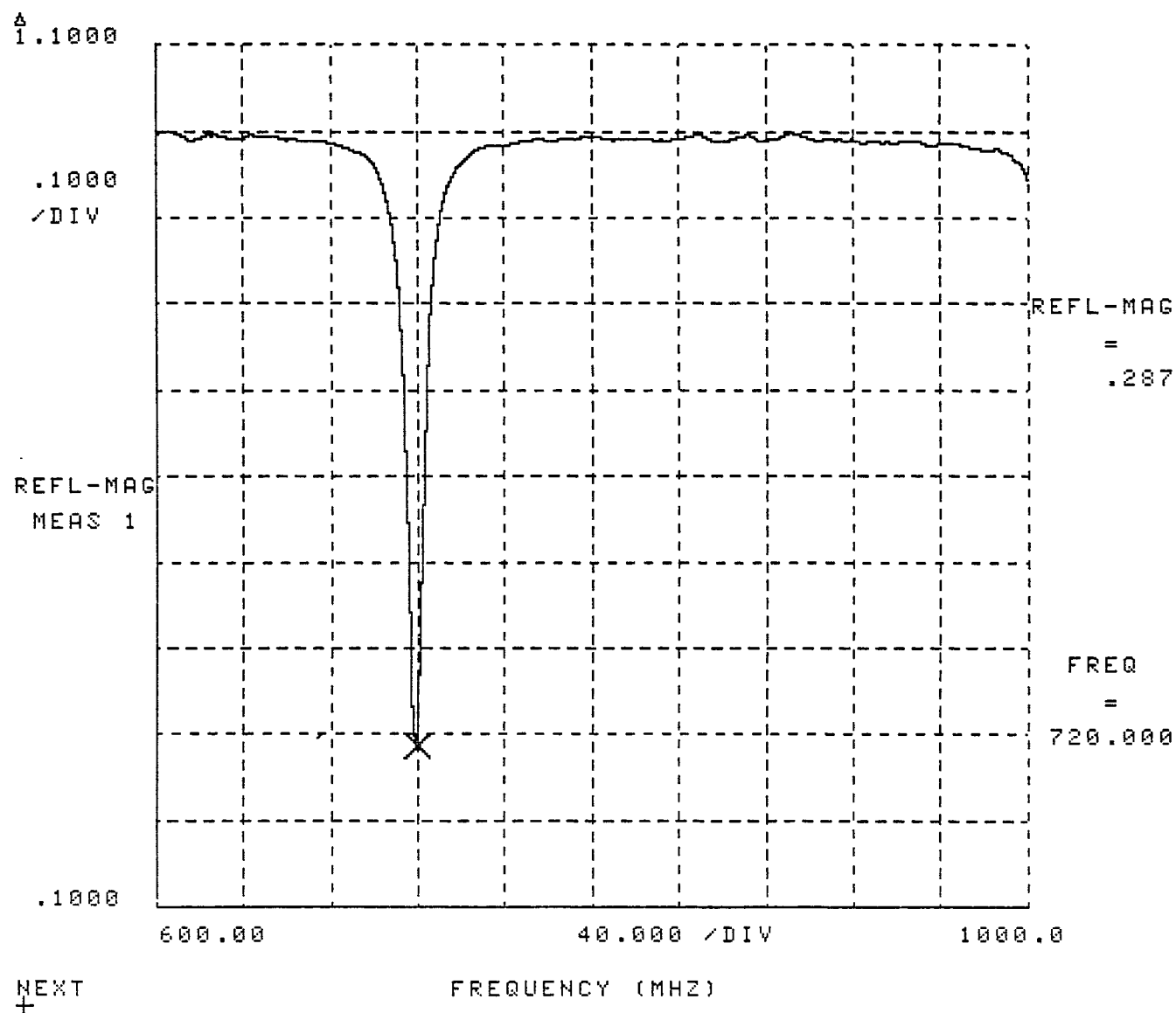


Figure 3-1-f: Continued

18 MAR 81

ANNULUS
4.09CM IR 12.26CM OR

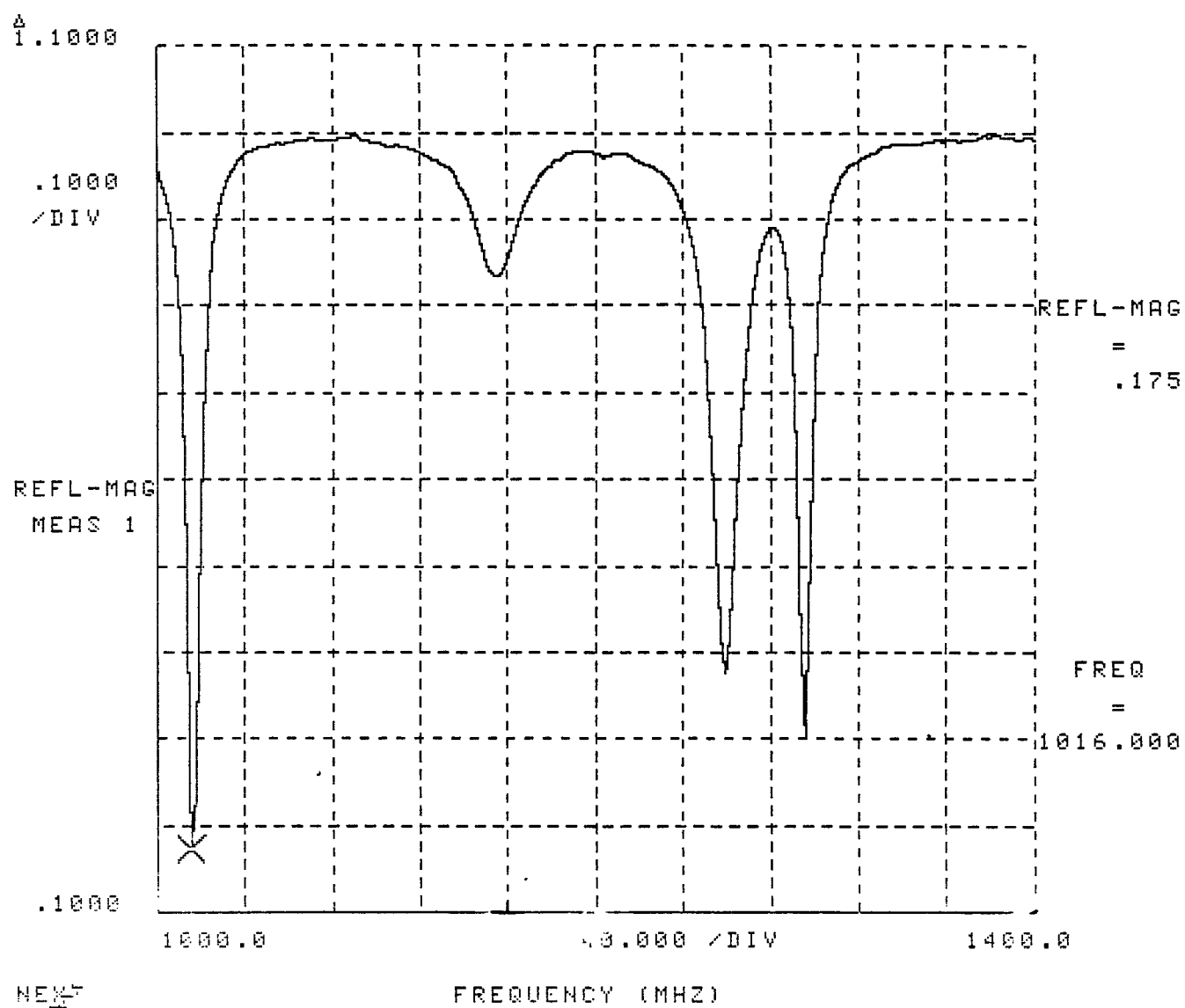


Figure 3-1-f: Continued

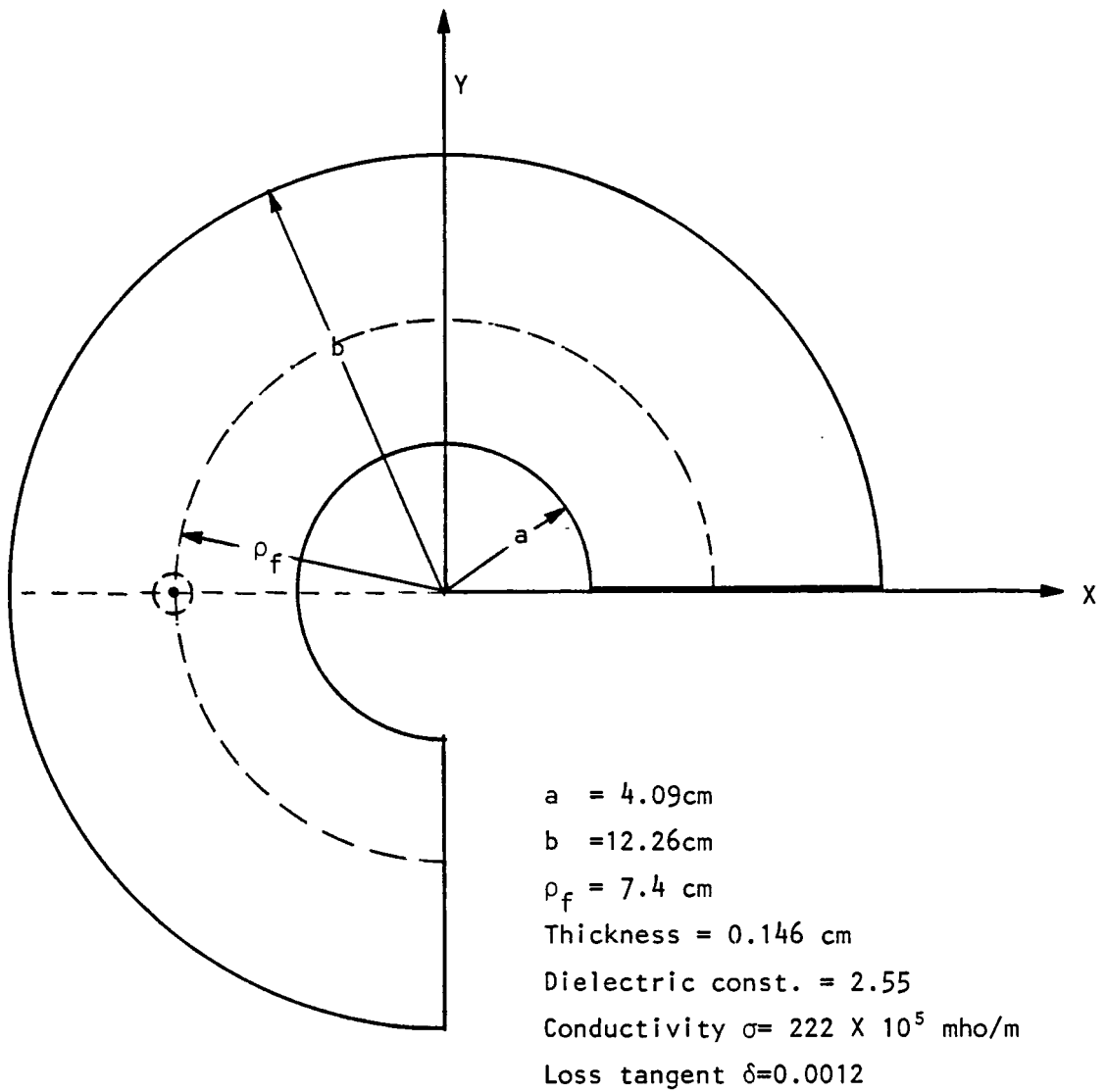


Figure 3-2-a

270 DEG. ANNULUS SECTOR
4.09CM IR 12.26CM OR

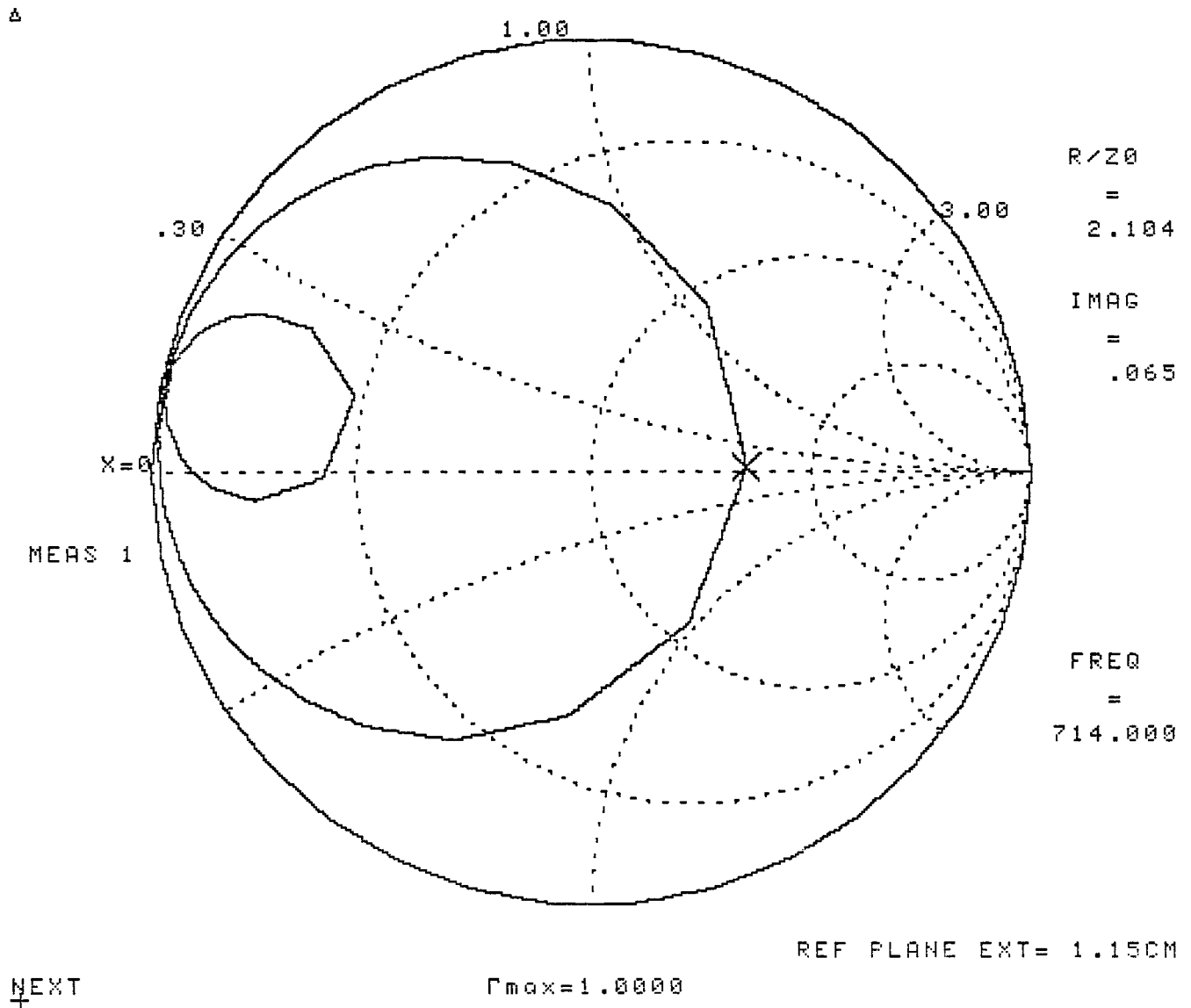


Figure 3-2-b: Measured input impedance for the antenna element of figure 3-2-a

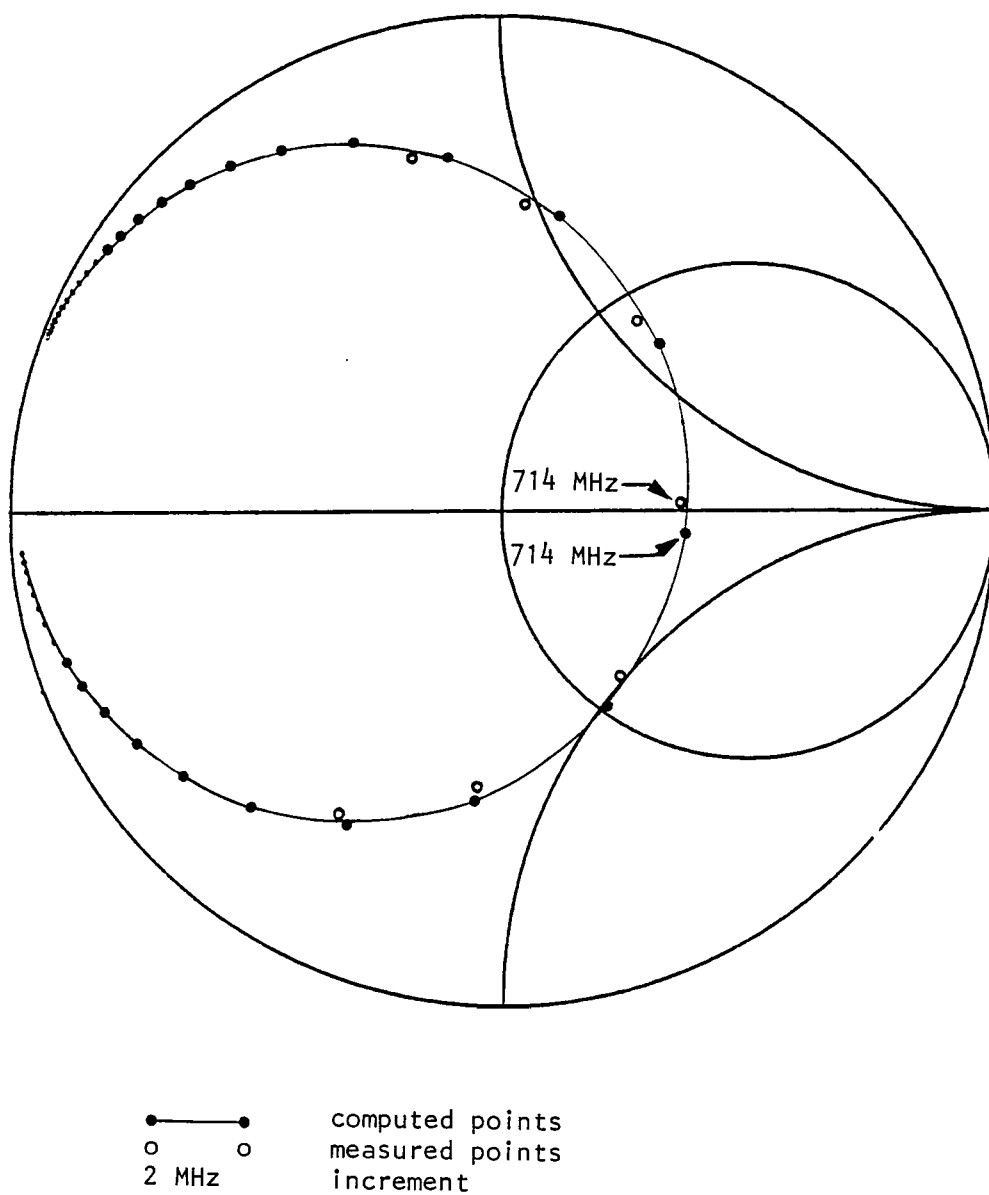


Figure 3-2-c: Calculated and measured input impedance loci for the antenna element of figure 3-2-a

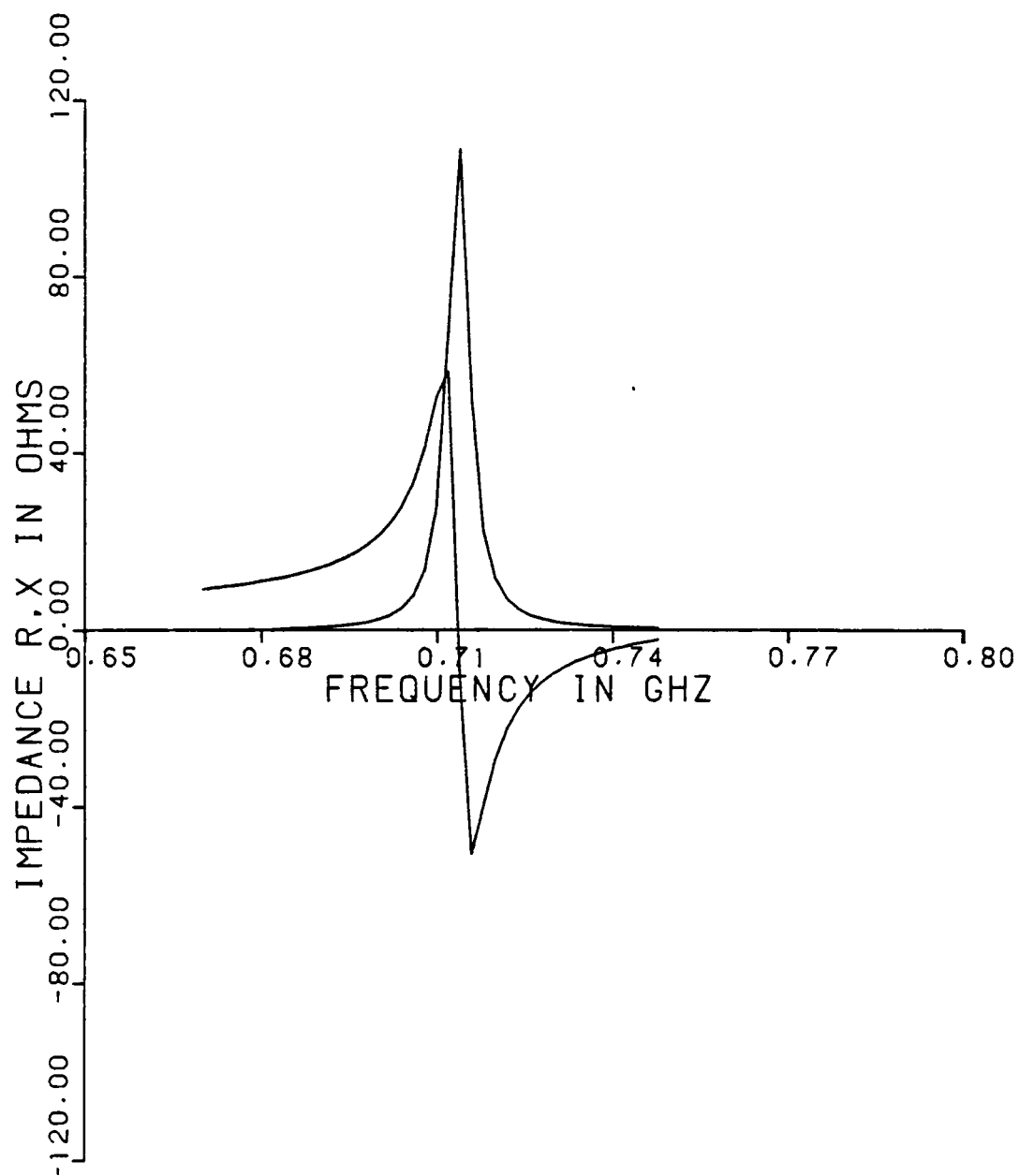
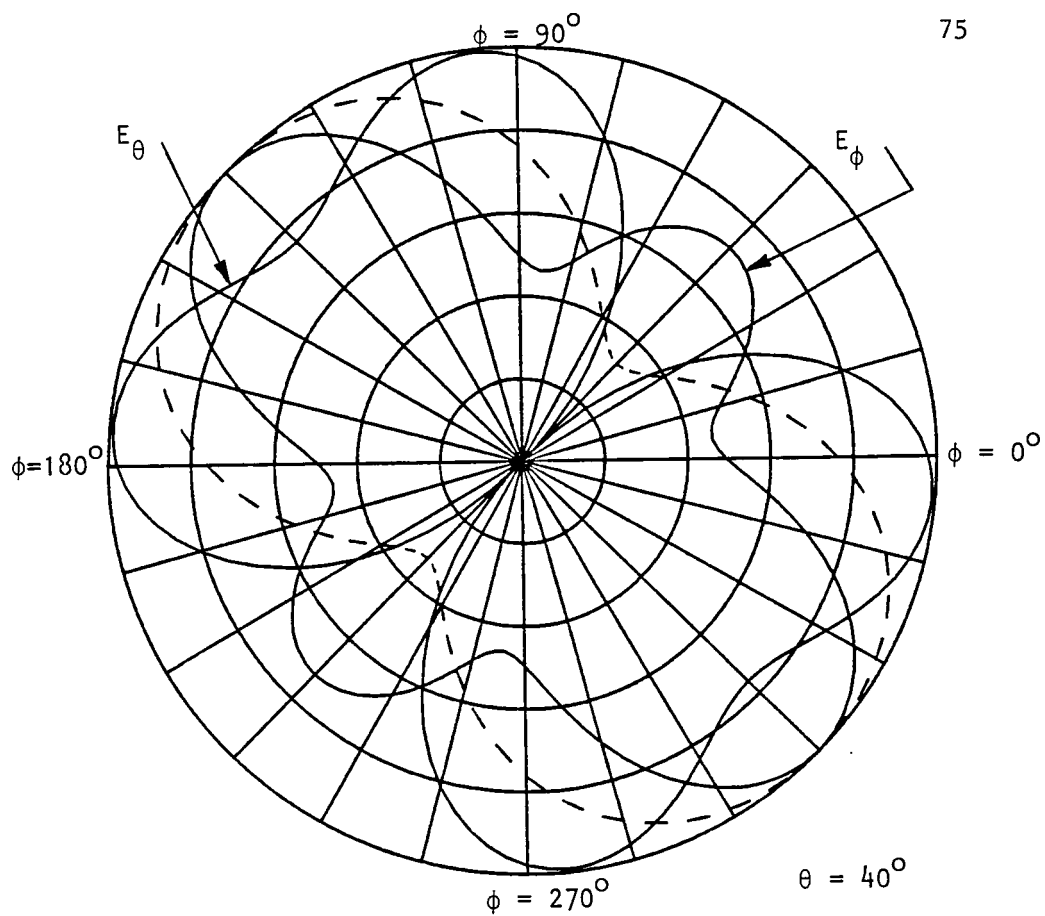


Figure 3-2-d: Calculated input impedance vs. frequency for the microstrip antenna element of fig. 3-2-a



Mode $(\nu, p, m) = (2, 3, 1)$

Frequency = 714.5 MHz

---- Poynting vector

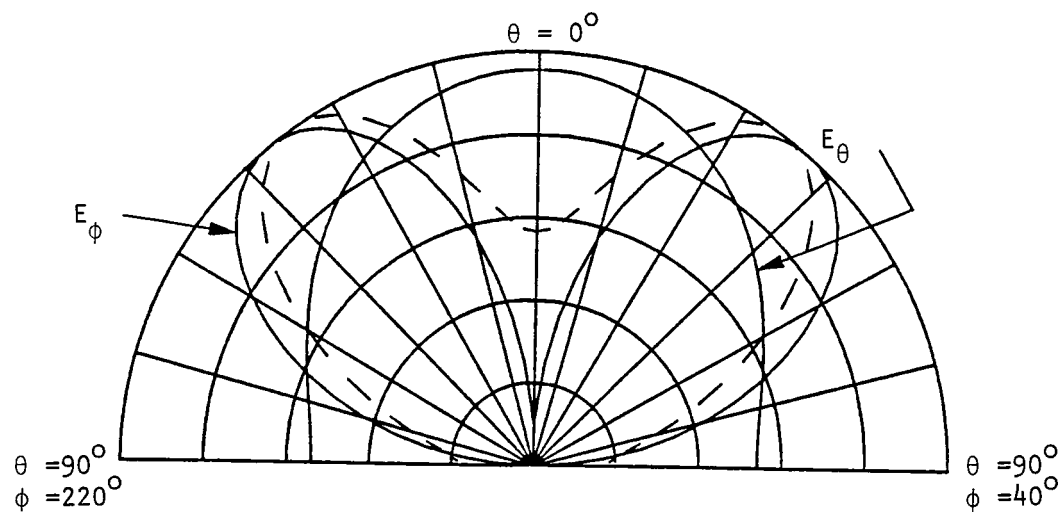


Figure 3-2-e: Calculated radiation pattern for the antenna element of figure 3-2-a

18 MAR 81

270 DEG. ANNULUS SECTOR
4.09CM IR 12.26CM OR

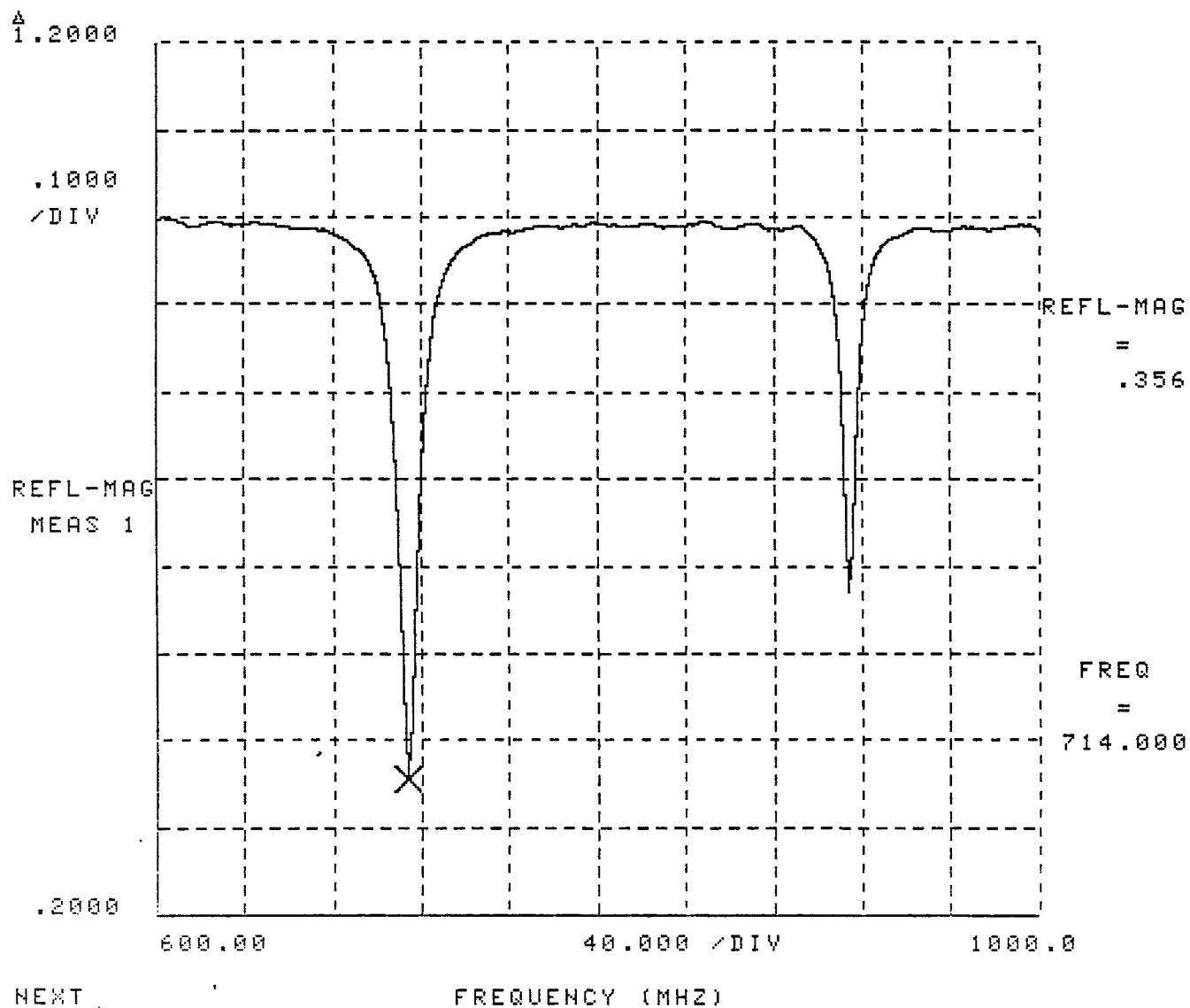


Figure 3-2-f: Experimental reflection coefficient vs. frequency
for the microstrip antenna element of figure 3-2-a.

18 MAR 81

270 DEG. ANNULUS SECTOR
4.09CM IR 12.26CM OR

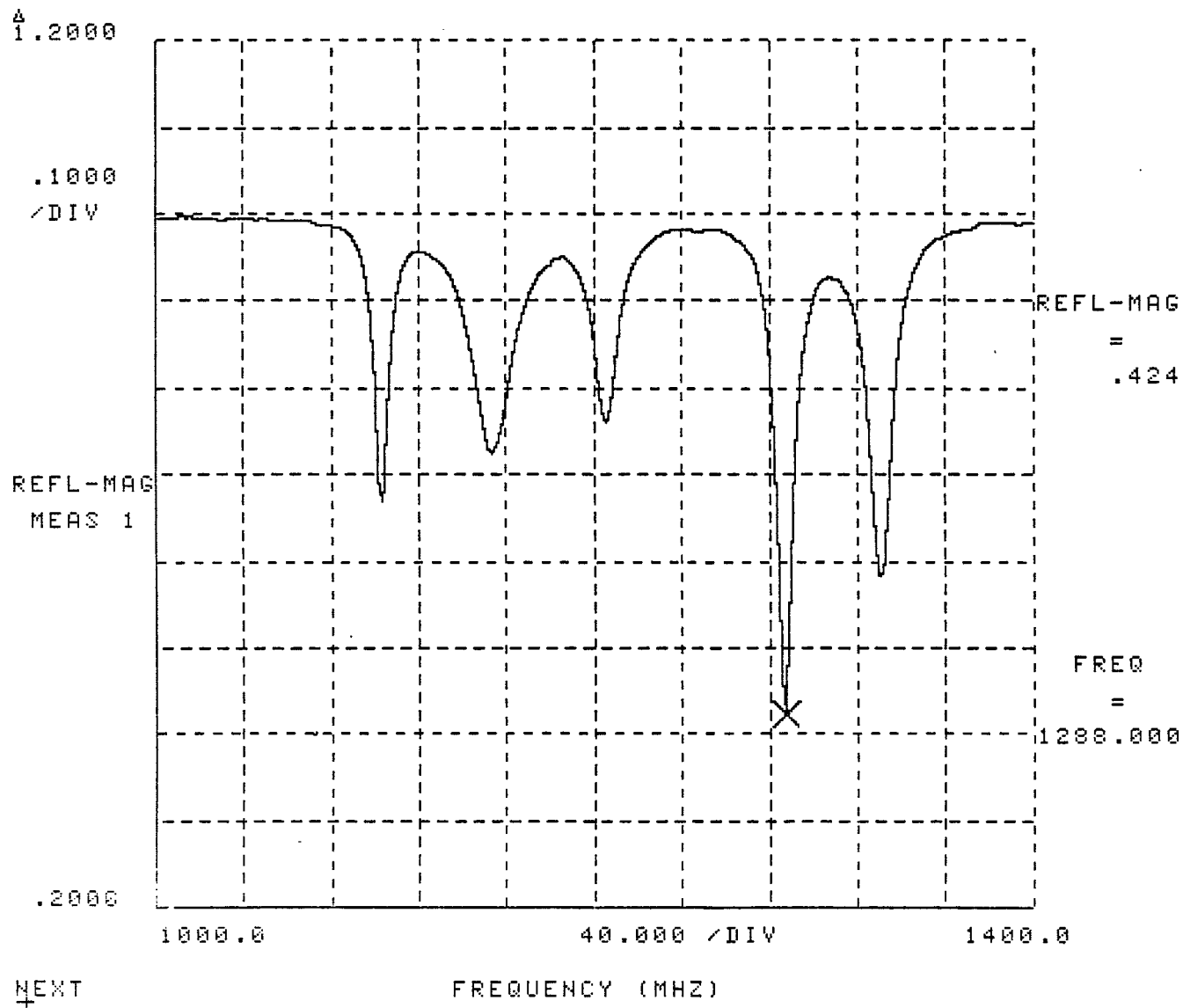


Figure 3-2-f: Continued

18 MAR 81

40 DEG CIRCULAR SECTOR
4.09CM IR 12.26CM OR

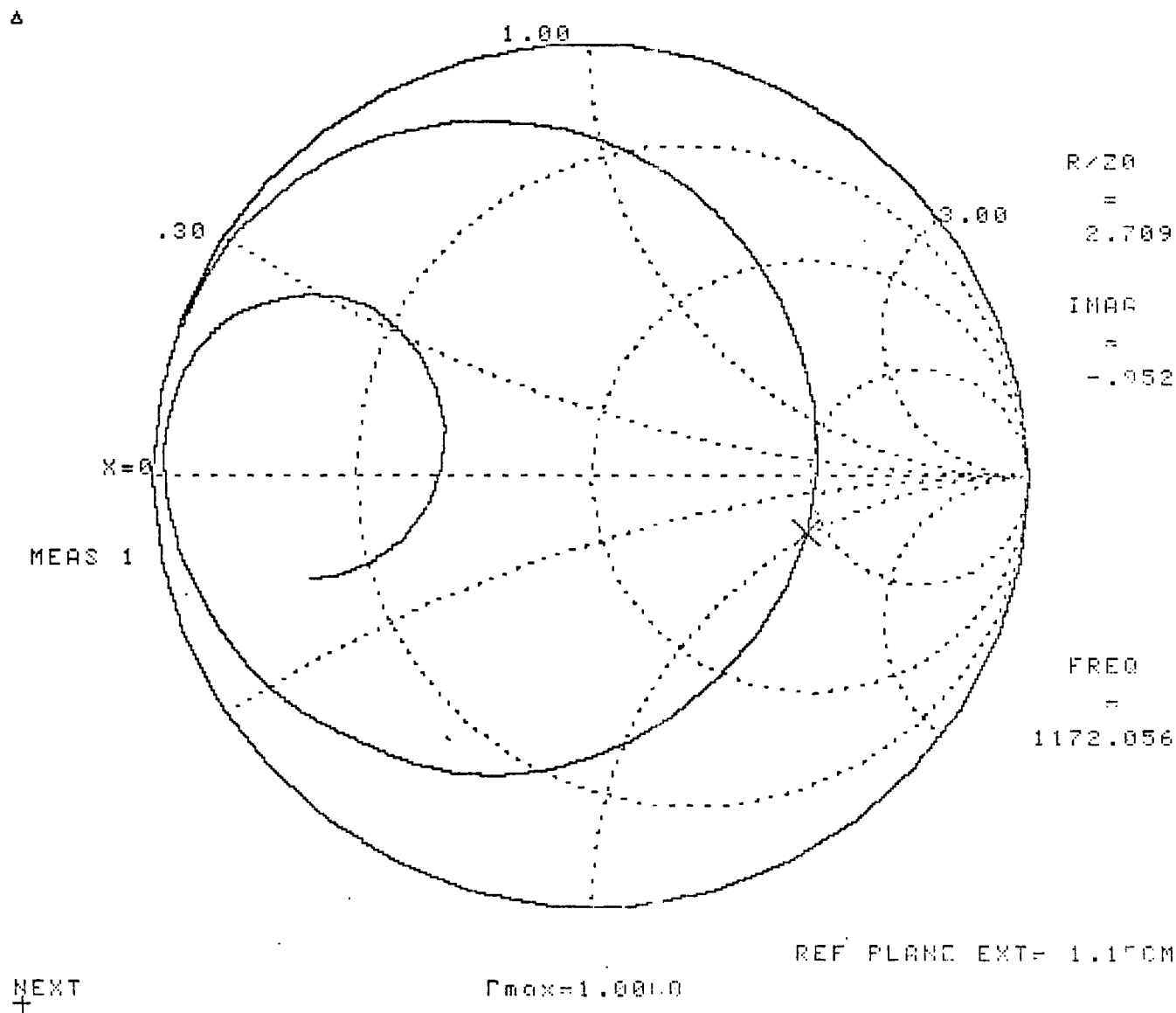


Figure 3-3-b: Measured input impedance for the antenna element
of figure 3-3-a

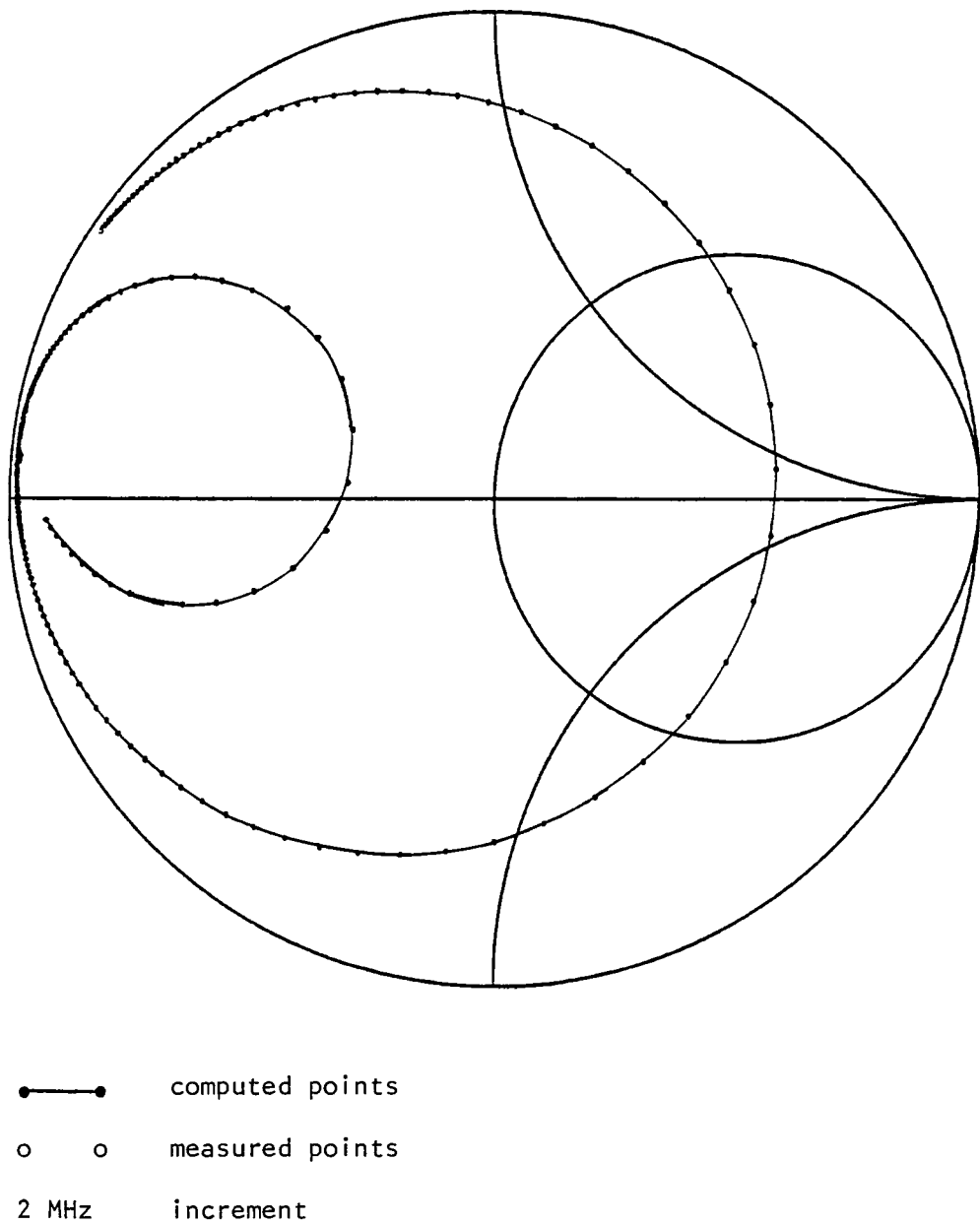


Figure 3-3-c: Calculated input impedance loci for the antenna element of figure 3-3-a

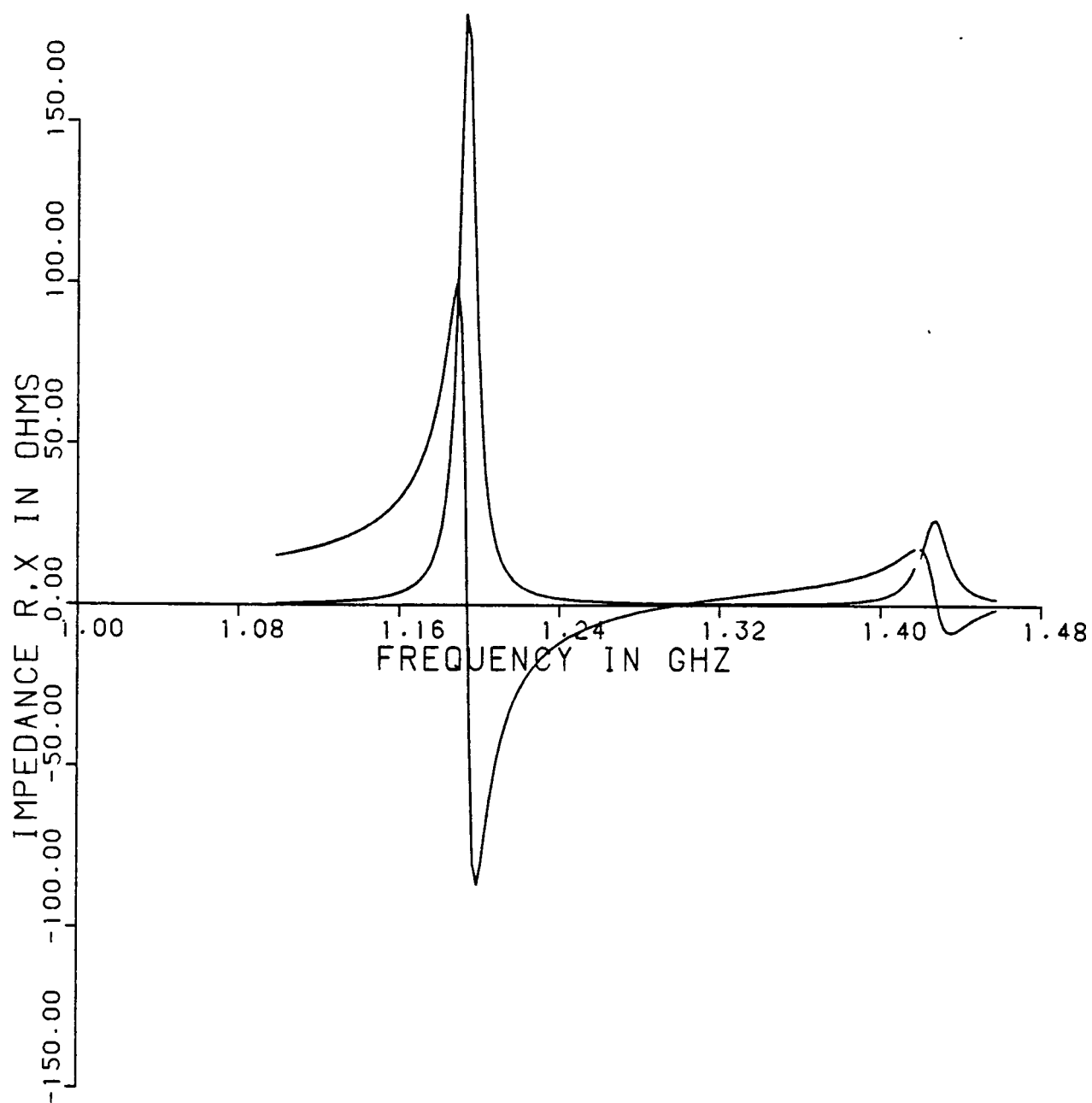
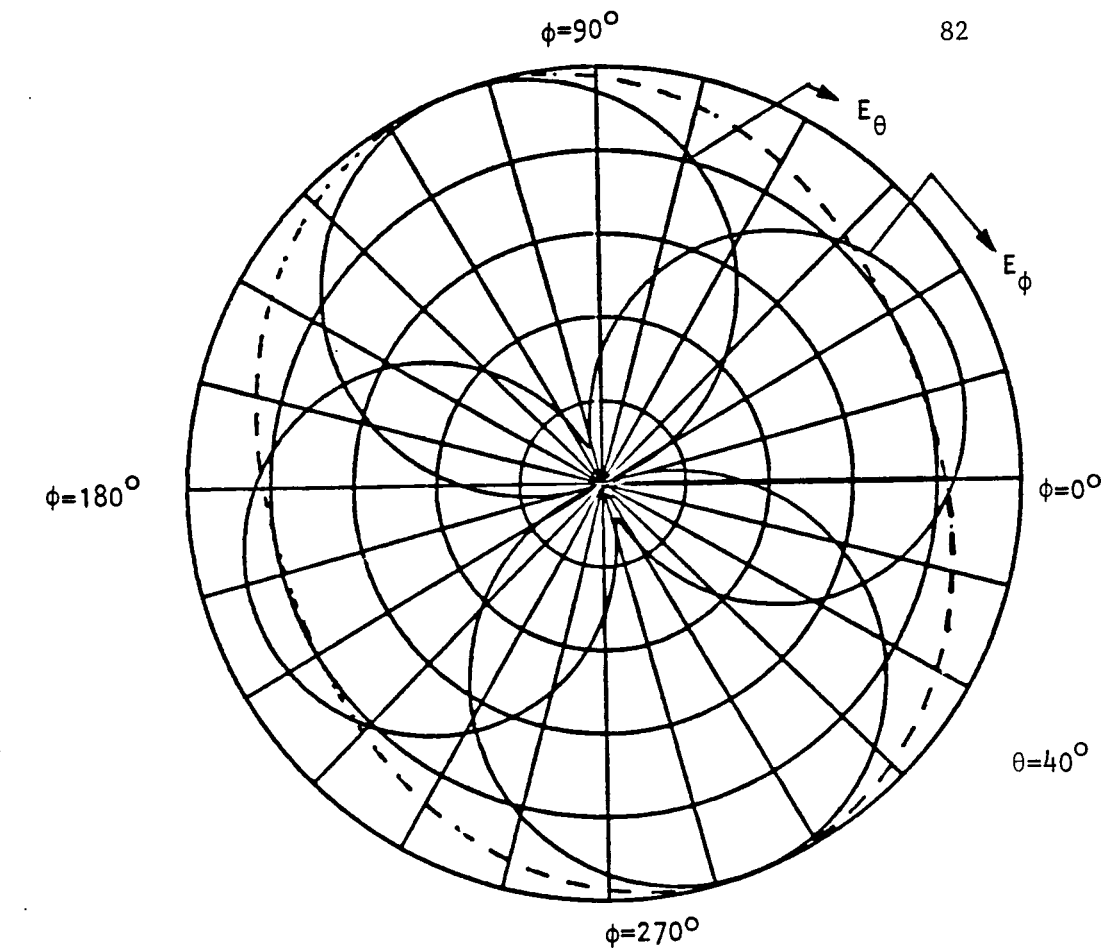


Figure 3-3-d: Calculated input impedance vs. frequency for the microstrip antenna element of figure 3-3-a



---- Poyntine vector

Mode $(\nu, p, m) = (4.5, 1, 1)$

Frequency = 1428.7 MHz

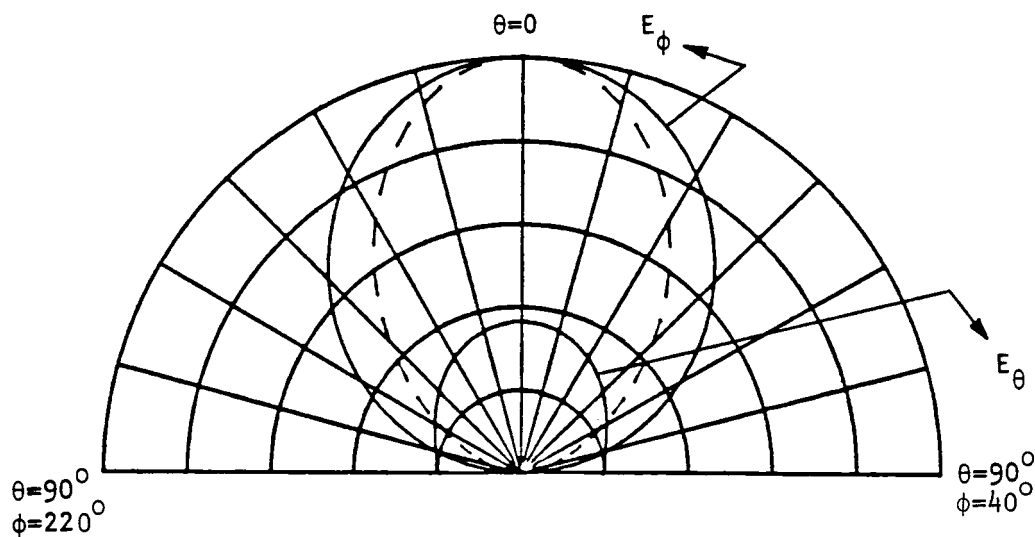


Figure 3-3-e: Calculated radiation pattern for the antenna element of figure 3-3-a

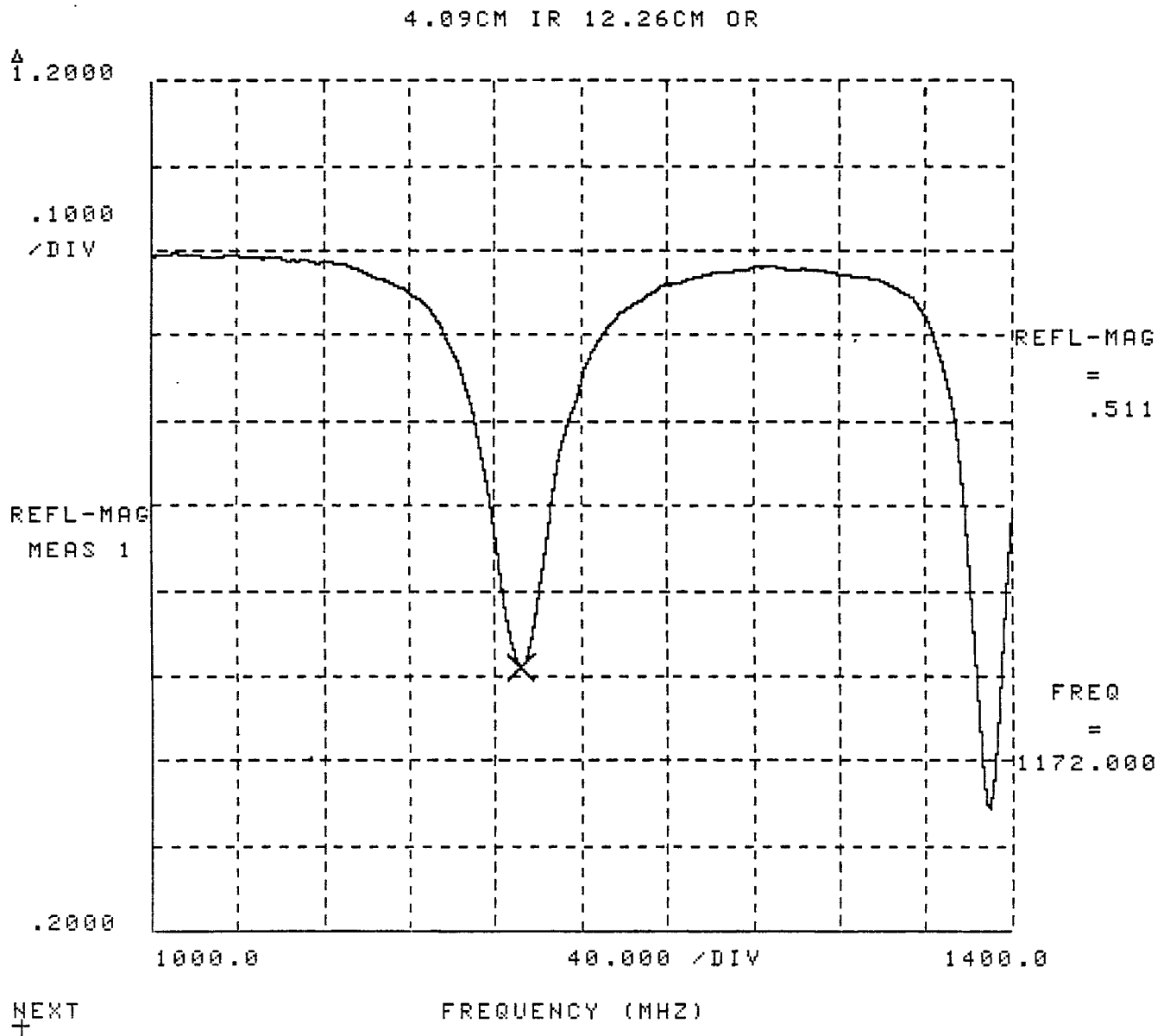


Figure 3-3-f: Measured reflection coefficient vs. frequency for the microstrip antenna element of fig. 3-3-a.

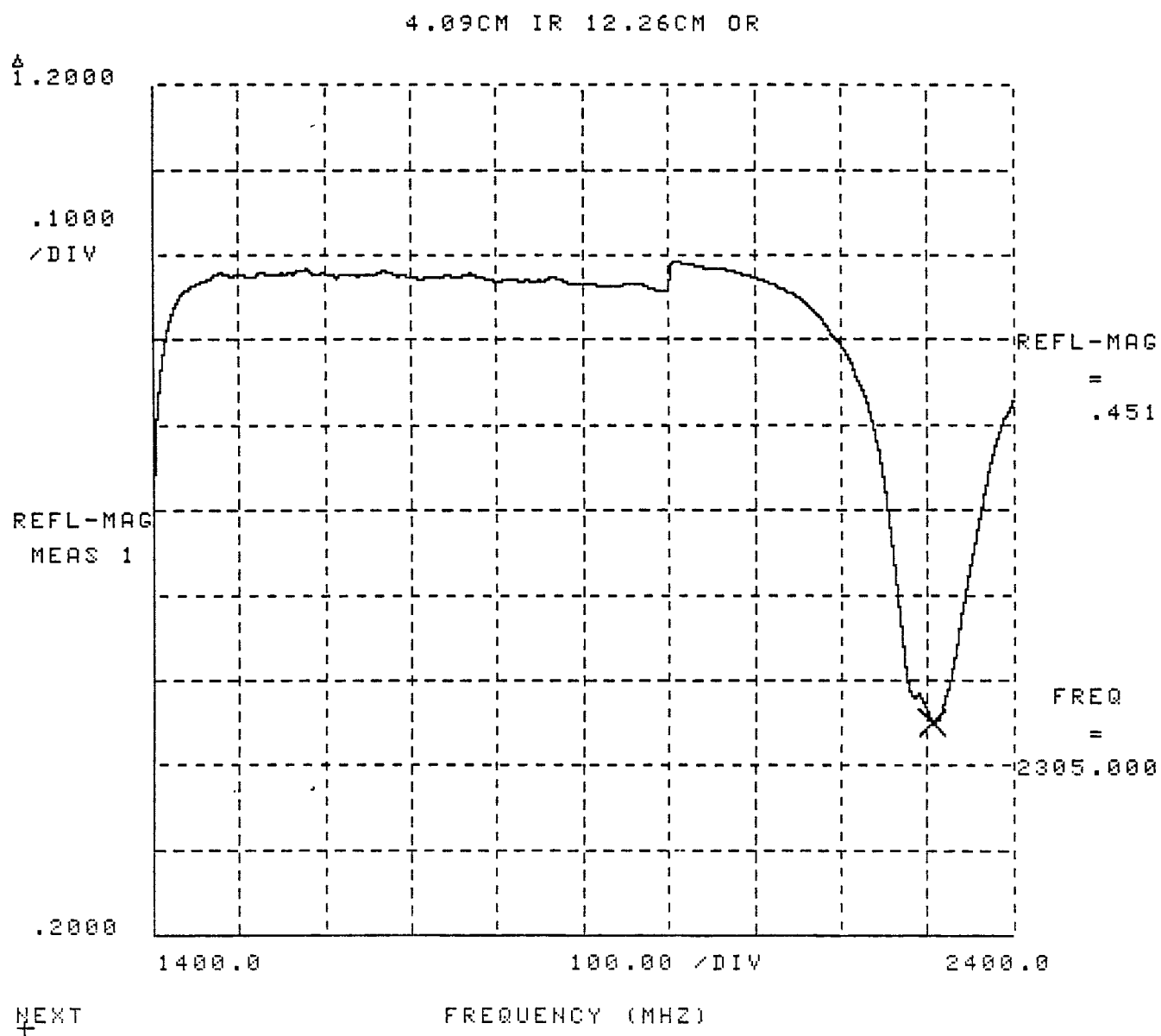
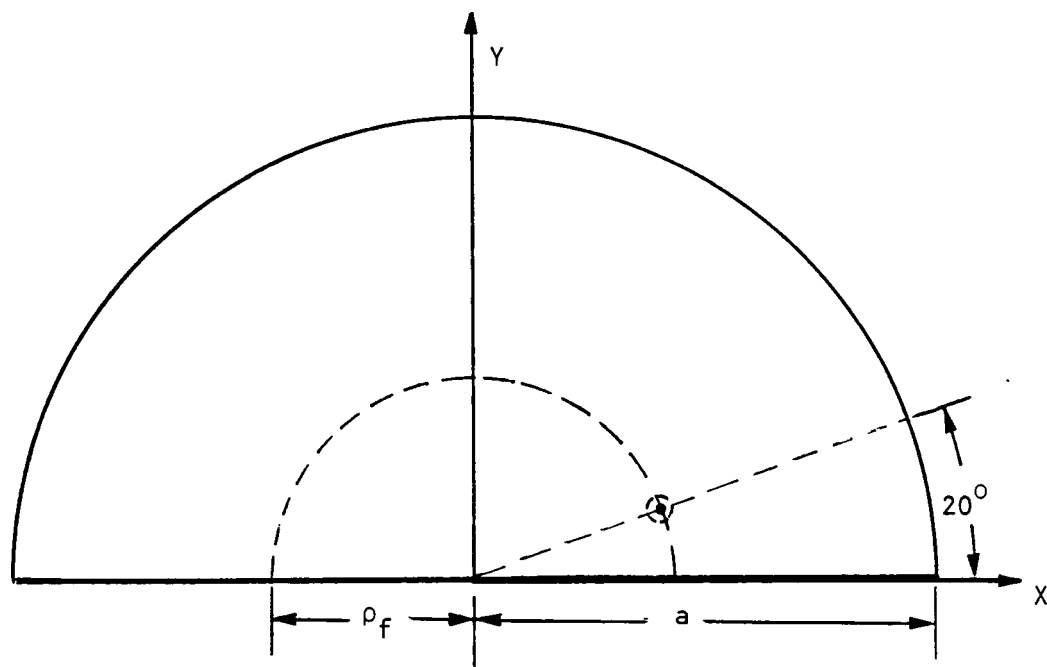


Figure 3-3-f: Continued



$$a = 11.7 \text{ cm}$$

$$\rho_f = 5.2 \text{ cm}$$

$$\text{Thickness} = 0.146 \text{ cm}$$

$$\text{Dielectric const.} = 2.55$$

$$\text{Conductivity } \sigma = 222 \times 10^5 \text{ mho/m}$$

$$\text{Loss tangent } \delta = 0.0012$$

Figure 3-4-a

18 MAR 81

HALF DISC
11.70 CM RADIUS

Δ

1.00

.30

3.00

R/Z_0
=
2.342

IMAG
=
-1.694

X=0

MERS 1

FREQ
=
470.000

NEXT
+

 $\Gamma_{max}=1.0000$

REF PLANE EXT= 1.15CM

Figure 3-4-b: Measured input impedance loci for the antenna element of figure 3-4-a

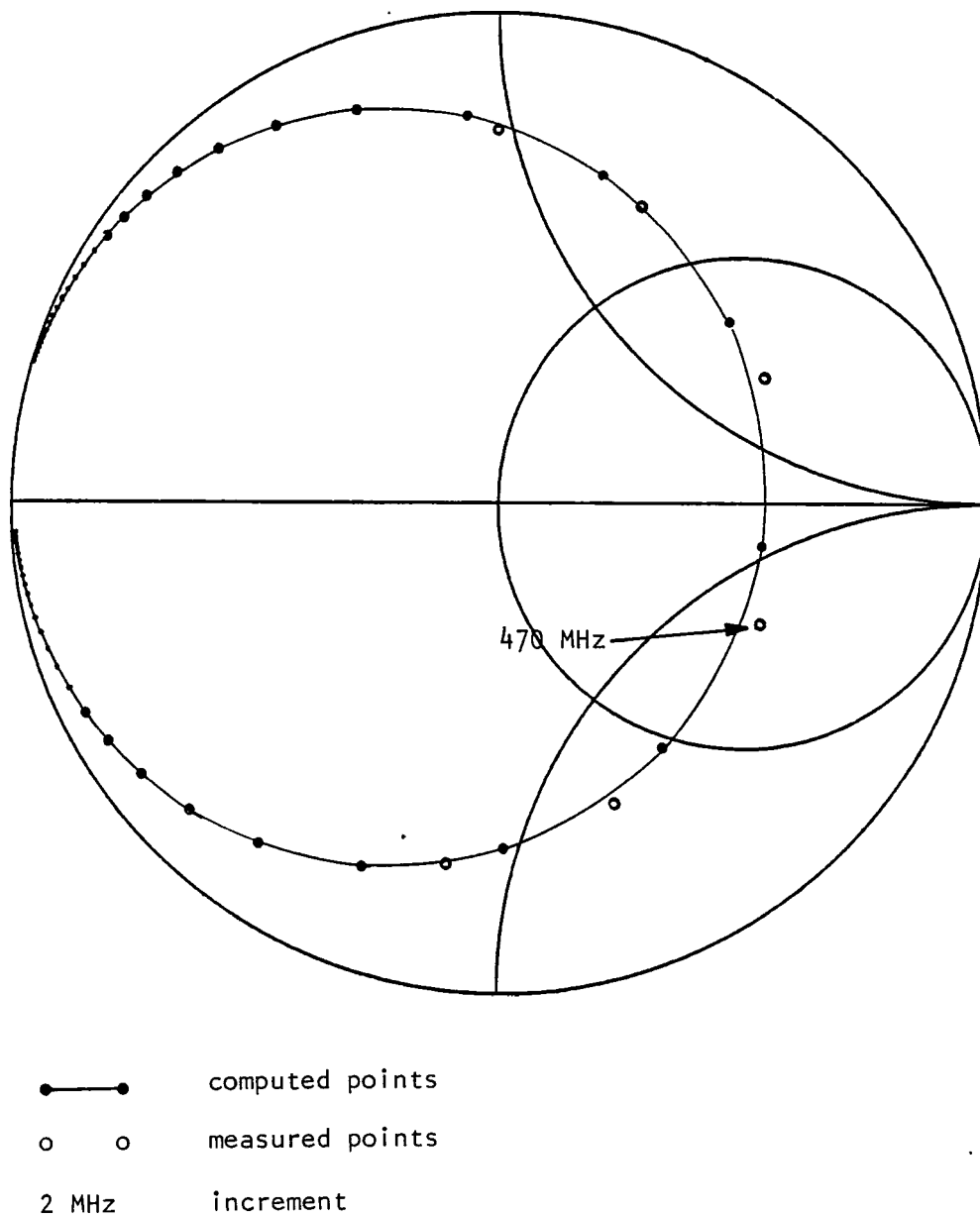


Figure 3-4-c: Calculated and measured input impedance loci for the antenna element of figure 3-4-a.

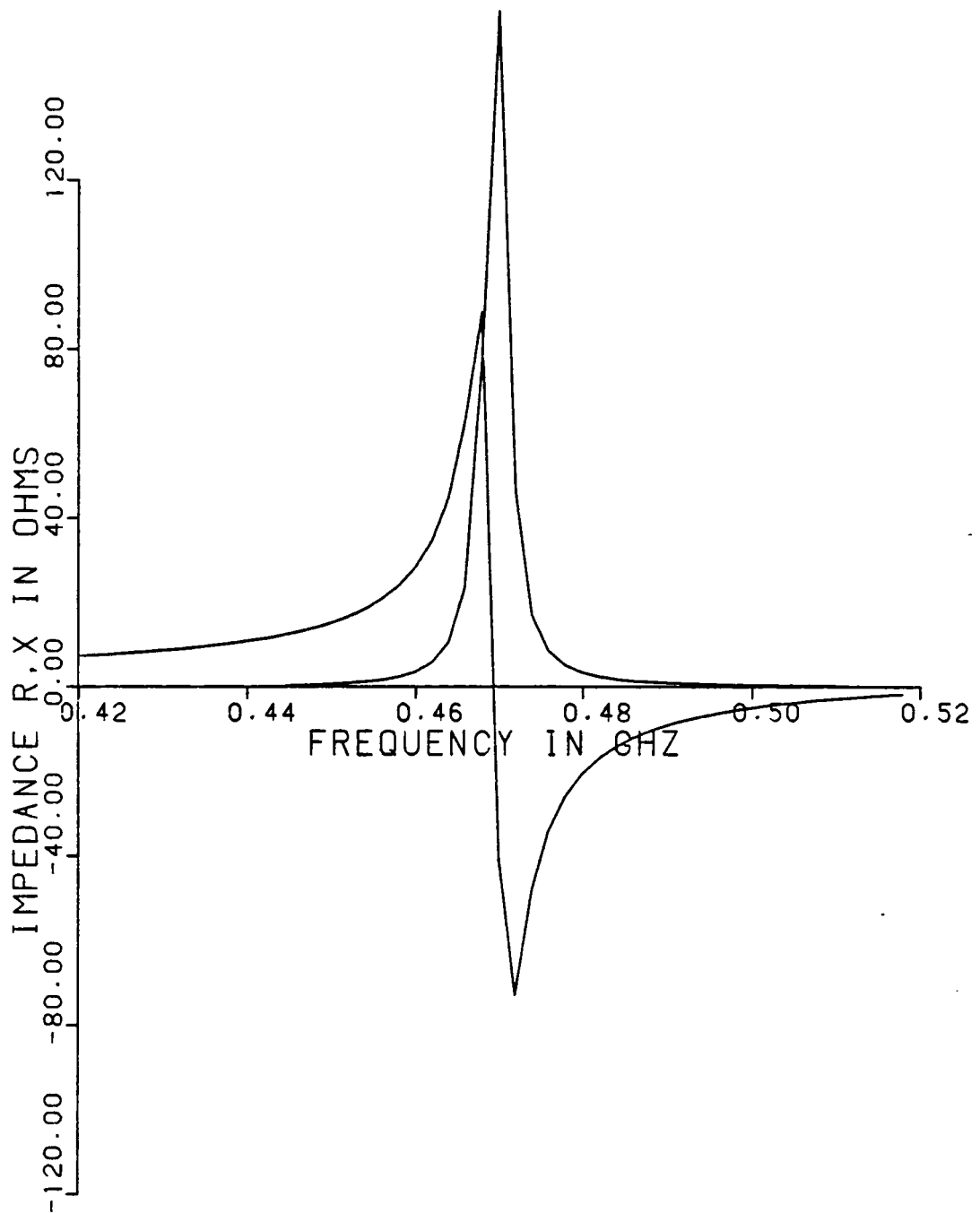


Figure 3-4-d: Calculated input impedance vs. frequency for the microstrip antenna element of figure 3-4-a.

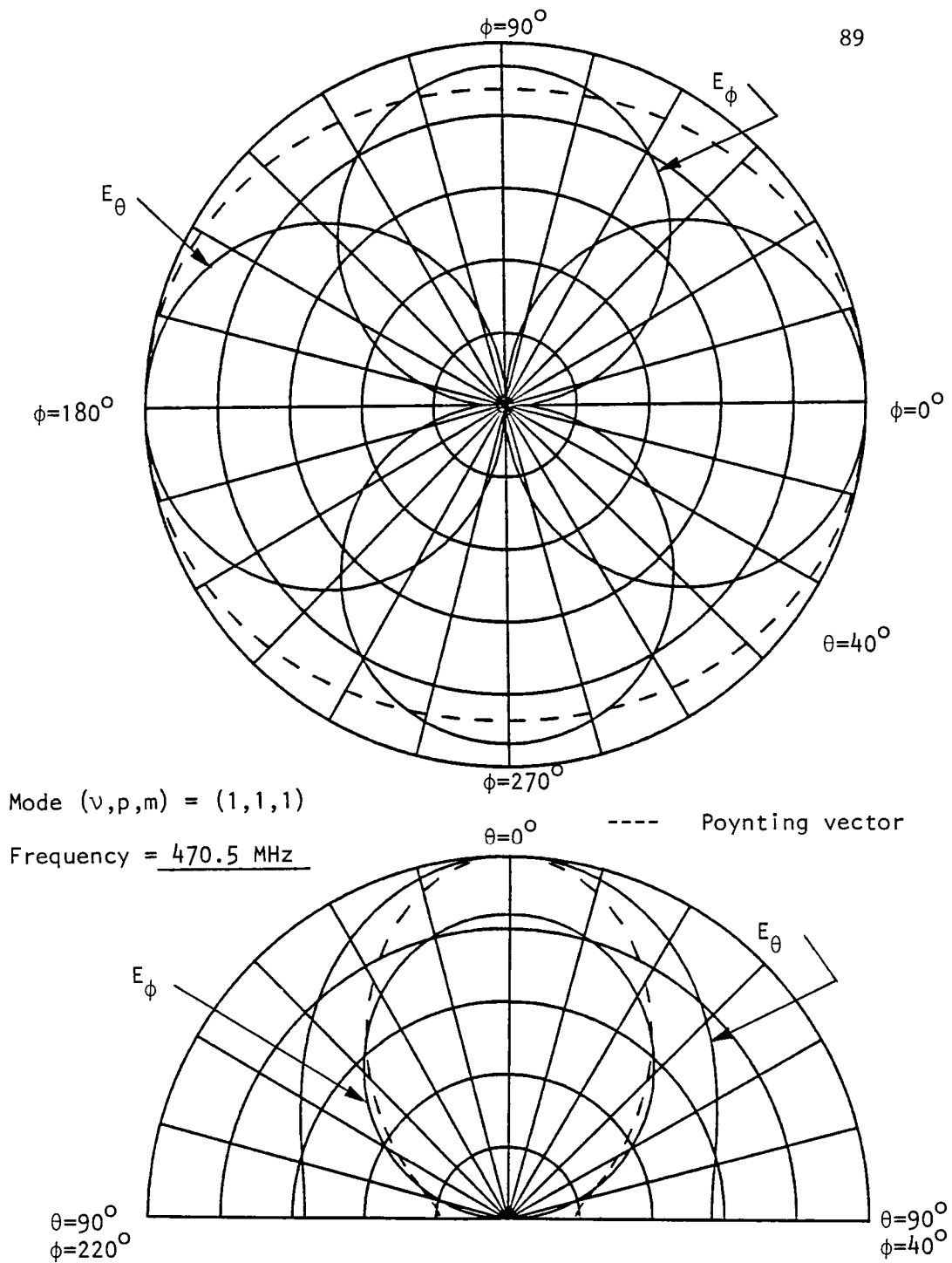


Figure 3-4-e: calculated radiation pattern for the antenna element of figure 3-4-a.

18 MAR 81

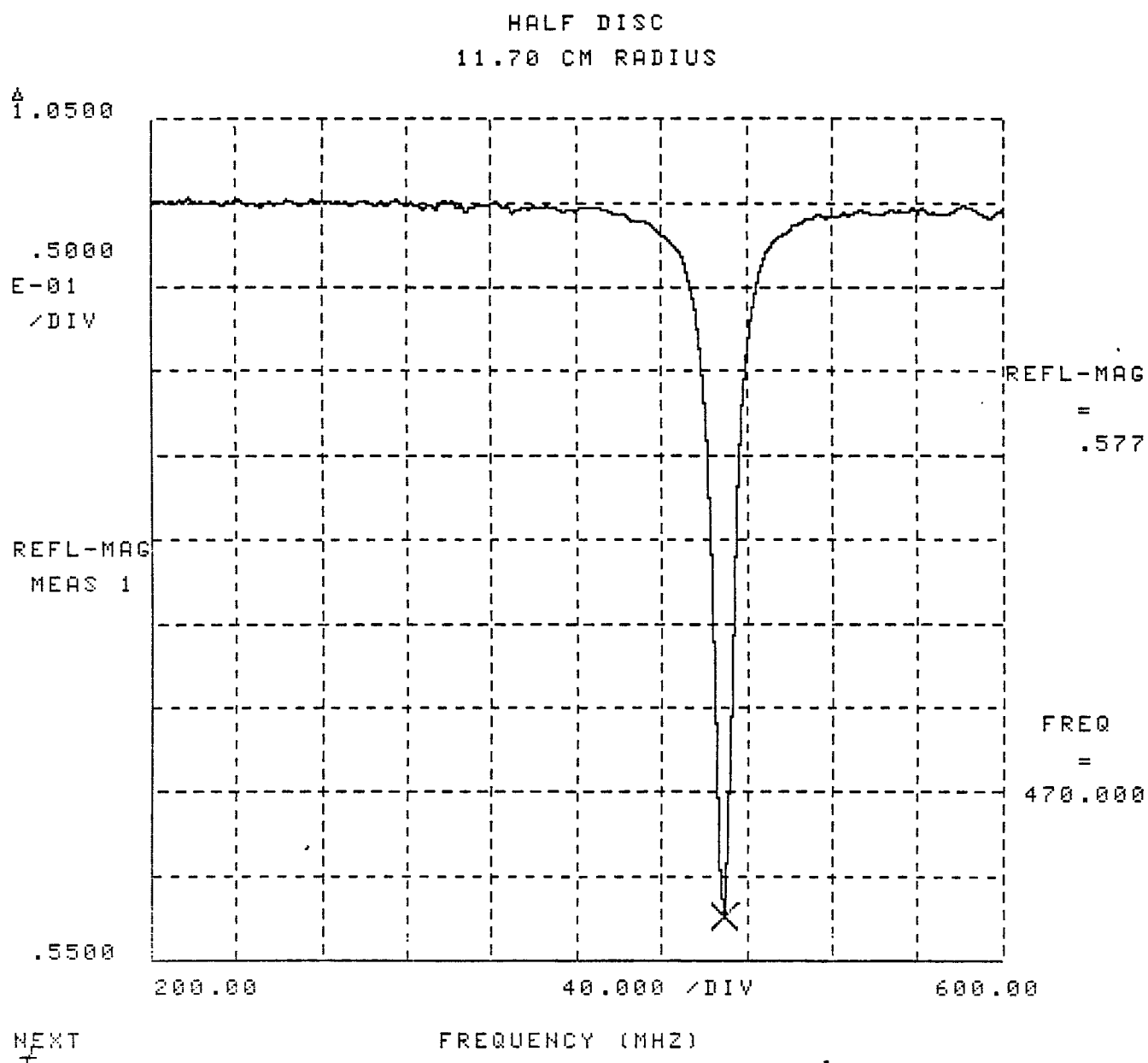


Figure 3-4-f: Measured reflection coefficient vs. frequency
for the antenna element of figure 3-4-a.

HALF DISC
11.70 CM RADIUS

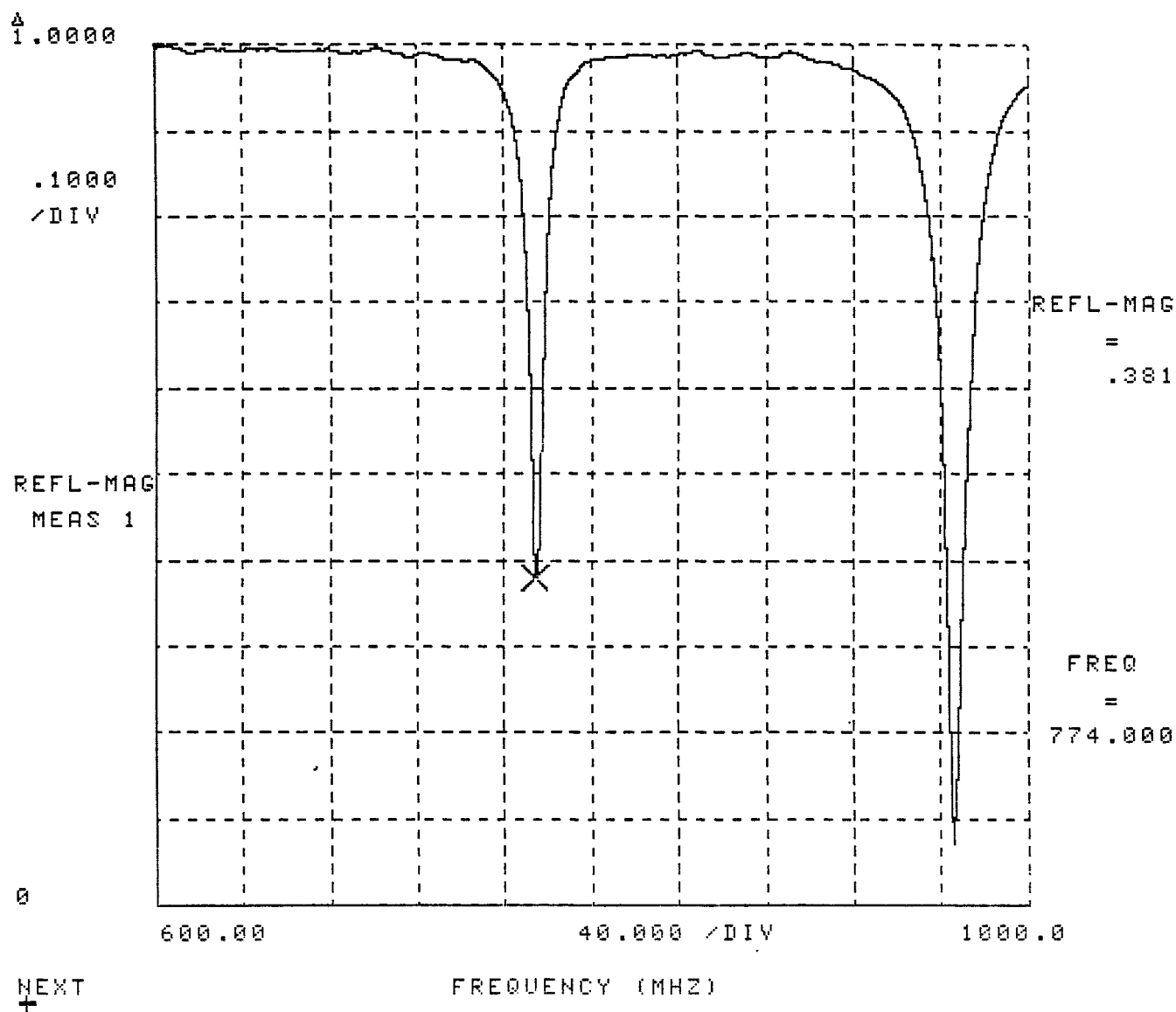


Figure 3-4-f: Continued

18 MAR 81

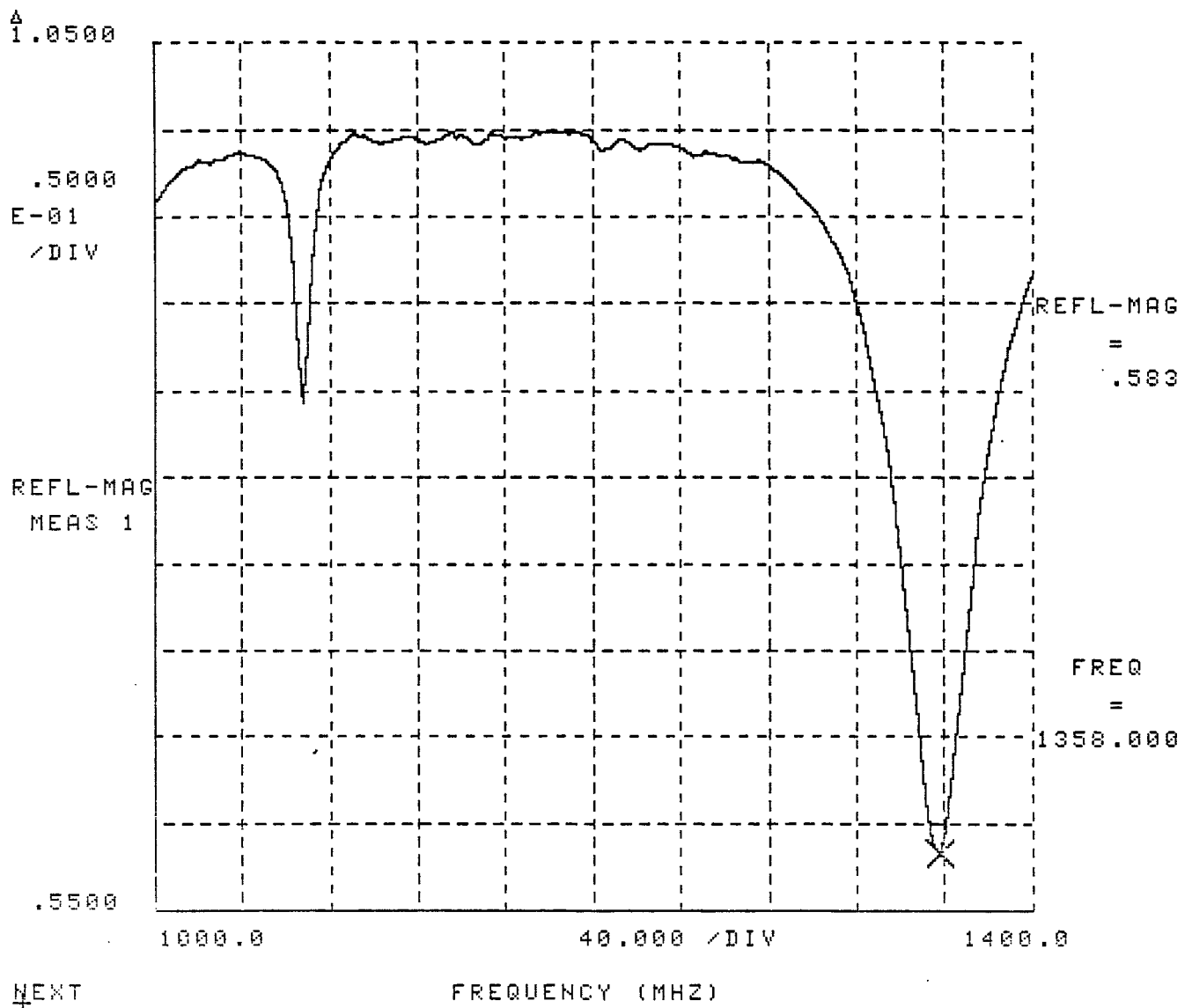
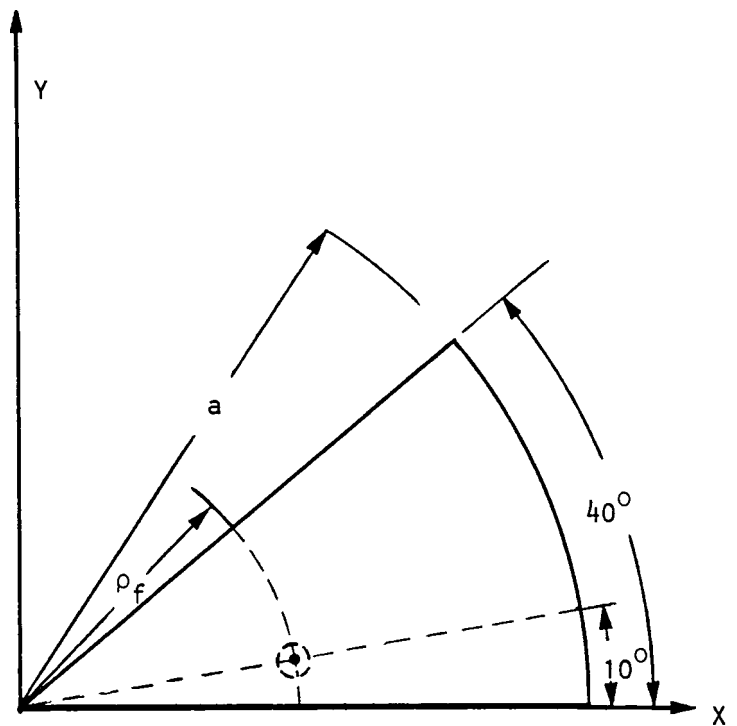
HALF DISC
11.7 CM RADIUS

Figure 3-4-f: Continued



$$a = 11.70 \text{ cm}$$

$$\rho_f = 5.20 \text{ cm}$$

$$\text{Thickness} = 0.146 \text{ cm}$$

$$\text{Dielectric const.} = 2.55$$

$$\text{Conductivity } \sigma = 222 \times 10^5 \text{ mho/m}$$

$$\text{Loss tangent } \delta = 0.0012$$

Figure 3-5-a

40 DEG. CIRCULAR SECTOR
11.7 CM RADIUS

1.00

.30

3.00

R/Z0
=
2.531

IMAG
=
-.386

X=0

MEAS 1

FREQ
=
1770.000

REF PLANE EXT= 1.15CM

 $\Gamma_{max}=1.0000$

NEXT
+

Figure 3-5-b: Measured input impedance loci for the antenna element of figure 3-5-a.

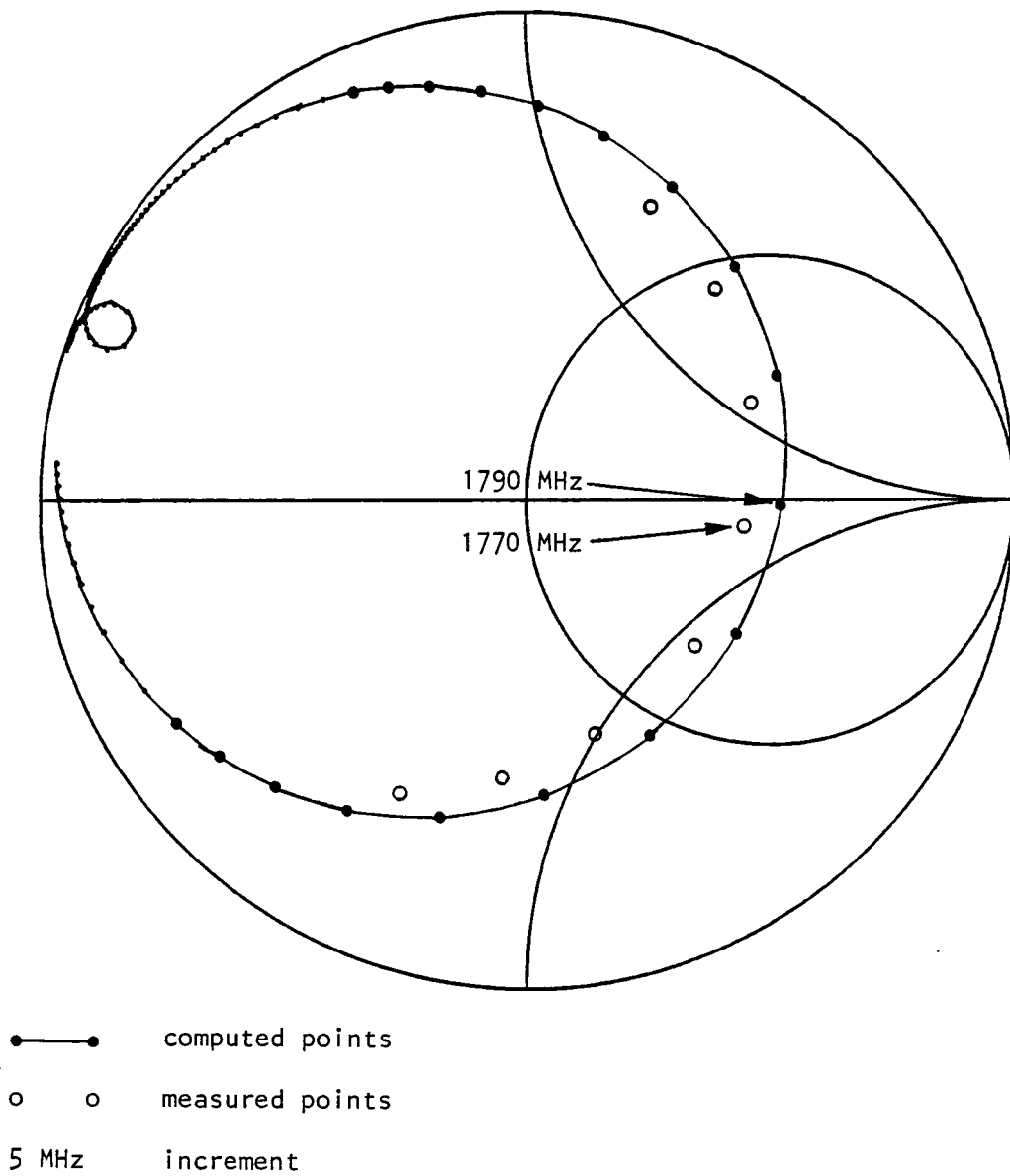


Figure 3-5-c: Calculated and measured input impedance loci for the antenna element of figure 3-5-c.

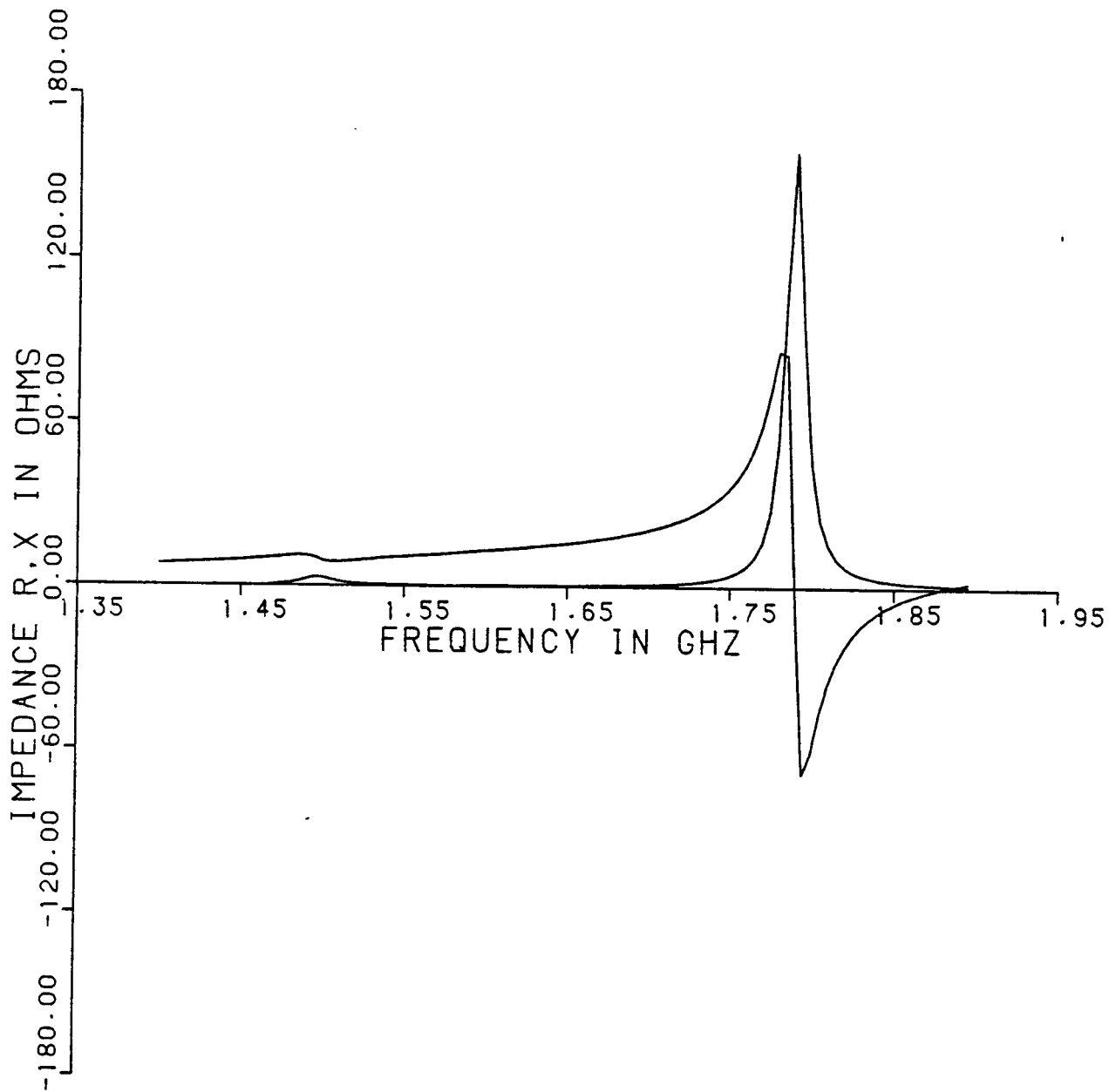


Figure 3-5-d: Calculated input impedance vs. frequency for the antenna element of figure 3-5-a.

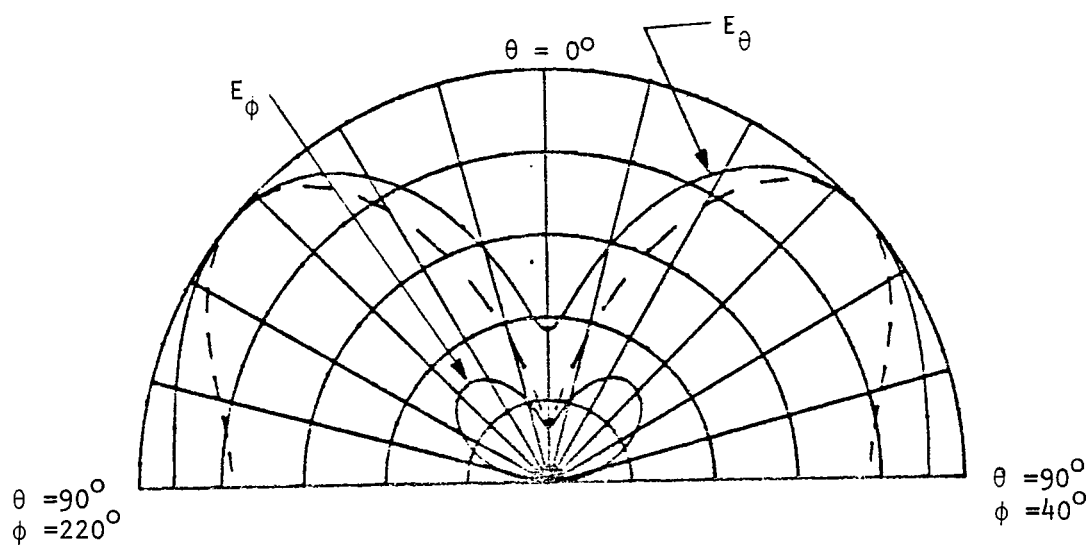
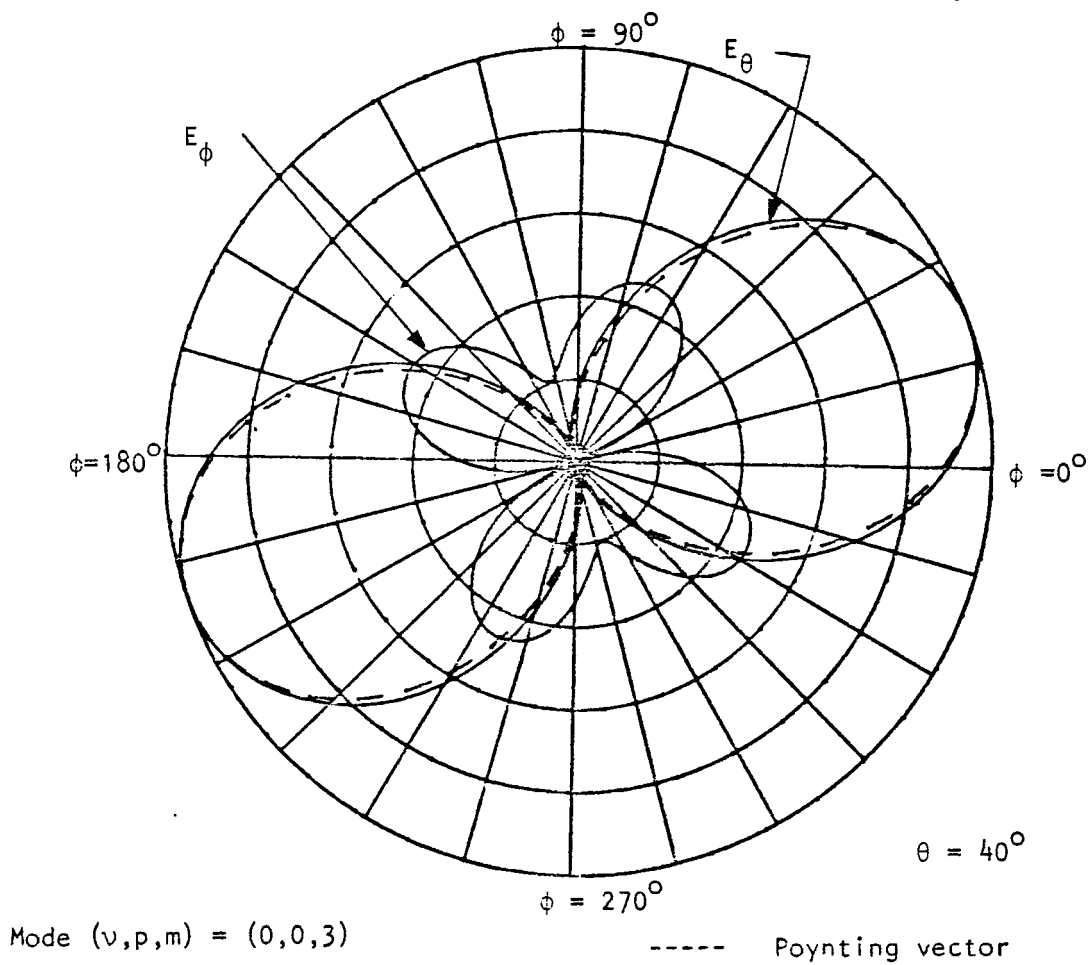


Figure 3-5-e: Calculated radiation pattern, for the antenna element of figure 3-5-a

18 MAR 81

40 DEG. CIRCULAR SECTOR
11.7 CM RADIUS

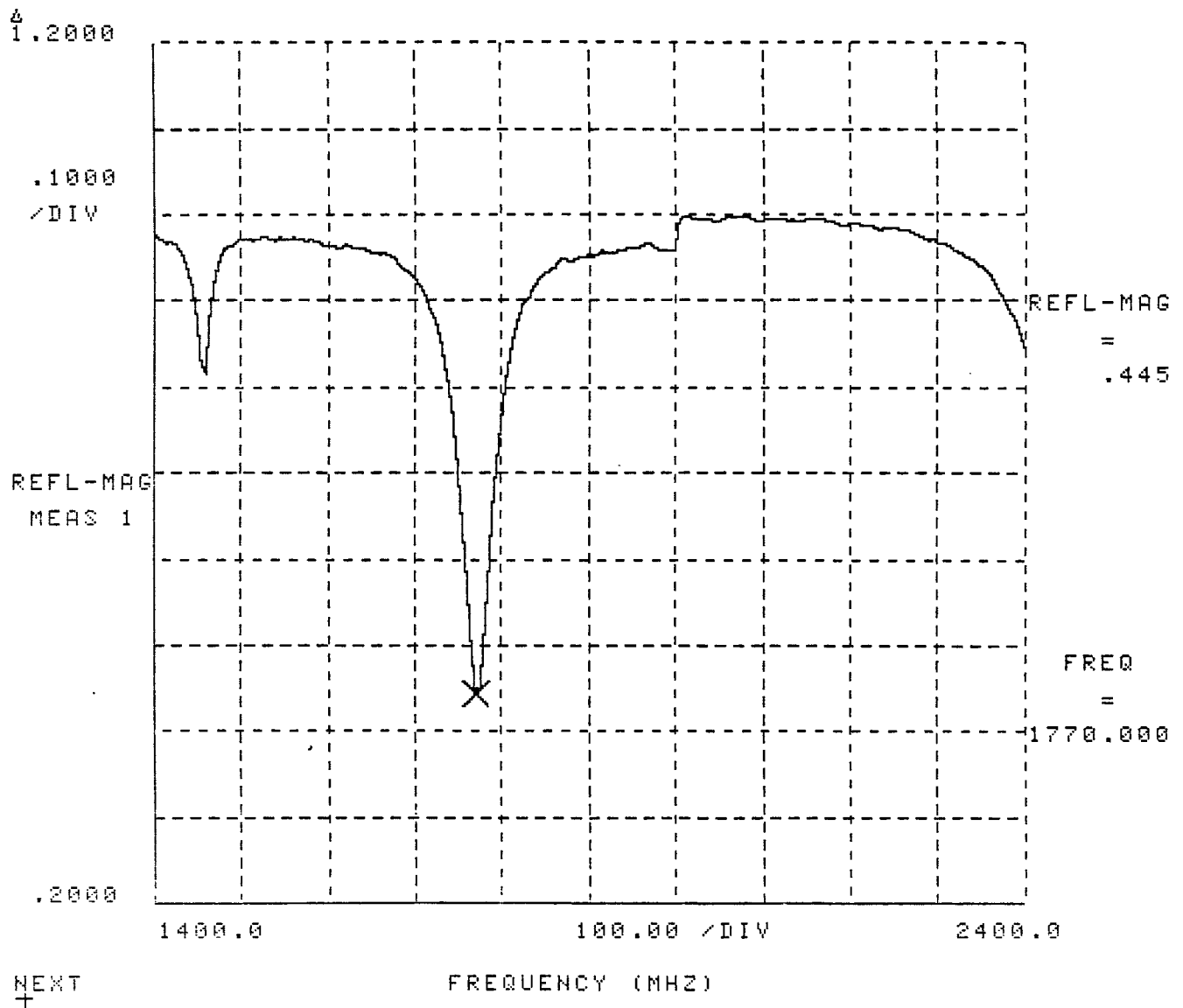


Figure 3-5-f: Measured reflection coefficient vs. frequency for the antenna element of figure 3-5-a.

CHAPTER 4

APPLICATIONS AND CONCLUSIONS

In this thesis, an approximate method (using the cavity model) was applied to analyze electrically thin microstrip antennas with three different shapes (categorized as annular, annular sector and circular sector patches). A detailed study of the internal fields, losses, radiation pattern, radiated power, input impedance and quality factor was made. For each case, the expressions for the internal fields were derived by using both a mode matching and a resonant mode expansion. The analytic and measured results of the input impedance and the resonant frequencies were compared. The agreement between theory and experiment was excellent and supports the validity of the approximations used in this research. (It must be noted, however, that the agreement between the measured and computed resonant frequencies may be more fortuitous than actual since the dielectric constant of the substrate material could vary from the manufacturer's supplied nominal value by several percent.)

One application of the annular patch that we studied can be inferred from tables 2-1 and 2-2. We notice that the resonant frequencies for the annular patch modes are lower than those of the corresponding circular disk patch modes. (We find that the pattern of the two antennas for the lower modes are very similar.) Thus, for a given operating frequency, we can realize a significant reduction in element size using an annular patch. This makes the annulus a more suitable element than the circular disk for array applications.

Another useful feature of the annular patch is that it provides space inside the ring for another patch, or other type of antenna element. For example, a rectangular patch with a rectangular hole cut in its center has been used to provide a dual frequency feed for a parabolic reflector. The microstrip element provided the L-band feed while an open ended waveguide protruding through the central hole provided the x-band feed [16].

The analysis presented in this thesis can be extended to predict the multiport parameters of the patches in the same manner as was done in [13]. In fact, it may be possible to provide a very wide band, multiport theory (that is, one in which the impedance characteristics far from resonance can be accurately predicted) using a method similar to that done for the rectangular microstrip antenna which was recently reported in [17]. However, the method that we have used has been proven to be accurate enough to be useful for much of the design of the annular, annular sector, and circular sector microstrip antennas.

REFERENCES

1. Richards, W. F., Lo, Y. T., and Harrison, D. D.: "Improved theory for microstrip antennas," Electronics Letters, 18th January 1979, Vol. 15, No. 2, pp. 42-44.
2. Long, S.A., Shen, L.C., and Morel, P.B.: "Theory of the circular-disk printed-circuit antenna," PROC. IEE, Vol. 125, No. 10, October 1978, pp. 925-928.
3. Shen, L.C.,: "Analysis of a circular-disc printed-circuit antennas," PROC. IEE, Vol. 126, No. 12, December 1979, pp. 1220-1222.
4. Chew, W. C., Kong, J.A., and Shen, L.C.: "Radiation characteristics of a circular microstrip antenna," J. Appl. Phys. 51(7), July 1980, pp. 3907-3915.
5. Lo, Y.T., Solomon, D., and Richards, W.F.: "Theory and experiments on microstrip antennas," IEEE Transactions on Antennas and Propagation, Vol. AP-27, No. 2, March 1979, pp. 137-145.
6. Chew, W.C., and King, J.A.: "Analysis of circular microstrip disk antenna with thick dielectric substrate."
7. Lo, Y.T., Harrison, D.C., and Richards, W.F.: "An analysis of the disk microstrip antenna part II," RADC-TR-79-132, Interim Report, May 1979.
8. Johnson, D.E., and Johnson, J.R.: "Mathematical methods in engineering and physics," The Ronald Press Company, N.Y., 1965.
9. Shen, L.C., Long, S.A., Allerdin, M.R., and Walton, M.D.: "Resonant frequency of a circular disk, printed-circuit antenna," IEEE Trans. on Antennas and Propagation, July 1977, pp. 595-596.
10. Lo, Y.T.: "Study of microstrip antennas, microstrip phased arrays, and microstrip feed networks," Final Report (October 1977).
11. Abramowitz, M., and Stegun, I.A.: "Handbook of mathematical functions," Dover Publications, Inc., N.Y., 1970.
12. Harrington, R.F.: "Time harmonic electromagnetic fields," Chapter 3, McGraw-Hill Book Company, N.Y., 1961.
13. Richards, W.F., Lo, Y.T., and Harrison, D.D.: "An improved theory for microstrip antennas and applications," IEEE Transactions on Antennas and Propagation, January 1981, Vol. AP-29, No. 1, pp. 38-46.

14. W. F. Richards, Y. T. Lo, and J. Brewer: "A simple experimental method for separating loss parameters of a microstrip antenna," IEEE Transactions on Antennas and Propagation, January 1981, Vol. AP-29, No. 1, pp. 38-46.
15. Mink, J.W.: "Circular ring microstrip antenna elements," IEEE Antenna and Propagation Society, June 1980, pp. 605-608.
16. Kerr, J.L.: "Microstrip antenna developments," Proceedings of the Workshop on Printed Circuit Antenna Technology, October 1979, New Mexico State University.
17. Richards, W.F. and Y. T. Lo: "A wide-band, multiport theory for thin microstrip antennas," 1981 IEEE APS Symposium Digest, June 1981, pp. 7-10.